FE-2029-6

GASIFICATION IN PULVERIZED COAL FLAMES

Second Annual Progress Report, July 1976—August 1977

By
P. E. George
R. C. Lenzer
J. F. Thomas
J. S. Barnhart
N. M. Laurendeau

August 1977

Work Performed Under Contract No. EX-76-C-01-2029

The Combustion Laboratory
Purdue University
West Lafayette, Indiana

U. S. DEPARTMENT OF ENERGY

DISCLAIMER

NOTICE

FE-2029-6
Distribution Category UC-90c

GASIFICATION IN PULVERIZED COAL FLAMES

Second Annual Progress Report
Energy Research and Development Administration
ERDA-FE-2029-6

P. E. George
R. C. Lenzer
J. F. Thomas
J. S. Barnhart
N. M. Laurendeau

August 1977

The Combustion Laboratory
School of Mechanical Engineering
Purdue University
West Lafayette, Indiana 47907
Report No. PURDU-CL-77-04

THIS PAGE

WAS INTENTIONALLY

LEFT BLANK

ACKNOWLEDGEMENTS

The following Purdue undergraduate students have assisted in various phases of this investigation: James Varnau, Scott Haag, Kris Dunn, Howard Schirtzinger, Wayne Stevens and Dickerson Huskey. Special thanks go to Mr. Varnau for his work on the exhaust system, Mr. Dunn for the cyclone particulate studies, and Mr. Haag for development and calibration of the coal feeder. Equipment acquisition was facilitated through the help of Mr. Frank Tymoski, Purdue Purchasing Department. The School of Mechanical Engineering provided funds for construction of the boiler facility. Prof. C. Ehresman aided us during many design phases especially with respect to various safety codes. The secretarial talents of Ms. Virginia Bass and Ms. Janelle Vehar are also appreciated. We are grateful for the help given to us by our contract monitors at ERDA, Dr. Michael Biallas and Dr. Robert Wellek.

TABLE OF CONTENTS

LIST OF TABLES

LIST OF FIGURES

LIST OF SYMBOLS

A	area
A_e	secondary air exit area
A_n	total cyclone nozzle area
A_p	primary air exit area
A_s	total free area of swirl block exits
A_t	Area of cyclone throat
A_v	Vessel lateral area used for heat transfer
a	particle radius, ft
a_r	area of one radial slot of swirl generator
a_t	area of one tangential slot of swirl generator
B	swirl block height
C	constant
C_1, C_2, C_3	swirling jet constants
D	chamber diameter
D_m	molecular diffusion coefficient
D_p	diameter of a coal particle
d	secondary air exit diameter
d_f	instantaneous fuel drop diameter
d_o	initial drop diameter
f	mass flow ratio, $\dot{m}_c/\dot{m}_g$

f_r	radiation shape factor
G_x	axial momentum flux
G_ϕ	angular momentum flux
g_c	gravitational constant
H_c	input coal enthalpy of combustion, kcal/kg coal
$H_{c,i}$	enthalpy of combustion of species i, kcal/g mole
H_{in}	chemical plus sensible enthalpy in
H_o	total enthalpy input per lbm product
H_{out}	chemical plus sensible enthalpy out
H_p	sensible enthalpy out per lbm product
H_{pg}	product gas enthalpy of combustion, kcal/kg coal
ΔH_{pr}	difference in sensible enthalpy between products and reactants, kcal/kg coal
H_2O_D	steam produced from coal by hydrogen, kg/hr
H_2O_{in}	steam feed rate, kg/hr
H_2O_{out}	steam discharge rate, kg/hr
h	convective heat transfer coefficient
K	radiative absorption coefficient
k	reaction rate coefficient, s^{-1}
k_K	Kaowool thermal conductivity
k_r	refractory thermal conductivity
k_s	steel thermal conductivity
L	chamber length
L_c	a characteristic length
L_t	length of tube extending from cyclone throat, ft
$\bar{M}$	average molecular weight of make gas, kg/g mole
M_i	molecular weight of species i

M_1	mass flow rate at cyclone wall
M_2	mass flow rate in cyclone at R_2
M_p	coal particle mass
$\dot{m}$	mass flow rate
$\dot{m}_a$	mass flow rate of primary air
$\dot{m}_c$	mass flow rate of coal
$\dot{m}_g$	make gas mass flow rate
$\dot{m}_o$	mass flow rate at jet exit
$\dot{m}_r$	recirculated mass flow rate
$\dot{m}_s$	mass flow rate of secondary air
$\dot{m}_t$	total mass flow rate
$\dot{m}_{uc}$	unburned carbon mass flow rate
N	number of nozzles in cyclone
Nu	Nusselt number
n	number of product gas constituents
P	axial distance to the point where a confined jet strikes the wall (see Fig. 28)
p	static pressure
Q	make gas heating value, kcal/kg gas
Q'	volumetric flow rate, ft^3/sec
Q_{cv}	heat transfer rate, gas to chamber wall via convection
Q_L	heat loss rate for reactor
Q_r	heat transfer rate, gas to chamber wall via radiation
Q_t	heat transfer rate, total from gas to chamber wall
Q_1	heat transfer rate, conducted through vessel wall
Q_2	heat transfer rate, vessel to surroundings via natural convection

Q_3	heat transfer rate, vessel to surroundings via radiation
q_1	radiation heat transfer to incoming reactants
q_2	heat transfer through the cyclone reactor walls
q_3	radiation heat transfer from the cyclone outer combustion region to the inner gasification region.
R	secondary air exit radius
R_t	radius of cyclone throat, ft
R1	cyclone combustor air/fuel entrance region
R2	cyclone reactor combustion region
R3	cyclone reactor gasification region
R4	cyclone reactor exit region
R_1	swirl block or cyclone radius (see Fig. 27 or 29)
R_2	arbitrary radius within cyclone, ft
RR	weight percent of particles greater than screen size
r	radius
r_v	vessel outside radius
r_w	inner refractory wall radius
r_1	radius of streamline tangent circle (see Fig. 27)
r_2	refractory/Kaowool interface radius
r_3	vessel inside radius
S	swirl number
S_s	secondary swirl number
S_t	total swirl number
T_v	vessel outside wall temperature
T_w	refractory inside wall temperature
t	time

U	primary air axial velocity
U_1	radial velocity at cyclone wall, ft/sec
U_2	radial velocity at R_2, ft/sec
u	secondary air axial velocity radial velocity of gas in cyclone, ft/sec
V	velocity
V_f	flow volume, ft^3
V_1	tangential velocity at cyclone wall, ft/sec
V_2	tangential velocity in cyclone at R_2, ft/sec
V_r	velocity through radial ports
V_t	velocity through tangential ports
v	tangential velocity of gas
w	tangential velocity
x	axial distance from jet exit
x_i	mole fraction of species i in product gas
x_o	axial distance from jet exit to start of theoretical entrainment (see Fig. 28)
x_s	screen size, μm
x_1	axial distance to point where entrainment stops and disentrainment begins (see Fig. 28)
Y	make gas yield, kg gas/kg coal fed
Y_p	combustible make gas yield, kg comb. gas/kg coal fed
z	number of radial and tangential entry pairs
α	swirl block angle (see Fig. 27)
β	swirl generator geometric parameter (see Fig. 27)
β_e	evaporation or combustion coefficient
Γ	swirled jet confinement parameter
δ	swirl generator geometric parameter (see Fig. 27)

ε	surface emissivity
ε_y	chemical yield, kg gas/kg coal reacted
ε_g	effective emissivity of particle laden gas
η_c	carbon efficiency, percent
η_{cg}	cold gas efficiency, percent
η_{hg}	hot gas efficiency, percent
θ	Thring-Newby parameter
μ	viscosity of gas, lbm/ft·sec
ξ	swirl block adjustment angle (see Fig. 27)
ξ_m	maximum swirl block adjustment angle (see Fig. 27)
ρ	density
ρ_a	density of primary air
ρ_c	density of coal
ρ_g	density of combustion gas
ρ_s	density of secondary air
σ	swirl block characteristic parameter
σ_B	Stefan-Boltzmann constant
τ_{co}	CO burnup time
τ_{eb}	fuel droplet lifetime
τ_f	fuel droplet flight time
τ_{hc}	fuel ignition delay and burning time
$\tau_{sl,co}$	eddy dissipation time in CO forming region of shear layer
τ_b	coal particle burning time
τ_r	coal particle residence time
ϕ	jet spread angle (half-velocity half-angle)
ϕ_o	jet spread angle for unswirled jet (half-velocity half-angle)

ϕ_t	Thiele modulus
χ	coal to total air ratio
ψ	mass flow ratio $\dot{m}_a/\dot{m}_s$
ω_C	carbon mass fraction, gC/g coal
ω_{CH_4}	CH_4 mass fraction, gCH_4/g gas
ω_{CO}	CO mass fraction, gCO/g gas
ω_{CO_2}	CO_2 mass fraction, gCO_2/g gas
ω_p	combustible mass fraction

ABSTRACT

This project concerns the production of power and synthesis gases from pulverized coal via suspension gasification. Swirling flow in both concentric jet and cyclone gasifiers will separate oxidation and reduction zones. Gasifier performance will be correlated with internally measured temperature and concentration profiles.

The test cell flow system and electrical system, which includes a safety interlock design, has been installed. Calibration of the UTI-30C mass spectrometer and construction of the gas sampling system is complete. Both the coal feeder, which has been calibrated, and the boiler are ready for integration into the test cell flow system.

Construction and testing of the cyclone reactor, including methane combustion experiments, is complete. The confined jet reactor has been designed and construction is underway. Investigation of combustion and gasification modeling techniques has begun.

I. INTRODUCTION AND SUMMARY

The need for a clean method of burning coal is clearly defined (Squires, 1974; Osborn, 1974; Lenzer, 1977). Power or synthesis gases from coal seem to offer the most promise for immediate coal utilization, particularly if they can be used in combined cycle plants. The primary emphasis of this research is to shorten the development time for a practical coal gasifier by demonstrating that existing coal burner technology may be used to design and optimize an entrained flow coal gasification reactor.

A. Fundamental Concepts

The chemistry of coal gasification has been covered elsewhere (Laurendeau, 1977; Batchelder et al., 1956; von Fredersdorff and Elliott, 1963). The characteristics of the three major reactor classifications (fixed bed, fluidized bed, and entrained flow) have also been reviewed (Laurendeau, 1975). Based on these observations, we believe that existing burner designs and the operating experience gained through widespread use of entrained coal combustion can be applied to produce an efficient coal gasifier acceptable to the utility industry.

We are presently considering two types of entrained coal firing — the cyclone and the swirling jet. Both the cyclone and swirling jet are characterized by high levels of turbulence and stable recirculation zones. In each case, the development of the internal fluid mechanics is strongly influenced by swirl. The swirl number S, defined as the ratio of the flux of angular momentum (G_ϕ) to the flux of axial momentum (G_x), non-dimensionalized by a characteristic radius ($S = G_\phi/G_x R$), characterizes both systems (Syred and Beer, 1974). Residence times, mixing times and recirculation zones can be controlled by varying the swirl number.

Figures 1 and 2 show schematically the two types of combustor/gasifier we are considering. The cyclone has coal and air feeds at the

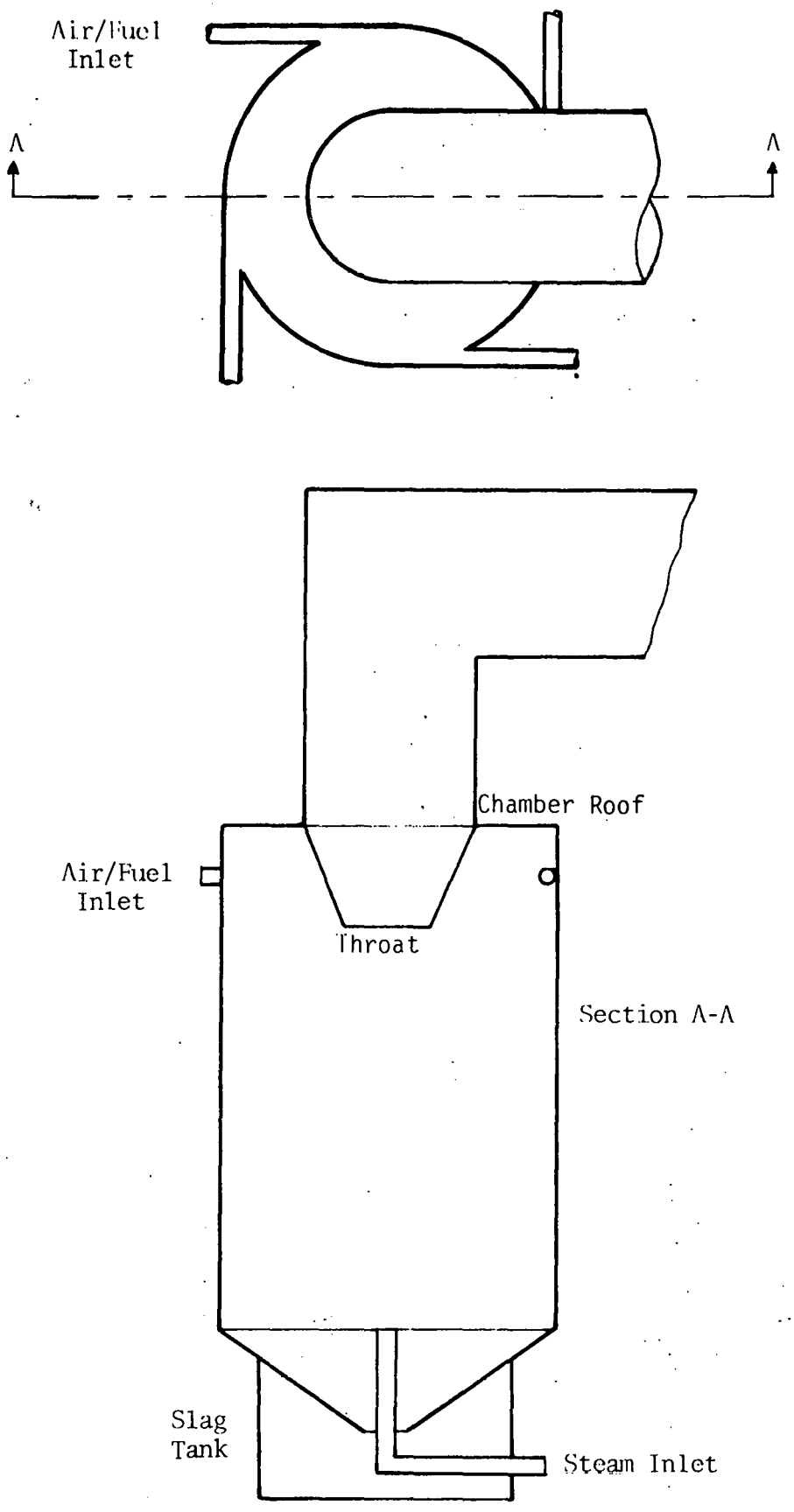

Figure 1. Vortex Gasifier Schematic

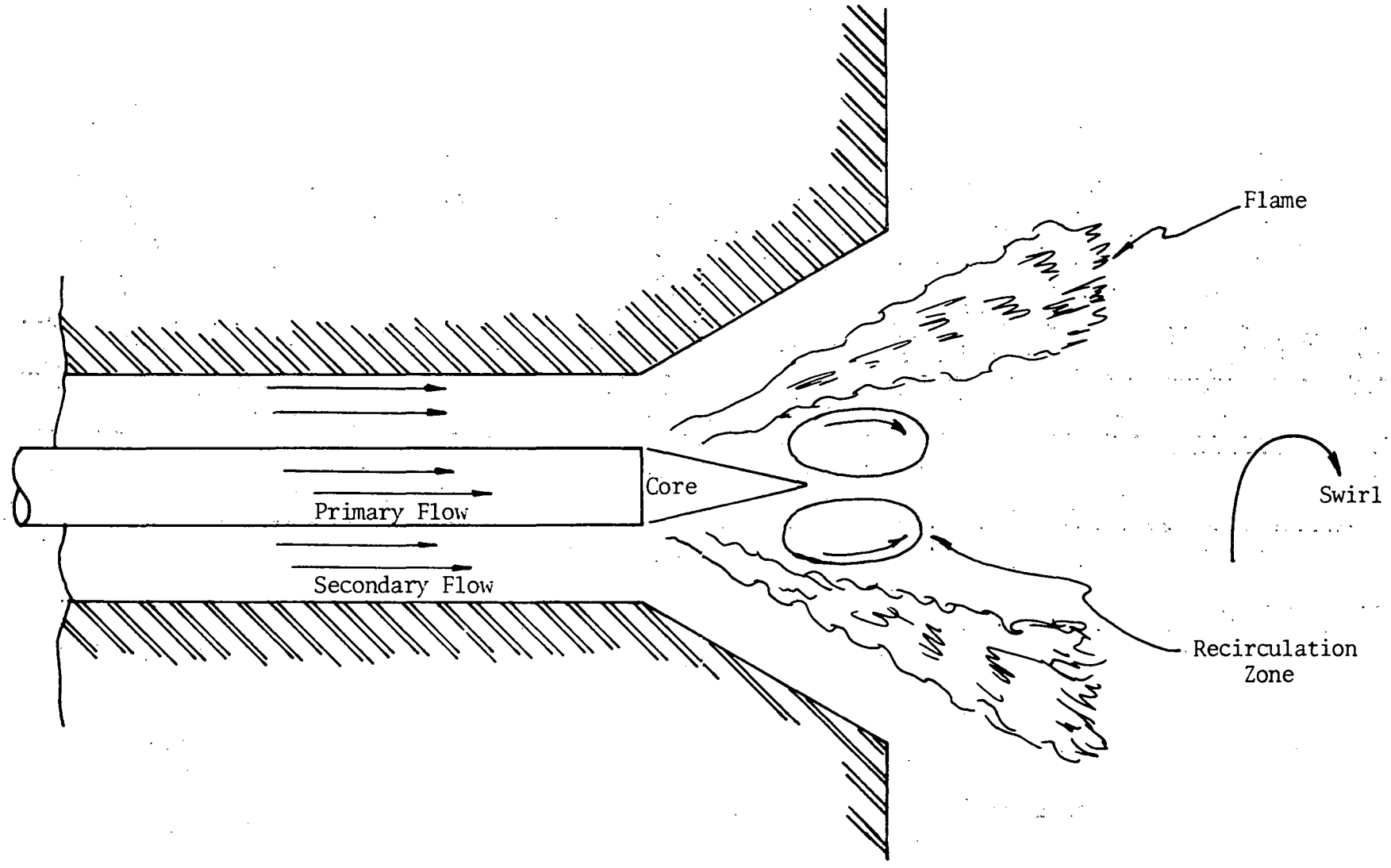

Figure 2. Concentric Jet Gasifier Schematic

top, firing tangentially to the chamber wall. Steam is fed axially through the lower end of the chamber and mixes with the central core where gasification takes place. Reactants are fed into the reactor in proportions which allow part of the coal to combust in the outer region of the cyclone. This provides heat to drive the endothermic steam-carbon reaction occurring in the core. The jet also depends on an endothermic zone surrounded by an exothermic combustion region. In this case, the endothermic region is the central recirculation zone which develops at swirl numbers greater than 0.6. The recirculation zone is charged with steam and coal from the primary feed pipe. A portion of the coal mixes with the swirling secondary air and combusts in the outer regions. Obviously, the concept of distinctly separate reaction zones is an idealization. Internal reactor probing will be required to determine the extent to which discrete reaction zones are present. It is clear, however, that swirl strongly affects the mixing and fluid mechanical behavior of the two systems; thus we have a measure of control not available in other gasifying schemes.

B. Criteria and Objectives

1. The Cyclone Gasifier

The tangential entry vortex gasifier is patterned after the cyclone burner (Fig. 1). Separation of oxidation and reduction zones is attained by tangential flow of coal/air mixtures coupled with axial steam injection. Fundamental experimental data for both homogeneous and heterogeneous (two-phase) cyclone chambers have been obtained for cold flow (Strickland, 1973), homogeneous combustion (Schmidt, 1970; Syred and Beer, 1974) and pulverized coal combustion (Syred and Beer, 1974). These results allowed design of our vortex gasification system (Chapter III).

The vortex gasifier possesses several advantages compared to the concentric jet system (Syred and Beer, 1974): (1) greater turbulent mixing levels, (2) ease of operation at high pressures and (3) larger particle residence times. These three factors promote high temperatures and slagging conditions, and hence good carbon and gasification efficiencies. There are disadvantages, however: (1) chamber wall temperatures

are much higher, causing material and heat transfer problems; (2) slagging operation presents difficulties due to heat losses and residue disposal; (3) injection of coal/air vs. coal/steam mixtures increases the opportunity for spontaneous combustion at high pressures.

Turbulent mixing and particle residence times in vortex systems are primarily determined by the tangential swirl velocity (Strickland, 1973). This dominant velocity profile is satisfactorily described by the Rankine model, i.e., potential or free vortex flow ($W \propto r^{-1}$) near the wall, and rotational or forced vortex flow ($W \propto r$) at the chamber core. In idealized rotary motion (Schmidt, 1970), the free vortex zone is characterized by downward axial flow, while the rotational zone is characterized by upward flow. Thus coal particles move downward via a helical path, followed by upward movement along a helical path of smaller radius. Lighter particles will of course undergo more rapid migration to the center of the chamber.

In Fig. 1, tangential air/coal injection occurs at the top of the cyclone to avoid slag buildup around the injection ports. If higher particle residence times are required, air/coal entry may be attempted at the bottom. In this case, two flow reversals occur; one at the throat annulus and another at the slag port (Schmidt, 1970). The half-angle of the throat quarl will probably determine much of the flow structure, regardless of bottom or top injection. Flow structure is also affected by the chamber end wall boundary layer (Schmidt, 1970); for example, average particle residence times are apparently increased by attaching rectangular fences radially to the closed end wall. Similarly, axial vs. radial steam injection will generate different mixing patterns, and hence affect gasification efficiency (axial injection promotes greater separation of oxidizing and reducing zones). At low steam velocities, mixing will be dominated by vortex entrainment in the core (Strickland, 1973).

Our proposed design is characterized by three important features: (1) entrained vortex flow, (2) coal/steam/air rather than coal/steam/oxygen and (3) separation of oxidation and reduction zones. The third characteristic is presently being considered by Combustion Engineering (Mehta, 1976); the first two have received limited attention, most notably in the Ruhrgas process (von Fredersdorff and Elliott, 1963).

To our knowledge, the only extensive investigation of pulverized coal gasification in a small-scale cyclone system was conducted by Yagi and Kunii (1957). Production of both power gas and synthesis gas was correlated with carbon efficiency, and hence reduction zone temperature (1300-1650°K). By externally heating the 20 cm diameter chamber, 70-80% of the ash appeared as slag. Their preliminary results are quite encouraging, thus providing impetus for our cyclone gasifier design.

2. The Confined Jet Gasifier

The concentric confined jet gasifier is patterned after the traditional pulverized coal burner (Fig. 2). Separation of oxidation and reduction zones is attained by using coal/steam mixtures in the primary flow and swirling air in the secondary flow. Fundamental experimental data applicable to confined and free jets have been obtained for cold flow (Beer and Chigier, 1972), homogeneous combustion (Beer and Chigier, 1972; Heap et al., 1973) and pulverized coal combustion (Beer and Chigier, 1969; Heap et al., 1973). These results allowed design of our confined jet gasification system (Chapter III).

The combustion process in a pulverized coal burner is dominated by the highly turbulent flow field produced by secondary swirl. At high swirl intensities ($S > 0.6$), a torroidal vortex recirculation zone, which promotes air/coal entrainment and high carbon efficiency, becomes stabilized in the flow. The size of the recirculation zone depends primarily on the swirl number and the shape of the divergent quarl at the burner exit. Increasing swirl generally lengthens the recirculation zone while divergence broadens the zone (Beer and Chigier, 1972).

Gasifier performance will depend quite strongly on the extent of turbulent mixing between the fuel rich recirculation zone and the outer air flow. Entrainment must be sufficient to promote combustion, but not enough to destroy the identity of the reduction zone. Previous work suggests that entrainment is largely controlled by the following burner parameters (Heap et al., 1973):

(1) secondary swirl
(2) primary/secondary composition ratios
(3) design and position of fuel injector
(4) primary velocity
(5) exit quarl divergence.

The first three parameters have the strongest effect, as they control flame shape during pulverized coal combustion. Our concentric gasifier is designed such that all parameters can be easily varied over reasonable ranges. To reduce entrainment and thus preserve the reduction zone, Heap et al. (1973) recommended a single hole, high velocity injector, with enough swirl to stabilize the reaction zone at the injector face. However, in view of carbon efficiency requirements, the appropriate choice of burner parameters is not at all obvious.

The included angle of the water-cooled exit quarl has been designed for maximum performance ($\sim 70°$), as suggested by Beer and Chiger (1972). Primary velocity and secondary swirl will be chosen to achieve both penetration (high primary velocity) and divergent (high swirl) flames. All fuel will be fed via the non-swirling primary jet. Secondary swirl will be controlled by a movable block swirl generator (Beer and Chigier, 1972).

For turbulent jets, comparison between model and prototype is aided by the unique profiles characteristic of all turbulent jets. More generally, however, partial modeling techniques have led to the development of rather simple similarity rules. If the following parameters are maintained equal in model and prototype, reliable extrapolation is assured (Beer and Chigier, 1972):

(1) stoichiometry and initial density
(2) residence time
(3) swirl number
(4) d_o/D and L/D
(5) $\dot{m}_{primary}/\dot{m}_{secondary}$
(6) $d_{primary}/d_{secondary}$.

C. Summary of Progress

Much of the second contract year has dealt with design, construction, and testing of hardware. Construction and shakedown of the test cell and the cyclone reactor are complete; fabrication of the confined jet reactor is underway. The mass spectrometer and pulverized coal feeder have been calibrated. A series of methane combustion experiments have been run.

Chapter II presents a preliminary investigation of entrained flow combustion and gasification modeling. Both microscopic and macroscopic models are considered at various levels of sophistication. Chapter III describes progress in system design and construction; experimental progress is described in Chapter IV.

II. MODELING TECHNIQUES FOR PULVERIZED COAL GASIFICATION

A. Introduction

Models for coal gasification range from simple thermodynamic equilibrium models to detailed numerical predictions based on the turbulent transfer equations coupled with chemical kinetic rate expressions. As with all modeling of combustion systems, as the degree of complexity increases, the potential for broadly applicable results increases, but the mathematical and practical tractability decreases. Equilibrium modeling is useful in defining gross performance trends and their variation with reactant inputs and heat loss characteristics (Laurendeau and Waite, 1977). Equilibrium cannot, however, predict performance for short residence time or mixing controlled reactors. In reviewing the modeling work pertinent to entrained coal combustors and gasifiers, we have concentrated on three major areas: macroscopic models, phenomenological models and microscopic models.

In macroscopic modeling, the reactor is broken into a network of plug flow (PFR) and perfectly stirred (PSR) reactors. The network may be as simple as a single reactor or as complex as the series of reactors proposed in Section B. When a series of reactors is used, the choice of type, size, residence time and input conditions depends on the physical nature of the actual reactor.

Phenomenological modeling is more concerned with actual reactor flow. In this case, overall behavior of the system is correlated by characteristic parameters. These take the form of nondimensional ratios and may include such items as swirl number, confinement ratio (in the case of jets), length to diameter ratio and equivalence ratios. In addition, characteristic times such as particle burn-out and mixing times can be defined and used to correlate performance.

The microscopic approach seeks to define not only the overall performance, but the details of the internal flow patterns based on a minimum of empirical constants and appropriate solutions to the turbulent transfer and chemical kinetic equations representative of the system. Our modeling efforts will be concentrated on the macroscopic and phenomenological types. We expect to work closely with Smoot and Hanks (1977)

in their efforts to develop a microscopic model. In this chapter we consider briefly each of the three model types.

B. Macromodels for Swirling Reactors

As a first effort in modeling the cyclone reactor, a relatively simple and versatile model was sought. The complex fluid mechanics coupled with the heterogeneous chemical reactions found in coal combustion and gasification are extremely difficult to model in detail or from basic governing equations. Also much information pertaining to the cyclone fluid mechanics and chemical kinetics remains unknown. For these reasons a PSR-PFR reactor model was chosen. Ideal PSR and PFR modeling is used extensively for chemical reactor models and certain modifications for nonideal behavior can be simply introduced.

1. Previous Modeling

A general review of entrained flow coal combustion modeling is presented by Field et al. (1967). Most previous modeling has been of the plug flow type with variations in chemical kinetics, heat transfer and particle sizing. Only models which have a direct bearing on PSR-PFR modeling are discussed here.

Beer and Lee (1965) modeled a pulverized coal furnace as a PSR in series with a PFR. Furnace experiments were done over a large swirl range. Both residence time distributions (measured by argon tracing) and carbon efficiency correlated well with the theoretical model. The relative volume of the furnace modeled as a PSR was correlated to the size of the recirculation zones caused by swirl. A global chemical kinetics model was used for heterogeneous reaction calculations.

A PSR-PFR model for a staged entrained flow coal gasification process has been presented by Mehta (1976). The process consists of three stages: a vortex combustor, a diffuser and a reductor. The vortex combustor is modeled as a PSR, based on the highly turbulent swirling flow. Within the diffuser, coal is mixed with the incoming combustor exit gases. The proximate volatile matter is assumed to react instantaneously to form CO and H_2. Steam is added in the reductor section, which is modeled as a one-dimensional, internally adiabatic plug flow reactor. In all stages gas-phase equilibrium is assumed.

2. Cyclone Reactor Characteristics

The cyclone reactor has been designed to form separate oxidation and reduction zones in gasification experiments (Lenzer, 1977). As shown in Fig. 3, the outer annular region will be primarily a combustion zone whereas gasification reactions will dominate in the inner region.

In general, the cyclone flow is characterized by high swirl and turbulence, with strong recirculation zones (Agrest, 1965; Schmidt, 1970; Ustimenko and Bukhman, 1968). Cyclone turbulence levels can be 10 or more times greater than for conventional straight flow furnaces (Ustimenko and Bukhman, 1968). These characteristics indicate that PSR modeling is appropriate.

The particle and gas residence time distributions must also be considered for modeling. Coal particles will remain within the reactor for a much longer time than the gas residence time (Schmidt, 1970; Agrest, 1965). The relatively heavy particles will tend to stay near the reactor walls due to inertial forces, and only the smaller particles will become entrained in the central region and flow out the exit stream (Semenov and Semenenko, 1969; Lewellen et al., 1977).

Heat transfer considerations are also very important. The reactor is externally heated to compensate for some heat losses, but heat loss through the reactor walls will be significant. Heat transfer within the reactor will be largely due to radiation transfer between reaction zones plus convection and radiation to the walls.

3. Proposed Model

The proposed model is explained by following the reactant paths into and through the cyclone reactor. Figure 4 is a schematic diagram of the proposed model.

The pulverized coal size distribution which enters the reactor will be approximately a Rosin-Rammler distribution. Field et al. (1967) have shown that considerable error can occur if a monosize distribution is used; hence, efforts will be made to incorporate the most realistic size distribution possible.

The coal/primary air and secondary air streams will be injected tangentially through four nozzles by coaxially arranged tubes (Fig. 2).

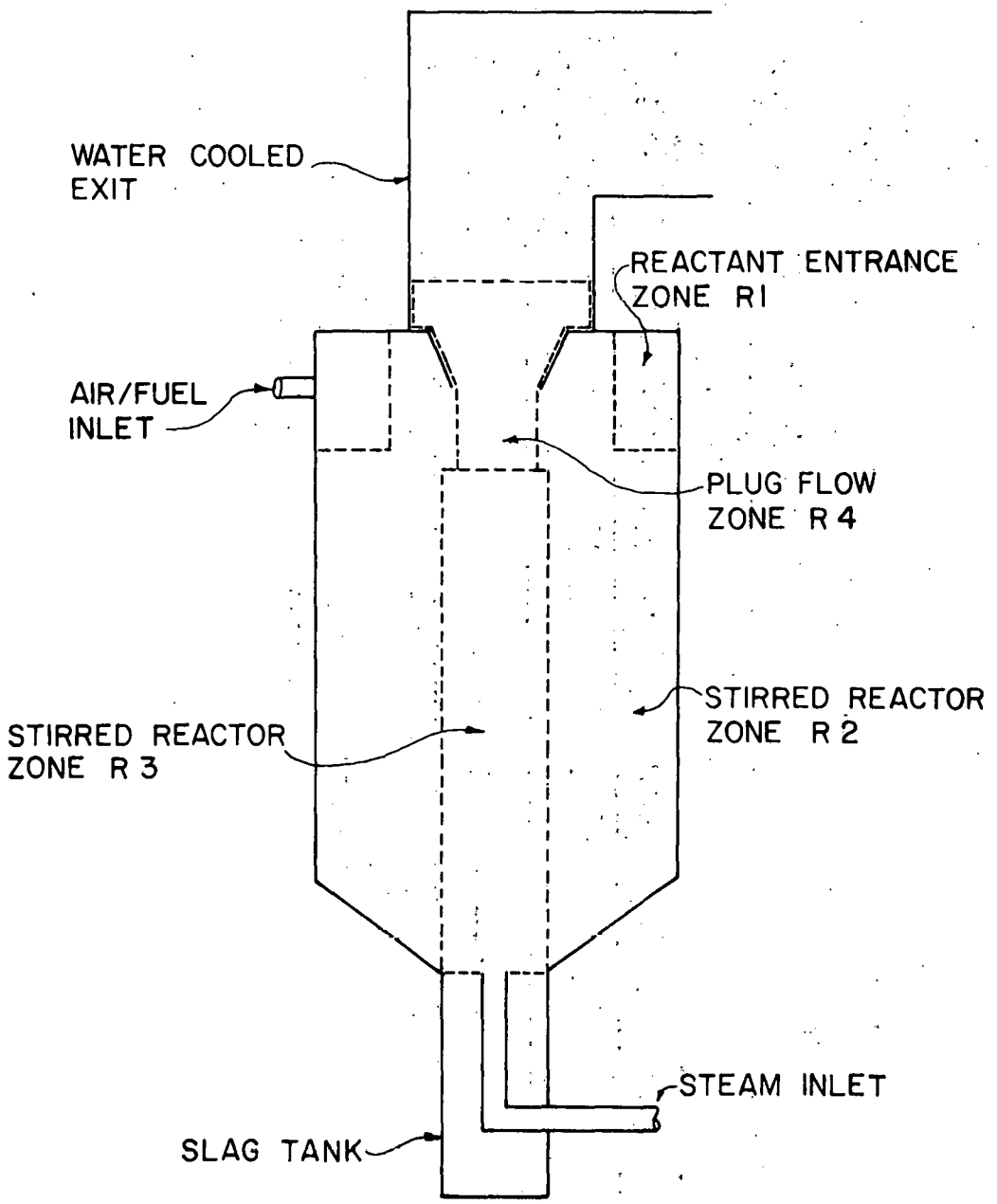

Figure 3. Hypothesized Cyclone Reaction Zones

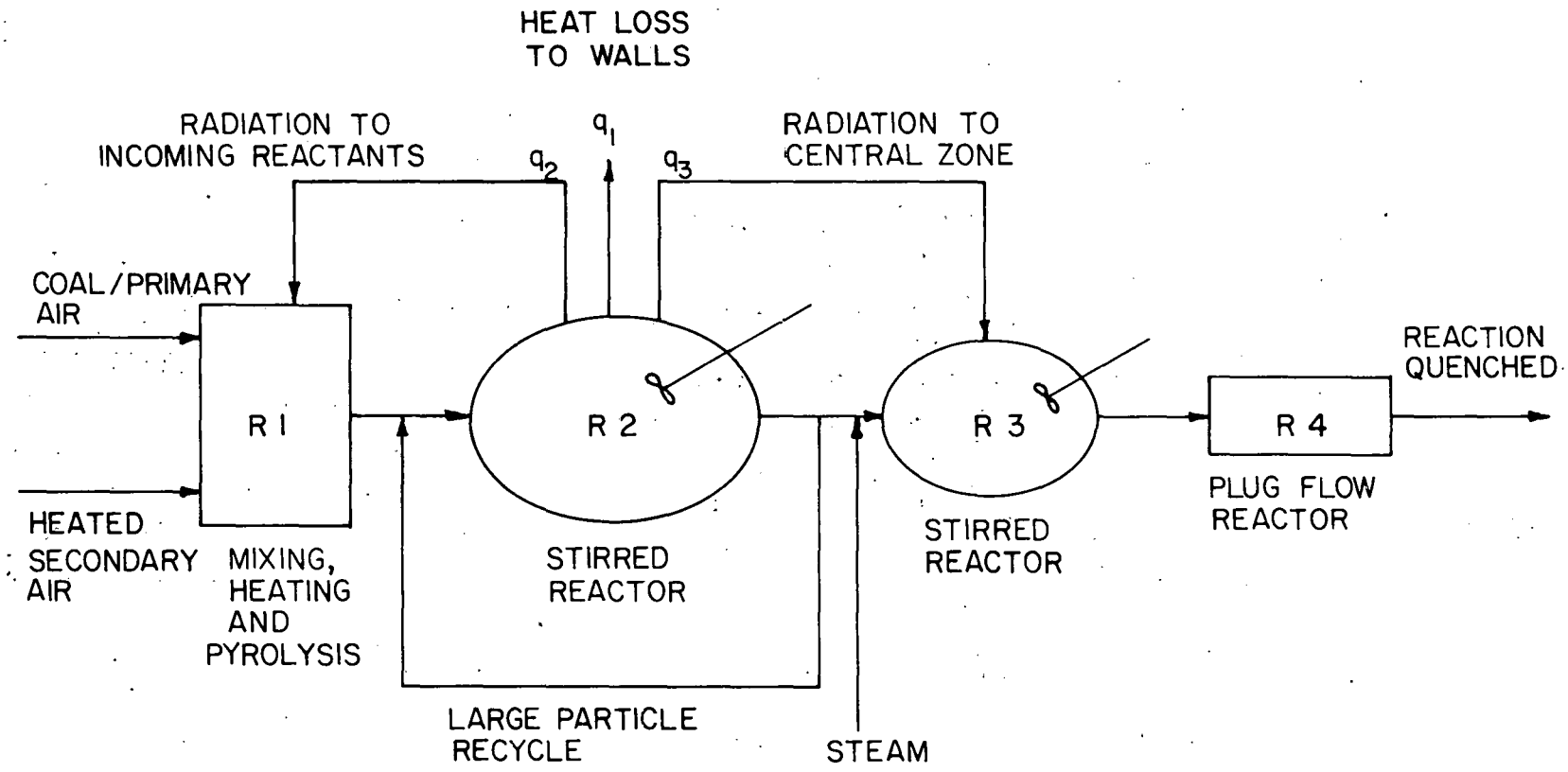

Figure 4. Proposed PSR-PFR Model Schematic

Secondary air will be preheated to 600-900°F. Entering coal particles will be quickly heated due to mixing with the hot secondary air stream and radiation from burning particles. Pyrolysis and swelling of the particles will ensue. A common assumption under such conditions is that the volatiles released will instantaneously react with oxygen to produce CO and H_2O (Batchelder et al., 1953; Field et al., 1967; Mehta, 1976). Reactor R1 shown in the model schematic represents the entrance zone of the reactor, where mixing, heating and pyrolysis occurs.

The char particles and gases then enter the combustion zone of the cyclone, which is represented by reactor R2 in the model schematic. Intense mixing and high temperatures occur in this zone which indicate that a micromixed rather than macromixed PSR model should be chosen (Beer and Lee, 1965). It is assumed for modeling purposes that no coal particles can leave the combustion zone until they are smaller than some characteristic size. The validity of this assumption is backed by our flow experiments (Section II.C). In the model, all particles which are greater than the chosen characteristic size are recycled back into the reactor (R2 in Fig. 4). A global expression will be used to calculate reaction of the char.

The gases and small particles will pass into the central region of the cyclone. The entrained particles will follow the gas stream, which moves upward towards the exit as rotational flow. A PSR model is proposed for this region on the basis of measurements by Ustimenko and Bukhman (1968), who found very high turbulence levels in the central region of a cyclone. In addition, steam introduction to this region should increase mixing.

The reactants will finally enter the throat region, which is represented by reactor R4 of Fig. 4. Reaction continues until the reactants are quenched in the water-cooled exhaust system. Mixing and turbulence should subside as the gases enter the throat region of the cyclone, which is modeled as a PFR.

Heat transfer occurs through the cyclone walls and between areas of the reactor. The net radiation transfer from the combustion zone to the incoming reactants is represented by q_1; similarly q_2 is the heat transfer through the reactor walls and q_3 represents the net radiation transfer to the reactants in the central rotational flow zone. An overall

heat transfer expression will be developed to calculate heat loss through the reactor walls. Methods of treating internal radiation heat transfer are currently being examined.

Only the general outline of a PSR-PFR modeling approach has been discussed. Many parameters, such as input particle size distribution, reaction zone size and mean residence time, will be defined by physical consideration of the cyclone. This type of model can also be adapted to the confined jet reactor. Further investigation and experience with PSR-PFR models will reveal what assumptions must be made or relaxed to produce accurate models of reasonable simplicity and flexibility. Information from actual combustion and gasification experiments will provide insight to the types of model alterations that are necessary.

C. Phenomenological Models

1. Characteristic Time Modeling

In addition to developing a PSR-PFR type model for gasification in entrained swirling flows, we hope to develop a model based upon a characteristic time approach. In characteristic time modeling, all physical phenomena that have a significant effect upon product composition are associated with appropriate time scales. The time scales are derived from readily identifiable reactor parameters, such as fuel composition, chemical reaction rates, pressure and fluid mechanic phenomena. Magnitudes of individual characteristic times are not nearly as important as ratios of times, since ratios rather than magnitudes are used to correlate experimental data. Rate-controlling steps can be readily identified by comparing the relative sizes of characteristic times.

According to Tuttle et al. (1976), Damköhler was one of the first investigators to use characteristic times in the analysis of combustion processes. Much of Damköhler's work applies only to homogeneous, premixed processes, but reaction and diffusion times identified by Damköhler may be applicable to heterogeneous processes such as coal gasification.

Tuttle et al. (1975) and Colket et al. (1977) successfully applied characteristic time modeling to the analysis of pollutant formation in gas turbine combustors. They identified droplet evaporation, air-fuel-burned gas mixing and chemical reaction as the dominant physical

processes influencing pollutant formation and combustor efficiency. Table I describes many of the characteristic times identified by Tuttle et al. (1976) and Colket et al. (1977).

The fuel droplet lifetime of Table I was derived from the "d^2 law" of Godsave (1953):

$$d_f^2 = d_o^2 - \beta_e t$$

where $d_f \equiv$ instantaneous fuel drop diameter
$d_o \equiv$ initial drop diameter
$\beta_e \equiv$ evaporation or combustion coefficient
$t \equiv$ time.

When d_f equals zero, the characteristic time for droplet evaporation has been reached and thus

$$\tau_{eb} = d_o^2/\beta_e \ .$$

This equation looks deceptively simple, since there is no uniform fuel droplet diameter and because β is a complicated function of many fuel properties that are difficult to determine for typical liquid hydrocarbon fuels. Colket et al. (1977) determined the sensitivity of τ_{eb} to errors in several important fuel properties and ambient conditions and found that relatively minor errors in those quantities could easily lead to errors of 20% or more in τ_{eb}. An accurate expression for coal particle lifetime may be even more difficult to determine because of the presence of ash, the lack of reliable kinetic data, reactions in the particle pores and the strong influence of local gaseous species.

Most of the fluid mechanic times identified by Tuttle et al. (1976) are ratios of turbulence scales to representative velocities. Note that since species mixing is the process of interest, a mixing time is chosen rather than a residence time. Several different mixing times may be required to specify all the processes of interest in a reactor.

Chemical reaction times identified by Tuttle et al. (1976) come from an Arrhenius-type expression in which the only operating

TABLE I

Examples of Important Characteristic Times

(Tuttle et al., 1976; Colket et al., 1977)

Time	Symbol	Physical or Chemical Process
Fuel droplet lifetime	τ_{eb}	Droplet evaporation or combustion
Fuel droplet flight time	τ_f	Particle flight over a characteristic distance
Eddy dissipation time in the region of the shear layer where CO is formed	$\tau_{sl,co}$	Large scale turbulent mixing between cold incoming air and hot, partially oxidized combustion products
Fuel ignition delay and burning time	τ_{hc}	Homogeneous, complete combustion of fuel
CO burnup time	τ_{co}	Homogeneous kinetics of CO oxidation

parameter is the temperature associated with the reaction of interest. Since they were interested in predicting pollutant emissions, they modeled times for NO_x formation and CO combustion. Chemical times for any reaction of interest could presumably be developed, however.

The characteristic times discussed above will all be important in modeling coal gasification in swirling entrained flow. A time analogous to τ_{eb}, the particle lifetime, will be of particular importance and will require an accurate model of coal particle devolatilization and subsequent char surface and pore reactions. The time required to devolatilize the incoming coal particle is expected to be very short in comparison to the total particle lifetime. In modeling pore reactions, a parameter similar to the Thiele modulus (Levenspiel, 1972) will be significant. The Thiele modulus is the ratio of chemical reaction rate to pore diffusion rate:

$$\phi_t = L_c\sqrt{k/D_m}$$

where $\phi_t \equiv$ Thiele modulus
$L_c \equiv$ a characteristic length
$k \equiv$ reaction rate coefficient (s^{-1})
$D_m \equiv$ molecular diffusion coefficient.

We propose to use swirl to create separate oxidation (combustion) and reduction (gasification) zones within each of our reactors. We expect the amount of time a particle spends in each zone to be a significant fluid mechanic characteristic time. These residence times will be difficult to represent in terms of simple reactor parameters since swirling, entrained flows are inherently complicated and because a clear division between oxidation and reduction zones will probably not be possible.

Chemical reaction times are expected to be numerous and complicated. Reactions in the gas phase, on the particle surface and within pores will all be going on simultaneously. Since char reactivity varies greatly among different varieties of coal and depends upon the thermal history of the particle, it may be difficult to arrive at reaction times that are suitable for a wide variety of coals.

Tuttle et al. (1976) and Colket et al. (1977) found that many of their correlating parameters were ratios of chemical reaction times

to fluid mechanic times. We expect correlating parameters for gasification to be of the same form. However, since some of the product gas constituents, particularly carbon monoxide, are formed in more than one reaction, sums and differences of ratios will probably be needed to generate effective correlating parameters.

In summary, characteristic time modeling is an approach that occupies the middle ground between models based on the fundamental conservation equations and models that employ a global, highly empirical approach. Since the characteristic times are derived from an analysis of the dominant physical processes in the reactor and are calculated from sensibly chosen reactor parameters, accurate predictions of product gas composition can often be made. Judicious selection of the dominant physical processes and accurate representation of these processes is the key to successful characteristic time modeling.

2. Two Phase Flow Model

An interesting and fruitful study of two phase flow in a swirling coal combustor-gasifier was recently published by Lewellen et al. (1977). Four basic performance parameters reflecting carbon efficiency, ash separation, combustor pressure drop and heat loss rate were developed as functions of several fundamental reactor parameters. Particle combustion, fluid mechanical and particle mechanical effects were included in the model and were derived from first principles as much as possible, at which point empirical correlations and simplifying approximations were imposed. Results of the model compare favorably with experimental data taken by the Pittsburgh Energy Research Center.

Lewellen et al. (1977) cite four regions of interest within their combustor and identify the dominant physical processes in each. Figure 5 shows the four regions of interest and the fluid and particle flow lines through each. Region I includes the boundary layer at the reactor walls and is perhaps the most important of the four regions. It is characterized by high particle concentration, high heat release rate and fluid-particle-wall interactions. Particles tend to remain in region I because centrifugal forces dominate over the radial pressure gradient

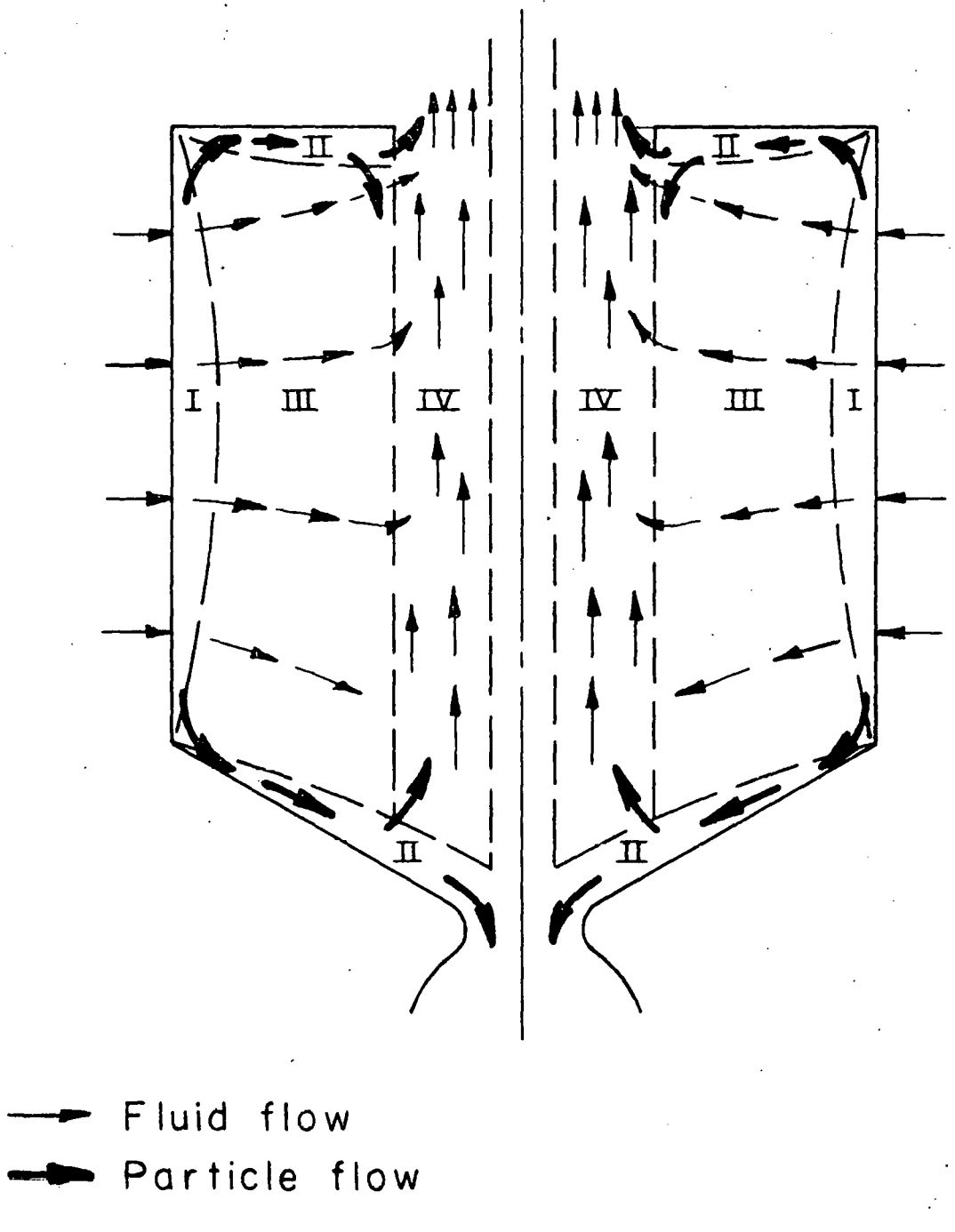

Figure 5. Flow Regions in Combustion Chamber

created by the swirling flow. Thus, virtually all the coal particles (except those that escape through region II) burn to completion in region I.

Region II consists of the boundary layer at the top and bottom of the reactor and is characterized by low tangential velocities due to frictional effects. The radial pressure gradient dominates and particles pass toward the center of the combustor through this region.

Regions III and IV dominate the internal combustor volume. Region III is an area of rapidly swirling gases that are only slightly particle laden. Regions III and IV are nearly isothermal since very little combustion takes place in them. In region IV the fluid velocity is primarily axial as the gases flow toward the combustor discharge.

It is interesting to note that many of the performance parameters developed by Lewellen et al. (1977) take the form of residence times and other characteristic times. Most of their times are derived such that direct comparisons can be made among them. The use of characteristic times by Lewellen et al. (1977) in modeling a swirling coal combustor lends credence to our belief that characteristic times will be useful correlating parameters in the analysis of coal gasification systems.

D. Microscopic Models

A very ambitious modeling approach being pursued by a few investigators attempts to describe the entrained gasification process in terms of the basic conservation equations supplemented by certain phenomenological relationships. Smoot and Hanks (1976) are developing a model based on the macroscopic form of the general conservation equations for a finite volume element within the gasifier. Their model includes the following aspects of the gasification process (Smoot and Hanks, 1976):

(1) mixing of primary and secondary streams
(2) recirculation of reacted products
(3) pyrolysis and swelling of coal
(4) oxidation of the char by oxygen, steam and carbon dioxide
(5) heat transfer between the coal/char particles and gases

(6) variation in composition of inlet gases and solids
(7) variation in coal/char particle size
(8) oxidation of the hydrocarbons produced from coal pyrolysis.

The rates of primary/secondary mixing and hot gas recirculation are particularly difficult to model accurately. Smoot and Hanks (1976) are using a combination of recently developed numerical techniques to form a comprehensive model that is applicable to entrained gasification processes.

Blake (1977) is developing models for both entrained flow and fluidized bed gasification based upon mass, momentum and energy conservation. The entrained flow model consists of a field description of steady, solid-gas flow in two dimensions. Both finite element and finite difference modeling techniques are being explored. The turbulent nature of the flowing stream is included, along with convective mixing effects. The presence of reacting solids and their interactions with the gas phase greatly complicate the formulation of the conservation equations. Blake (1977) also relies on a great number of phenomenological relationships to describe particle and gas properties, heat transfer and chemical phenomena.

III. GASIFICATION FACILITY

A. Test Cell

Test cell flow, control and data monitoring systems are nearly complete and have been tested extensively during the past six months. The air and nitrogen systems have been hydrostatically tested and have performed satisfactorily during several test runs. New flow meters were designed and calibrated and are now in service. A forty point temperature monitoring station has been installed and tested and is currently in use. The interlock system and all power wiring except for the steam heater wiring are installed and in service and all control panels are complete and in service. The coal feeder has been calibrated and modified to permit remote monitoring and operation. The exhaust system is installed and operational. The boiler has been installed in a concrete block building erected for that purpose. Power wiring to the boiler has been installed.

1. Air and Nitrogen Systems

Figure 6 is a schematic showing the air, nitrogen, steam and methane systems. Following extensive leak testing and a few modifications, the air, nitrogen and methane systems were put into service. The primary air and secondary air controllers were moved to a location downstream of the flow meters, allowing the meters to operate at a more nearly constant pressure. The flow meters from Thermal Instrument Company were returned to the manufacturer, and orifice meters are being used in their place. Metering devices have also been installed on the methane and ignition air lines, and methane and ignition air flow control valves have been relocated to permit operation from the control room. Bleed valves have been installed on the air and nitrogen manifolds.

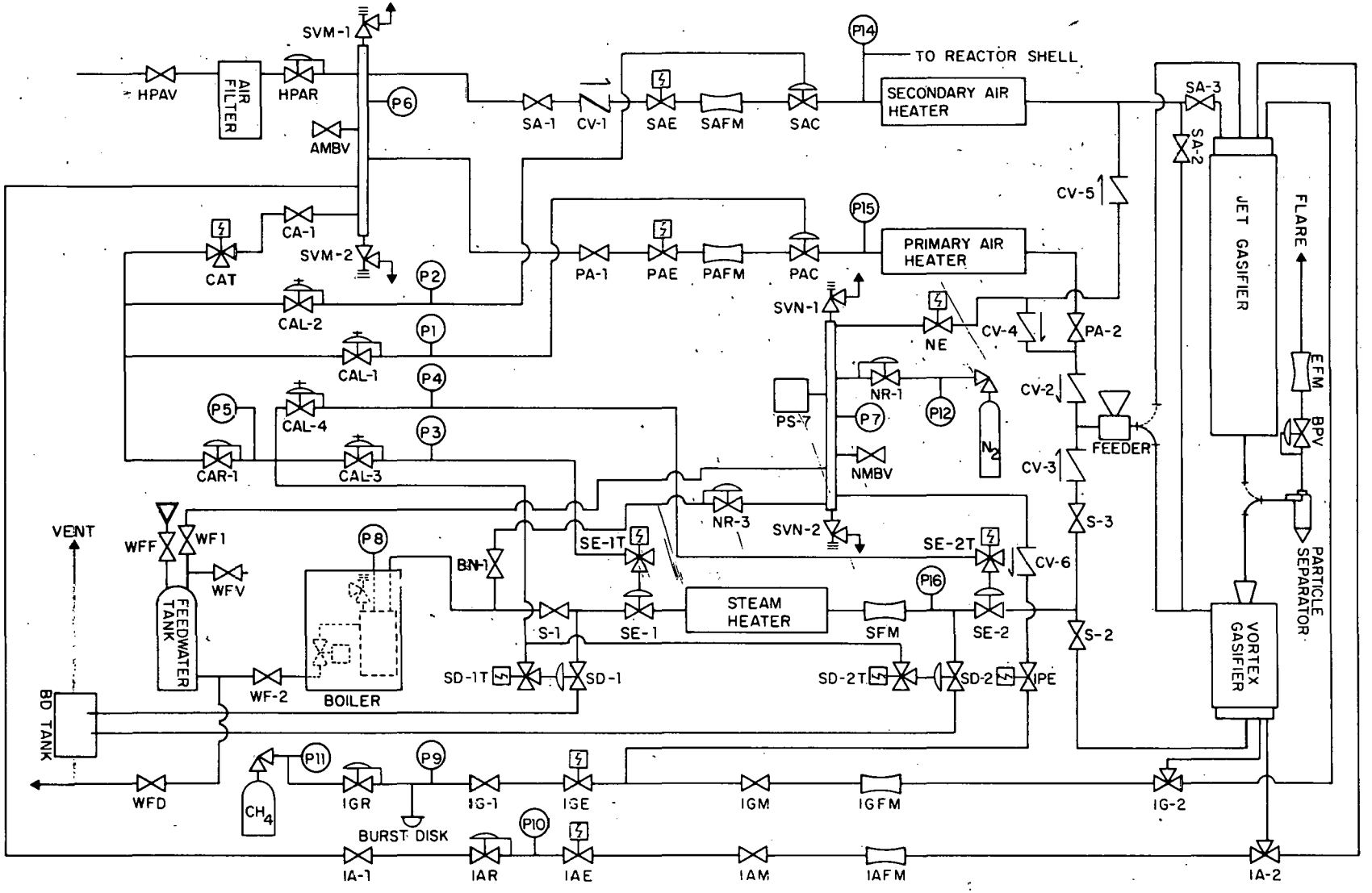

Figure 6. Flow System Schematic

2. Flow Metering and Temperature Measurement

Flow metering devices from Thermal Instrument Company for measuring primary and secondary air and steam were found to be unacceptable and have been returned to the manufacturer. Several weeks were spent trying to calibrate the meters with consistently poor results. To replace the Thermal Instrument meters, we have designed, fabricated and calibrated orifice meters for primary and secondary air. A steam meter will be made in the near future. Figure 7 is a schematic of the primary and secondary air metering systems showing the orifices and the data monitoring devices. Solid state pressure transducers will eventually replace the manometers and the pressure gages, making data acquisition easier and more precise.

Interchangeable low and high range secondary air orifices were required to stay within the sixty inch range of the secondary air manometer and still provide good readability at low flow rates. A single orifice was sufficient to cover the anticipated range of flow for the primary air. All three orifices are made of stainless steel and are made to ASME specifications. Mounting flanges with integral pressure taps were designed to provide easy access to the plates. Table II lists important dimensions and anticipated flow rate ranges for each orifice.

The primary air orifice and both secondary air orifices were calibrated against standard ASME orifices whose discharge coefficients as functions of Reynolds number are known. A computer program was used to reduce the experimental data, yielding a tabulation of discharge coefficient versus Reynolds number for each orifice tested. Figure 8 shows the calibration curves for the primary, low range secondary and high range secondary air orifices. The discharge coefficient, K, is a factor which accounts for the area reduction and for viscous effects which cause the flow rate to be less than that predicted by the inviscid form of the Bernoulli equation. Thus K is a function of orifice to tube diameter ratio and Reynolds number. We intend to use the indicated average values for discharge coefficient for determining all mass flow rates. Each of the three orifice meters was calibrated with two different reference flow meters, and data points for both calibrations are shown for each orifice meter in Fig. 8. Most of the scatter near the low end

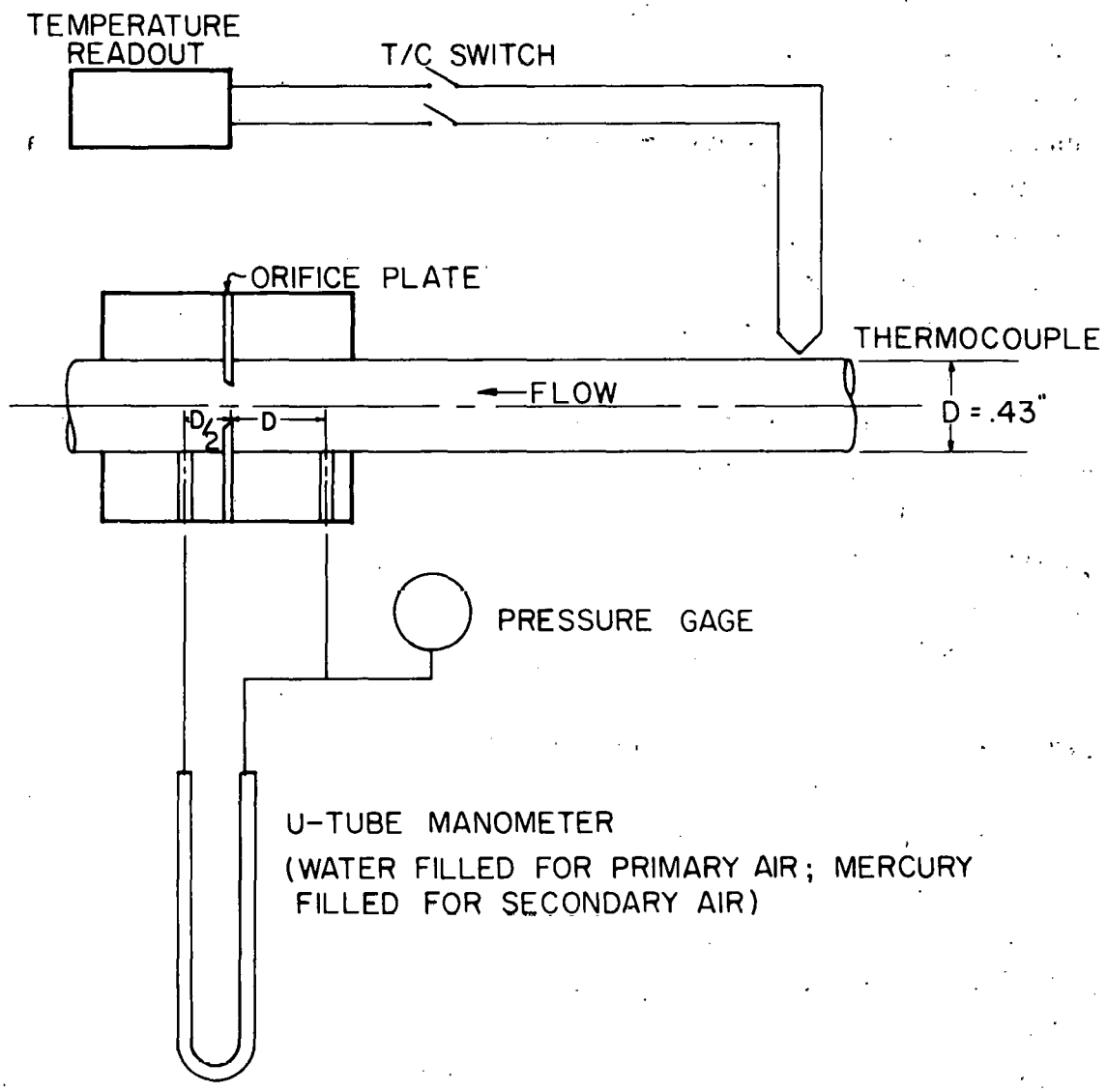

Figure 7. Primary and Secondary Air Metering Systems

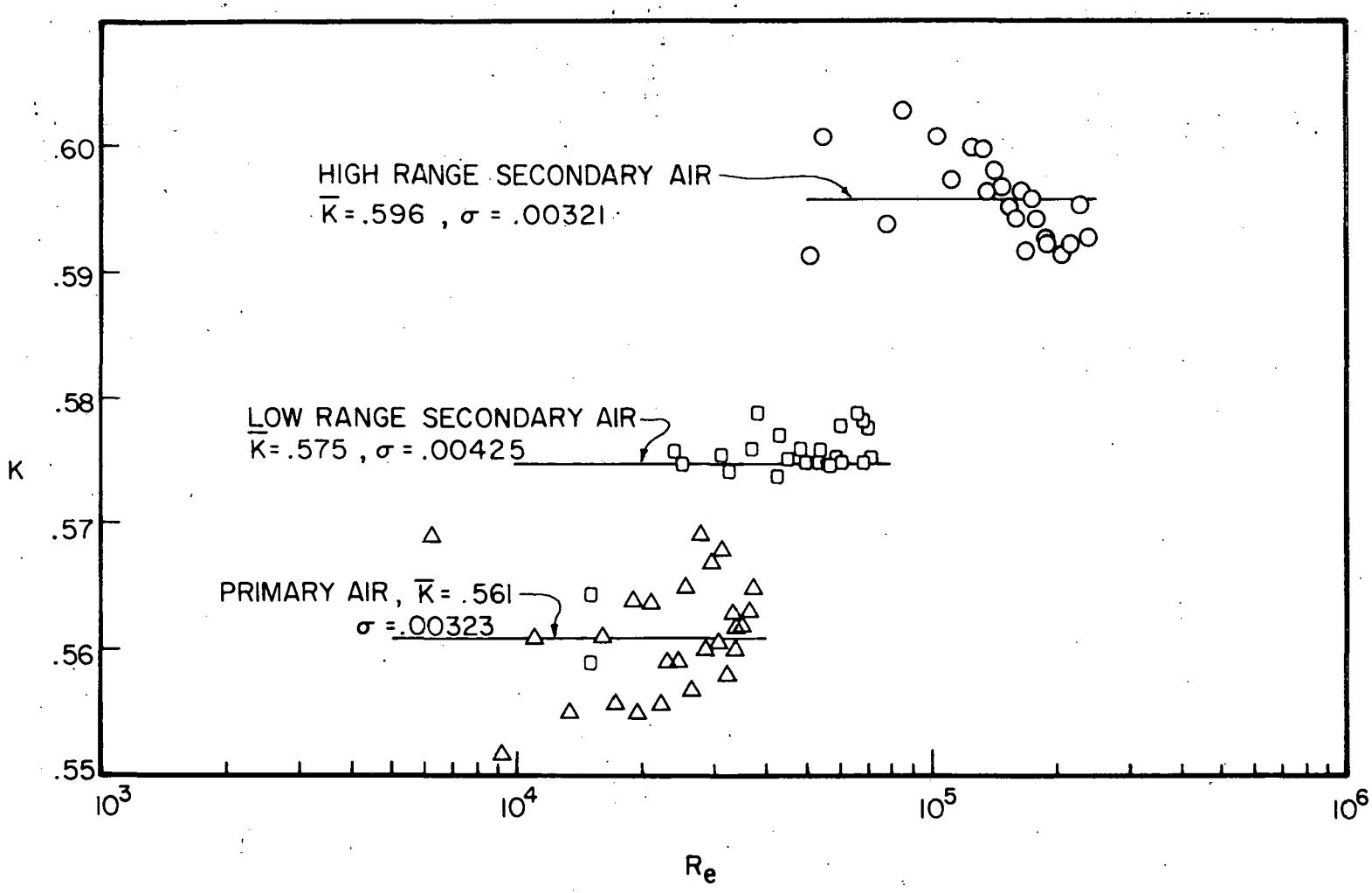

Figure 8. Primary and Secondary Air Orifice Meter Calibration Curves

of the scale on each plot was due to marginal readability of the manometers at very low flow rates. We expect this problem to be eliminated when the solid state pressure transducers are installed.

TABLE II

Orifice Dimensions and Flow Ranges

Orifice	Orifice Diameter, in.	Tube Diameter, in.	Flow Range, lb/hr.
Primary	.161	.43	14 - 50
Low range secondary	.113	.43	20 - 90
High range secondary	.209	.43	90 - 310

Thermocouples are being used to provide temperatures of reactant and product streams, structural and insulating components and to provide feedback to heater controllers. A total of 46 thermocouples have been installed, six of which provide temperature feedback to heater controllers. The other thermocouples are connected to a 40 position switch (Omega Engineering model no. OSW5-40). Temperature readout is provided by an Omega model 175KC1 digital readout device which includes an electronic ice point and has a range from -180°C to 1260°C. A sixteen point strip chart recorder and two single point recorders are also available to indicate trends and fluctuations in temperatures.

3. Interlock System

The interlock system is complete to a point that permits safe operation of the cyclone reactor during methane combustion runs. All control relays and switches are installed and operational, and all but three safety interlocks have been installed. These three are the loss of air flow, loss of flame in the reactor and loss of coal feed interlocks. Air flow and reactor flame are currently being closely monitored with data acquisition equipment. We expect to have all interlocks operational before coal combustion runs are commenced.

4. Power Wiring

Power wiring for the primary and secondary air heaters and the cyclone reactor heaters is installed and in service. All temperature controllers are also installed and in working order. Wiring of the coal feeder and steam heaters will be completed when the equipment is installed. All power wiring and conduit is installed according to National Electrical Code and Combustion Laboratory safety requirements.

5. Coal Feeder

The Vibra Screw coal feeder has been calibrated and fitted with remote monitoring and control devices. Section IV:A contains details of the calibration results, and Fig. 19 is a schematic of the control and monitoring devices. A stand for the coal feeder has been fabricated, and the feeder itself will be moved into the test cell shortly after methane combustion runs have been completed.

6. Exhaust System

The exhaust system has been designed and fabricated and is in service. The line is cooled by a water jacket to maintain temperatures at the particle separator at less than 250°F due to material limitations. An ASME standard orifice is located downstream of the particle separator to provide an indication of the make gas flow rate. A backpressure valve will be installed in the line prior to high pressure gasification tests.

7. Steam System

As noted previously, a concrete block building was erected behind the test cell for the purpose of housing the boiler. The boiler is installed and power wiring for it has been pulled and connected. Our work bench and a utility cabinet have also been moved to this building to make more room in the test cell. The feedwater tank and the remainder of the steam piping system will be installed shortly after coal combustion runs have been initiated.

B. Cyclone Reactor Design

1. Reactor Sizing

Reactor size is influenced by the cyclone geometric parameters and coal throughput (lbm coal/hr·ft^3). Residence time, although important, is not an independent consideration; both gas and particle residence times are indirectly related to coal throughput.

Geometric parameters for cyclone chambers are reviewed elsewhere (Lenzer, 1976). Table III lists the geometric design parameters for our cyclone reactor. These can be modified later to improve high pressure operation. Coal throughput was the most influential consideration in the sizing process. A successful design objective is the ability to operate at throughputs similar to those achieved in both industrial and pilot plant gasifiers without exceeding coal feed rates of 40 lbm/hr. Surface area heat release rates of 3.5×10^5 BTU/hr·ft^2 (the same order of magnitude as industrial scale) can also be achieved at coal feeds under 40 lbm/hr (assuming a coal heating value of 12000 BTU/lbm) in 5 to 6 inch diameter reactors with L/D = 1.67.

TABLE III

Geometric Design Parameters for the Cyclone Reactor

Swirl number, S	17.5
Length/diameter ratio, L/D	1.67
Throat/cyclone diameter ratio, D_t/D	0.417
Number of tangential nozzles, N	4
Total nozzle/throat area ratio, A_n/A_t	0.137

Due to the reduction in throughput at increased reactor volume, cyclones with diameters larger than 6 inches were eliminated from consideration. The increased flow disturbance due to sampling probe insertion in a smaller diameter cyclone precluded further increases in throughput capability. Consequently, a 6 inch diameter, 10 inch long cyclone was selected. At high pressures, however, a smaller chamber (or higher coal feed rate) may become desirable.

2. Reactor Heat Transfer

Heat transfer calculations were performed to determine thermal losses and to aid the materials selection process. Heat loss estimates are imperative due to the high surface to volume ratio of laboratory cyclones. Temperature profiles of the reactor assembly under various operating conditions help determine the type and amount of refractory and insulation. These calculations formed the basis for heating element selection and pressure vessel design.

Heat transfer calculations were based on the following assumptions: (1) steady state, (2) one-dimensional conductive heat transfer, (3) isothermal refractory surfaces and (4) negligible radiative heat transfer. One dimensional heat transfer calculations were made in both radial and axial directions, and then summed. A first set of calculations was made for inner refractory wall surface temperatures ranging from 1000 to 3000°F. To compensate for two dimensional effects, a second set of calculations was made for outer refractory wall surface temperatures over the same temperature range.

3. Reactor Construction

The reactor assembly is shown in Figure 9. Major aspects of this design are high pressure gasification, a symmetric reactant inlet arrangement, separate combustion and gasification zones promoted by independent steam injection, slagging operation and the use of air with no oxygen enrichment. While various combinations of these features have been previously employed by others, the incorporation of all of them is apparently unique. Details of the assembly are discussed in the following sections.

3.1 Pressure Vessel. The pressure vessel has been designed in accordance with the ASME Boiler and Pressure Code to operate at 300 psi (20 atm). It is fabricated from a 30 inch length of 24 inch schedule 20 seamless pipe, A-53 grade B carbon steel (Mutual Pipe and Supply Co., Inc., Indianapolis, Ind.). A 3 inch A-36 circular steel plate forms a flat head at the bottom. At the top, a blind flange and an asbestos gasket are bolted to a class 300 carbon steel slip-on flange

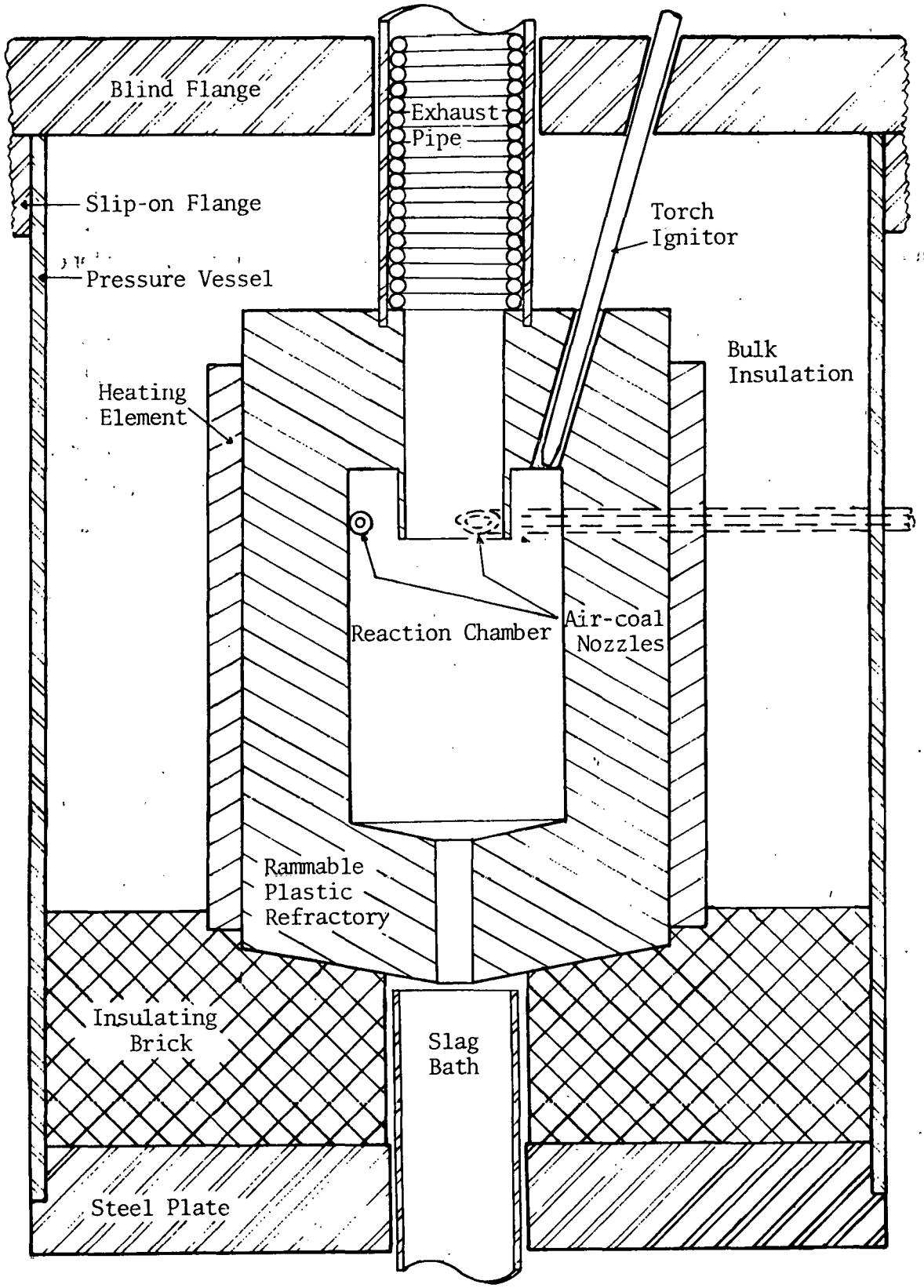

Figure 9. Cyclone Reactor Assembly

(Mutual Pipe and Supply Co., Inc.). A 3/16 inch blind flange is used for atmospheric operation; at high pressure, a class 300 blind flange is used (Mutual Pipe and Supply Co., Inc.).

3.2 Reactor Materials. The wall and ends of the cyclone are formed from four molded cylinders of Jade-Pak-88-P rammable plastic refractory (A. P. Green Refractories Co., Mexico, Mo.). This material resists attack by slag and can withstand temperatures as high as 3400°F (2140°K). Satanite slag resistant mortar (A. P. Green Refractories Co.) was used to cement the cylinders together. The cyclone wall is 3 inches thick; the roof and floor are approximately 4.5 inches deep. A 1 inch diameter hole in the refractory floor permits slag removal. Unexpected swelling of the refractory during curing resulted in an internal reaction zone height approximately 3/4 inch in excess of the planned 10 inches.

A 6 inch long, 2.5 inch inner diameter mullite tube (McDanel Refractory Porcelain Co., Beaver Falls, Pa.) extends 2 inches into the reaction zone from the cyclone roof. The tube, which helps center the vortex and minimizes short circuit flow in the cyclone, is secured to the refractory roof with Sauereisen Electrical Refractory Cement No. 75 (Sauereisen Cements Co., Pittsburgh, Pa.).

The floor of the cyclone is supported and insulated by two layers of G-23 Insulating Firebrick (A. P. Green Refractories Co.). The side and top of the reactor are insulated with Kaowool bulk fiber (Babcock and Wilcox Co., Oak Brook, Ill.).

3.3 Torch Ignitor. A stainless steel torch ignitor (Fig. 10) for coal ignition and final refractory preheating fires downward from the annulus at the reactor roof. Unmixed air and methane flow through the inner and outer tubes, respectively. A 0.050 inch diameter tungsten electrode, electrically insulated by a 0.125 inch outer diameter mullite tube (McDanel Refractory Porcelain Co.), extends the ignitor length to provide a 5000 Vac continuous spark at the ignitor tip.

3.4 Air/Coal Nozzles. Upstream of the reactor, the primary air/coal and secondary air flows are each split into four reactant streams Air and pulverized coal then enter the reactor through four coplanar

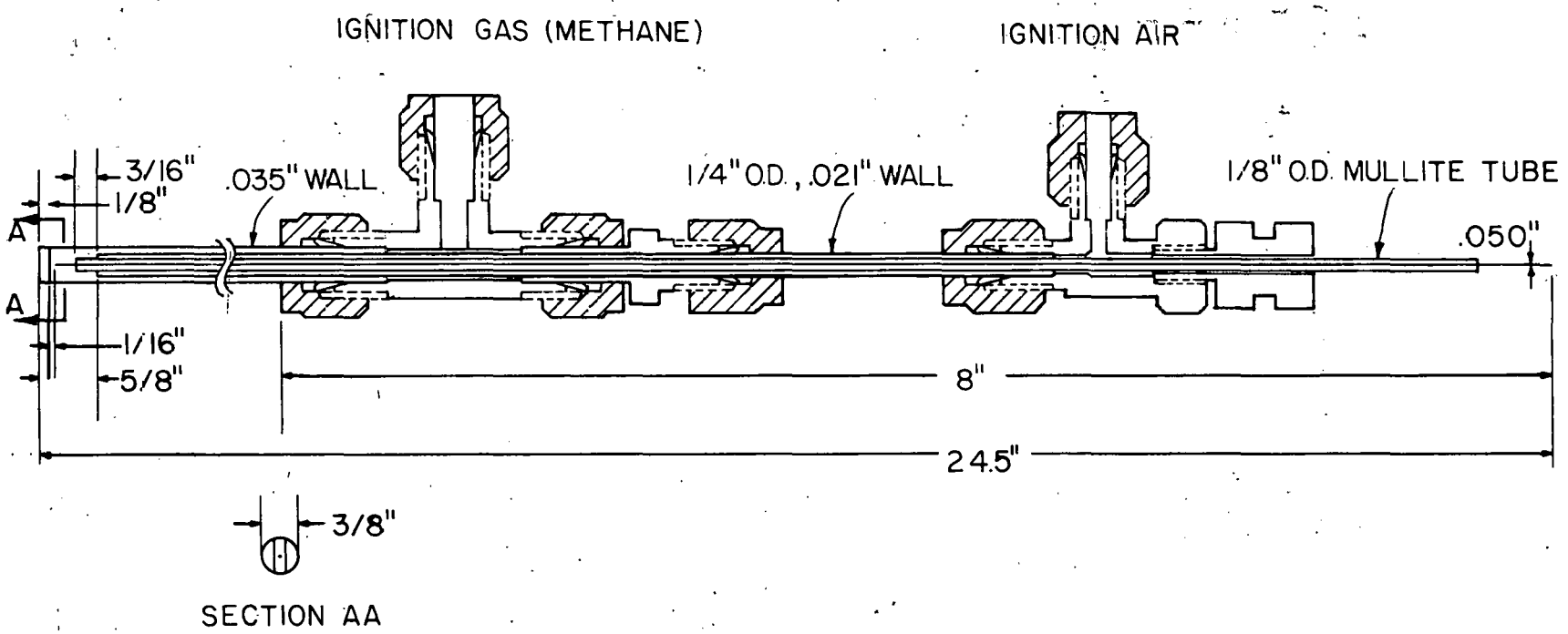

Figure 10. Cyclone Torch Ignitor

tangential nozzles near the cyclone roof. The nozzles are sealed to the refractory wall with Sauereisen Cement No. 75. Each nozzle has a concentric tubing arrangement; primary air and coal are injected through the inner tube, secondary air through the outer tube. Entrance velocities will range from 100 to 300 ft/sec for primary air/coal and from 30 to 500 ft/sec for secondary air.

3.5 Steam Injection. Steam for gasification will be injected to the core of the cyclone by one of two possible injection arrangements: (1) by a steam cooled stainless steel replacement for the 2.5 inch diameter mullite tube described earlier, or (2) by an injection tube near the refractory floor. This separate injection of air/fuel and steam, coupled with cyclone flow characteristics, should establish two zones of reaction within a single reactor stage: exothermic combustion reactions in the annular zone and endothermic gasification reactions in the core.

3.6 Slag Quench Bath. The slag quench bath consists of a seamless 4 inch schedule 40, A-53 grade B vertical steel pipe (Mutual Pipe and Supply Co., Inc.) closed at the bottom by a 3000 psi forged steel pipe cap (Mutual Pipe and Supply Co., Inc.). The pipe is threaded into a 3000 psi forged steel half coupling (Mutual Pipe and Supply Co., Inc.) which has been welded to the bottom of the pressure vessel. A 3 inch diameter stainless steel tube welded to the pipe extends upward to the exit of the slag tap. Currently, water replenishment is a batch operation; a more sophisticated system is being considered.

3.7 Reactor Cooling Coil. Product gas leaving the reaction zone is immediately cooled by a system consisting of a 10 inch long, 4 inch diameter stainless steel tube lined with a water conducting coil of 1/2 inch diameter stainless steel tubing. A flange at the base of this assembly is secured to the refractory roof with Sauereisen Cement No. 75, thus providing a seal. At the top of the pressure vessel, high temperature packing seals the 4 inch stainless tube to a 3000 psi forged steel half coupling (Mutual Pipe and Supply Co., Inc.).

3.8 Sampling Probe and Observation Window. From the pressure vessel, reaction products flow through a 1 foot length of 4 inch schedule 40 stainless steel pipe (Mutual Pipe and Supply Co., Inc.) to a reducing tee where they enter the water jacketed make gas cooling system. A 4 inch 3000 psi forged steel pipe cap (Mutual Pipe and Supply Co., Inc.) threads onto the tee and supports the sampling probe and observation window. The water cooled sampling probe consists of a triple walled stainless steel tubing arrangement which extends downward to a point slightly above the cooling coil. The window is a 1 inch diameter, 1/2 inch thick quartz disk. A small mirror positioned above the observation window permits monitoring of combustion activity from the control room.

3.9 Overpressure System. A simple overpressure system has been developed to prevent leakage of reactants and products from the reaction zone to the insulated portion of the pressure vessel. Pressure in this void volume is raised to secondary air static pressure via a 1/4 inch stainless steel tube. In addition to preventing leakage, this system protects the refractory by equalizing internal and external pressures. The cyclone vessel pressure gage is incorporated into this system.

3.10 Heating Elements. Four quarter-cylindrical electric heating elements (Electro-Applications, Inc., Canonsburg, Pa.) which enclose the refractory wall provide preheat capability and minimize wall heat losses. These elements, 16 inches long, extend beyond the chamber end walls to promote a flat temperature profile in the reaction zone. The elements are slotted to permit passage of the air/coal nozzles.

The heating elements operate between two phases of the 240 Vac three phase system. Power leads penetrate the vessel via two electrical conductor sealing glands (Conax Corporation, Buffalo, N. Y.). Maximum allowable element temperature is 1200°C; total heating capability is 8 kW.

3.11 Thermocouples. An extensive thermocouple system provides reactant and product temperatures, critical material temperatures, and feedback for temperature controllers. Within the cyclone pressure

vessel, nine inconel sheathed chromel-alumel thermocouples (Omega Engineering, Inc.) serve the following functions: two provide feedback to the reactor heater temperature controller; five, located at the ends and seams of the refractory cylinders, provide a profile of refractory temperature; one measures product gas temperature; and another remains as a spare. Eight of these thermocouples, all 1/16 inch in diameter, enter the pressure vessel through a multi-hole packing gland (Conax Corporation). A single hole packing gland (Conax Corporation) facilitates replacement of the 1/8 inch diameter product gas thermocouple should it fail due to severe conditions in the product stream.

C. Jet Gasifier Design

The reactor is designed to demonstrate, on a laboratory scale, that the fluid mechanical properties of a swirling jet can be used to enhance performance and control of a coal gasification reactor. Major reactor variables (inlet velocities, confinement ratio, etc.) can be varied independently to assist in characterizing their effects. This procedure will elucidate those areas of existing burner technology which can be directly applied to gasification, and indicate new directions for areas in which simple extrapolations are not possible. The reactor is designed to combust coal initially; after combustion has been stabilized and investigated, the reactor will be shifted to gasification. Combustion of other fuels such as oil, char or low BTU gas could be studied in the reactor with appropriate injector modifications.

Figures 11 and 12 show the general layout and dimensions of the reactor. Reactor sizing was based on an upper limit of 28 lbm coal/hr and combustion at 20% excess air. A four to one turn-down ratio should be possible without reactor modifications. Higher feed rates will be possible under pressure operation, and for gasification at atmospheric pressure.

Reactor design began with the primary air injector. As each successive component was designed, it was checked to insure that sufficient flexibility was available to allow for the reduced mass flow rates of gasification. Since vertical firing was selected to avoid coal settling, a reactor which could be tilted for maintainance and probe insertion was required to avoid the length limitations exerted by the test cell ceiling height.

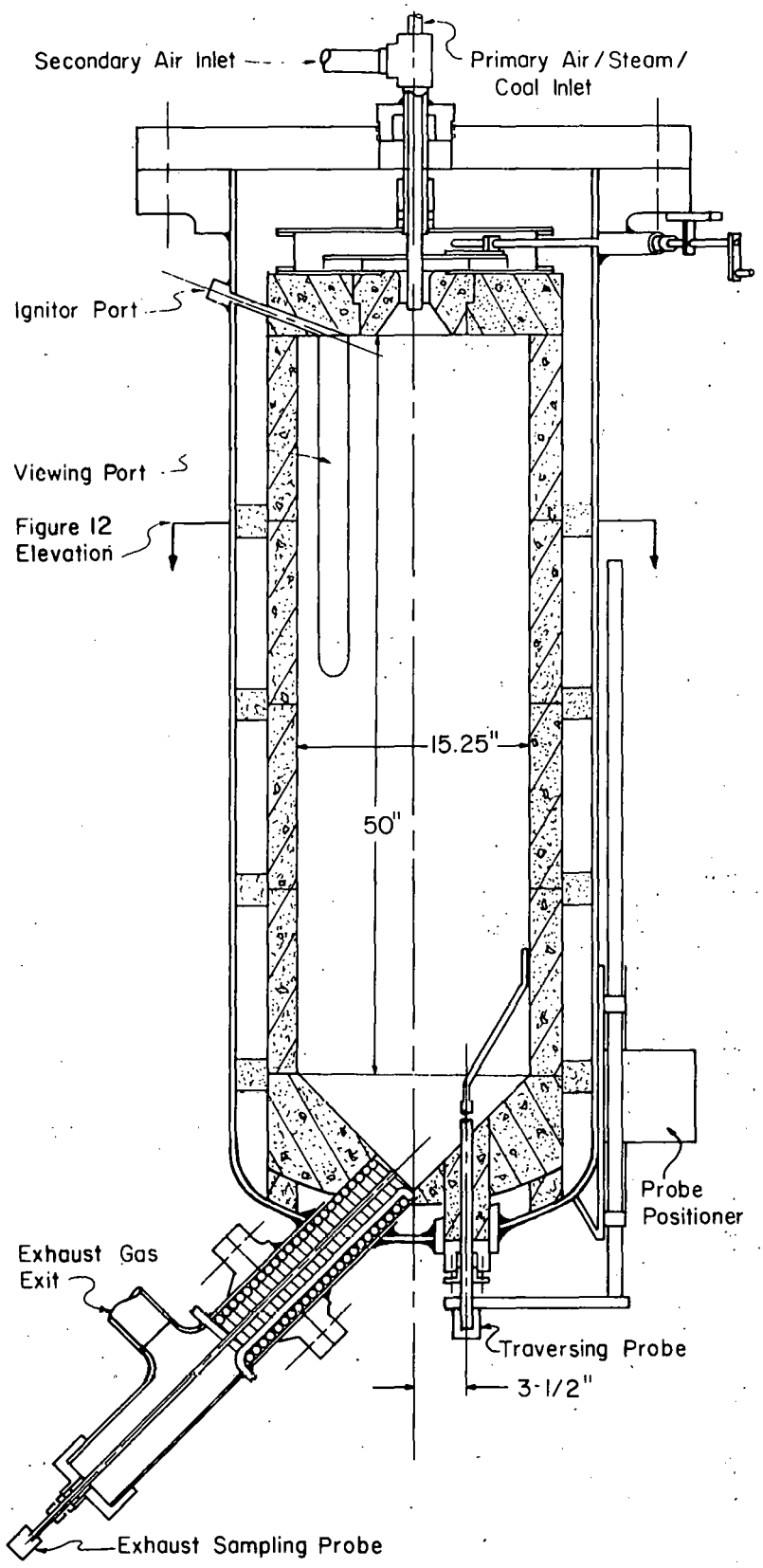

Figure 11. General Layout of the Jet Reactor

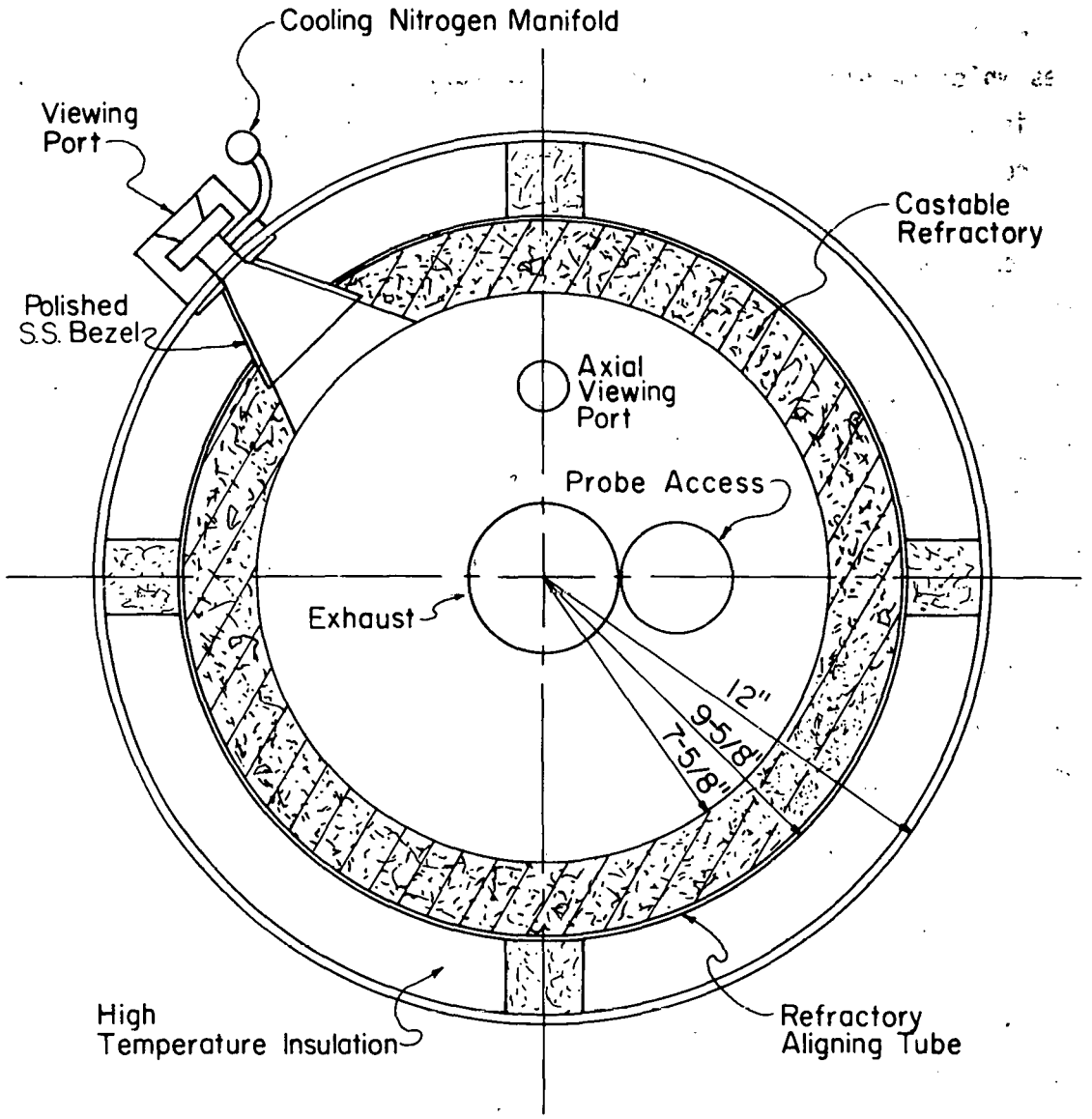

Figure 12. Cross-section of the Jet Reactor

1. Primary Injector

By controlling the axial and radial velocities of the primary stream, the primary injector can alter flame shapes (Heap et al., 1973) and govern mixing with the secondary stream. Ideally, the primary injector should have the capability of directing the primary stream and controlling its velocity with a minimum of "bluff body" effects. The recirculation zones which develop behind bluff bodies frequently cause soot deposition on injectors. With swirl, geometrically induced recirculation is not required and should be avoided.

Figure 13 shows the primary injector which will be used in the gasifier. Unlike many other lab scale injectors, it does not have significant bluff body effects, yet it provides axisymmetric flow with varying amounts of radial momentum. This injector is patterned after the concentric ring arrangement suggested by Babcock and Wilcox (1963). Table IV gives the axial velocities for three different configurations and indicates operating conditions where they will be useful.

The size of the outer tube of the injector can be varied by reducing the size of the swagelok adaptors and pressing a sleeve over the smaller tube to seal against the adapter plate at the top of the swirl generator (see Fig. 14). Changing the primary configuration will require approximately 4 hours of reactor down time, since the reactor must be tilted to provide sufficient head room to remove the primary tube.

2. Secondary Air Throat

As shown in Fig. 11, the secondary air throat and the divergent quarl are cast into a removable section of refractory in the upper chamber end wall. Changing the secondary velocity can be accomplished by changing throat blocks, secondary air temperature, or primary to secondary air ratio. Changing the divergent angle will require changing blocks.

For combustion, the secondary air throat will be 2 inches in diameter. Velocities will be less than 125 ft/sec, as recommended by Babcock and Wilcox (1963). Divergents with an included angle of 90° or less and a length/throat diameter ratio of unity can be incorporated into the block. Initially an included angle of 70° will be used as recommended by Beer and Chigier (1972).

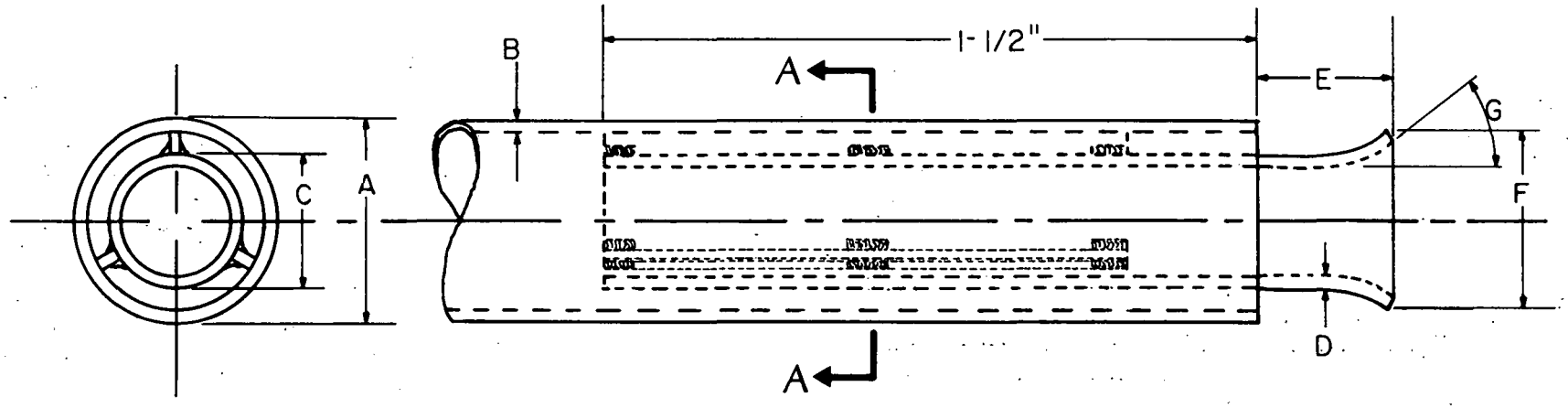

Section AA

Injector No.	A∓	B	C	D	E	F	G
P-1	0.750	0.035	0.500	0.035	0.50	0.688	37°
P-2	0.750	0.065	N.A.	N.A.	N.A.	N.A.	N.A.
P-3	0.500	0.035	0.250	0.035	*	*	*
P-4	0.375	0.035	0.250	0.035	*	*	*

∓ All dimensions in inches
* Not yet determined

Figure 13. Jet Primary Injector

TABLE IV

Primary Stream Velocities (ft/sec)
at Atmospheric Pressure*

Flow Rates (lbm hr)			Injector Type**		
Coal	Air[a]	Steam	P-1 or P-2	P-3	P-4
7	15	--	33.1	90.1	≠
20	30	--	66.3	180.1	≠
20	45	--	99.4	≠	≠
20	60	--	132.6	≠	≠
28	42	--	92.8	≠	≠
7	--	2[b]	≠	42.7	102.6
14	--	10[b]	76.5	≠	≠
28	--	20[b]	153.1	≠	≠
7	--	2[c]	≠	30.8	74.5
14	--	10[c]	55.4	154.4	≠

* Recommended minimum velocity is 35 ft/sec for down firing (Babcock & Wilcox, 1963)
** See Figure B

[a] Velocities based on 660°R(ρ = 0.06013 lbm/ft^3)
[b] Velocities based on 1460°R(ρ = 0.01691 lbm/ft^3)
[c] Velocities based on 1060°R(ρ = 0.02333 lbm/ft^3)
≠ Injector not used for these conditions

Exchanging nozzle blocks will require 2 days of reactor down time. The blocks are designed to slip quickly into place, but lowering the reactor and removing the top closure will be required for each block change. For initial atmospheric runs before internal probing is required, the reactor will be left in the lowered position with a light top closure. This will reduce the exchange time and experience gained in early runs should reduce the number of changes necessary for "up position" pressurized runs.

3. Swirl Generator

The key to performance of the gasifier is swirl. The swirl number (see Chapter I) has been shown to effectively characterize swirling flames (Kerr and Fraser, 1965; Beer and Chigier, 1972; Syred and Beer, 1974). Swirl should therefore be both easily variable and precisely determined. The moving block swirl generator developed by Leuckel at IJmuiden can provide continuously variable swirl and the position of the blocks correlates well with swirl number (Beer and Chigier, 1972; Grant et al., 1977). Figure 14 shows the movable block swirl generator for the gasifier.

As noted by Grant et al. (1977), primary velocity has a significant effect on the swirl number for some conditions. In gasification, primary flows may be as high as 30% of the total mass flow. Hence, total swirl number (S_t) must include both primary and secondary flows; the secondary swirl number (S_s) (commonly used for characterizing industrial units) is not adequate. Both total and secondary swirl numbers can be correlated with swirl generator block position, although additional flow information is required for the total swirl number. In both cases, the velocity through the swirl generator does not enter explicitly, so one swirl generator will be useful for all flows and pressures. Swirl numbers are correlated by (Appendix A):

$$S_t = \frac{\sigma A_e A_p \rho_a}{2\pi BR[\rho_a A_p + \rho_s A_e(1 + f)\langle\psi^2\rangle]}$$

$$S_s = \frac{\sigma A_e}{2\pi BR}$$

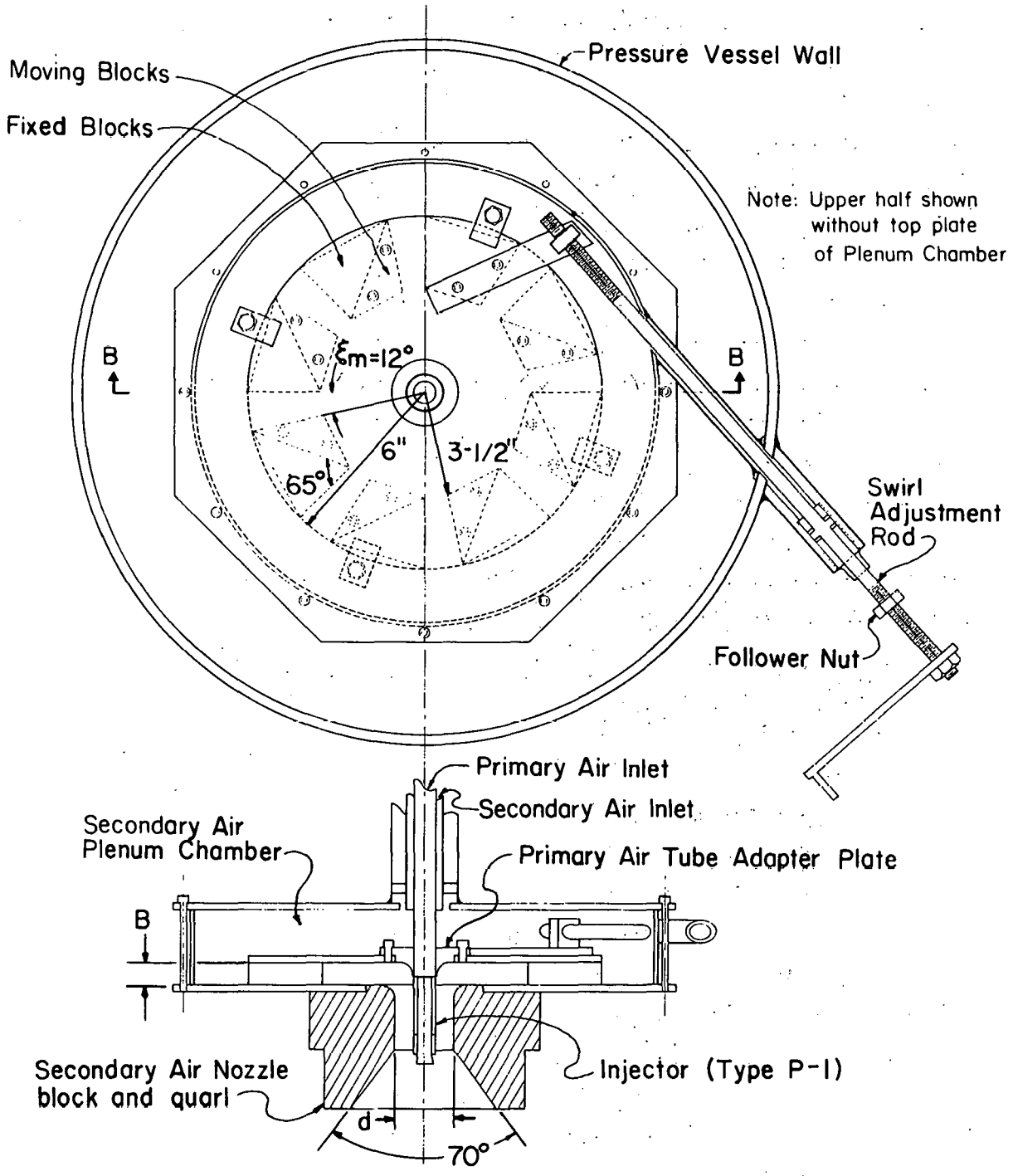

SECTION BB

Figure 14. Moving Block Swirl Generator

where

$$\alpha = \frac{\pi \tan \frac{\xi}{2} \cos \left[\alpha - \frac{\xi}{2}\right] \sin \alpha}{Z\left[\tan \frac{\xi}{2} \cos \left(\alpha - \frac{\xi}{2}\right) + \sin \left[\frac{\xi_m - \xi}{2}\right]\right]^2} \quad ;$$

f and ψ are the mass flow ratios of coal to primary air and primary air to secondary air, respectively. A_e is the secondary throat area, A_p the primary injector area, ρ_a the density of the primary air excluding coal and ρ_s the secondary air density; the remaining variables are geometric parameters defined by Fig. 27 in Appendix A.

The swirl blocks were designed with a larger block angle (α) than the original IJmuiden generator to insure that recirculating flows will be available under gasification conditions. The swirl generator is capable of total swirl numbers in excess of 1.0 for all combustion and gasification conditions expected. Much higher swirl numbers will be possible under combustion conditions where the primary momentum is small with respect to the secondary momentum.

The position of the swirl blocks is varied by a rod passing through the reactor shell. The rod and positioning nut have fine threads to insure precise placement of the swirl block. The swirl block position is determined by the location of a follower nut on the outside of the vessel. The position of the nut with respect to a stop will be measured with a vernier caliper and correlated with the swirl block parameter σ. Coarse threads are used for the follower nut to magnify the position indication and reduce readability errors. Safety regulations will not allow entering the cell to change swirl while reaction is taking place, but reactor down time should be no more than 5 minutes. If changing swirl during a run is found to be desirable, the swirl adjustment will be motorized.

The swirl generator will be constructed entirely of stainless steel to avoid warpage and corrosion at the high temperatures expected in this area. Ninety percent of the material has been purchased, and machining is underway on those portions which are not dependent on pressure vessel design.

4. Reaction Chamber and Pressure Vessel

The refractory lined reaction chamber is housed in a pressure vessel designed for 20 atm operation. Access to the chamber is provided for an ignitor, two probes and two observation windows. The reactor can be tilted or lowered for assembly or probe exchange. Figures 11 and 12 show the arrangement of the reactor internals. Note that the use of an offset probe will allow complete mapping of radial and axial profiles.

4.1 Reaction Chamber Size. The initial objective was to design a reactor which would allow free jet development of the coal flame. However, the large rates of spread characteristic of swirled jets (Kerr and Fraser, 1965; Beer and Chigier, 1972) would require a prohibitively large chamber. Further, most industrial flames experience some degree of confinement either by walls, tube banks, or surrounding burners. Pershing and Wendt (1975) operate their coal burner at an apparent confinement ratio (diameter of chamber/diameter of the secondary air throat) of 4.4:1. Beer (1976) suggests that a 6:1 ratio is probably a reasonable approximation to industrial practice.

Since the confinement ratio has a strong effect on the external recirculation zone (which may be very important in stabilizing gasification reactions), flexibility of confinement ratio was included as a design criterion. An initial confinement ratio of 7.5:1 was chosen. This value is greater than industrial practice, yet the chamber can still be accomodated within a 24" pipe.

As Fig. 11 shows, the refractory shell is cast in sections with the top two sections covering ~50% of the reactor length. These two sections will be exchanged with sections of smaller I. D. to change confinement ratio. By maintaining the original chamber diameter, confinement ratios up to 30:1 are possible at 20 atm.

Table V predicts the point of wall contact and mass recirculation ratio (recirculating mass flow/initial mass flow) at several swirl numbers for the initial configuration. The values presented are based on a modified Thring-Newby analysis with extrapolation of the Kerr and Fraser (1965) jet spread and entrainment data (Appendix B). These predictions show that

TABLE V

Point of Wall Contact and Recirculation Ratio†

	Total Swirl Number					
	0	0.6	1.0	1.5	2.0	2.5
Wall Contact Point	2.92D	1.02D	0.683D	0.446D	0.297D	0.190D
$\dot{m}_r/\dot{m}_o$	3.38	2.49	2.23	1.88	1.48	1.02

†Nozzle Diameter (d) - 2 in.
Chamber Diameter (D) - 15.25 in. = 7.625 d
Chamber Length (L) - 50 in. = 3.28D

the recirculated mass flow outside the jet decreases with swirl. For the gasifier then, the effectiveness of the outer recirculation zone as a flame stabilizer will decrease with swirl. A recirculation ratio greater than one can be maintained up to a swirl number of 2.5. Unlike industrial units with cooled walls, the recirculated gases will retain most of their temperature and a recirculation ratio of unity may be sufficient for stability.

The chamber length is sufficient to allow even an unswirled jet to contact the wall before the chamber end. The chamber volume allows the volumetric heat release to vary from 1.6×10^4 to 6.3×10^4 BTU/hr•ft^3. As shown by Table VI, these heat releases are of the same order as other successful laboratory scale coal combustors.

4.2 Refractory and Insulation. The refractory walls will be cast of Harbison Walker Lightweight Castable No. 30. This is an insulating castable with an upper recommended use temperature of 3460°R. Since it has very poor resistance to slagging and abrasion, a coat of A. P. Green Satanite approximately 1/8" thick will be applied to all inner surfaces. Satanite is a slag resistant mortar for use up to 3660°R.

A 1/32 inch stainless steel sheet surrounds the refractory; it serves as an alignment tube for the refractory sections and maintains the integrity of the Kaowool insulation should refractory cracking occur. A port is provided in the refractory and stainless sheet for the observation window.

Two inches of Kaowool bulk insulation surround the refractory. The Kaowool provides the major resistance to heat flow out of the reactor. It will be packed to an 8 lbm/ft^3 density, but will not have sufficient compressive strength to prevent the refractory lining from shifting when the reactor is tilted. Small blocks cut from insulating fire brick will be placed between the refractory aligning tube (stainless steel sheet) and the vessel wall to steady the refractory.

A polished stainless steel bezel will surround the viewing port and extend into the refractory opening (Fig. 12). This serves to hold the Kaowool in place and protect the vessel wall from radiation. Cooling nitrogen will be supplied through the base of the sight glass.

TABLE VI

Heat Release Rates for Coal Reactors

	Coal flow (lbm/hr)	Throughput (lbm coal/hr·ft^3)	Volumetric heat release (BTU/hr·ft^3)	Surface heat release (BTU/hr·ft^2)
How, Kear, and Whittingham (1954)	1.0 - 4.5	0.7 - 3.0	0.9×10^4 - 3.6×10^4	---
Kurtzrock, Bienstock and Field (1963)	1 - 4	0.7 - 2.7	0.9×10^4 - 3.5×10^4	$< 6.5 \times 10^3$
Pershing and Wendt (1975)	6.6	5.6	7.6×10^4	9.6×10^3
Present reactor	7 - 28	1.3 - 5.3	1.6×10^4 - 6.3×10^4	0.4×10 - 1.7×10^4

The chamber ends are also made of insulating castable refractory. The upper end is cast in two sections to allow changing the secondary throat and divergent quarl. The lower end contains the gas exit, probe opening and axial viewing port. A two piece refractory insert is used around the probe to provide a close fit while still allowing removal of the off-set probe.

All refractory pieces will be cast in wooden molds. The molds will be removed after the refractory has been heated to 690°R and further curing will be done with temperatures up to 2000°R. After the high temperature cure, the refractory should allow rapid initial heat up with the methane ignitor. The thin sections of refractory promote short heat-up and cool-down times.

4.3 Thermal Analysis of the Refractory Chamber. In order to determine the suitability of the refractory wall and predict exit gas temperatures, a stirred reactor-equilibrium model was employed. The model assumes that the contents and properties of the reaction chamber are uniform throughout and that all the coal reacts to completion. The analysis is presented in detail in Appendix C.

Figure 15 gives the shell vessel temperature as a function of the refractory inner wall temperature. As long as inner wall temperatures are below 4000°R, the vessel temperature will remain below 960°R with only natural convection and radiation cooling. The vessel is designed for 1110°R.

Figure 16 shows the gas temperature as a function of heat loss rate for various coal flow rates at stoichiometric and 20% excess air. Also shown is the refractory inner wall temperature as a function of heat loss rate. If refractory temperature is assumed to equal the gas temperature, the points of intersection represent stable operating conditions. These intersections indicate that stability should be no problem even at the lowest flow rates. Pershing and Wendt (1975) report auto-ignition of their coal jet with wall temperatures as low as 2360°R. Even if heat losses are greater than predicted and incomplete combustion leads to lower heat release rates, stable operation will be possible, particularly at higher flow rates.

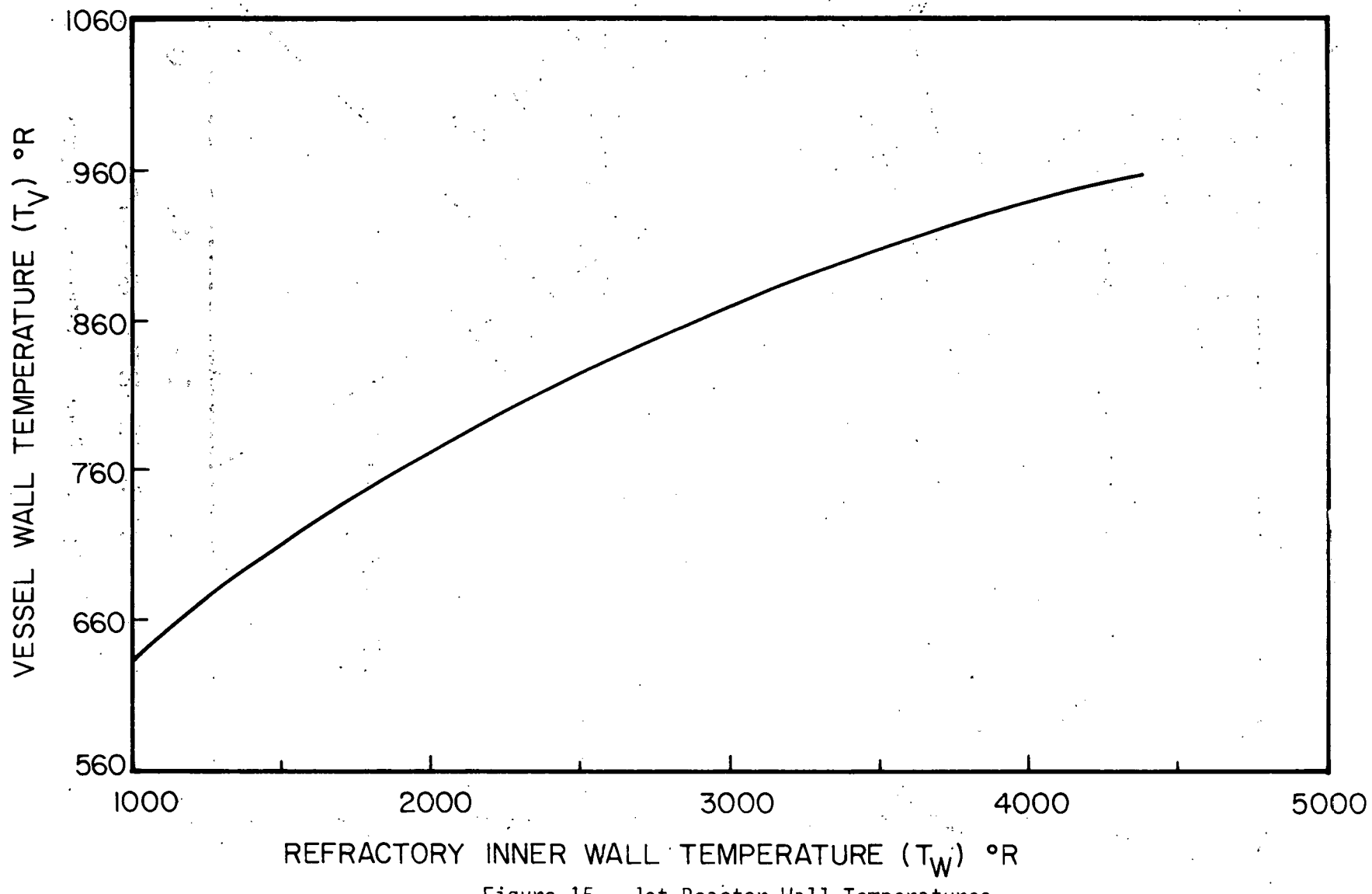

Figure 15. Jet Reactor Wall Temperatures

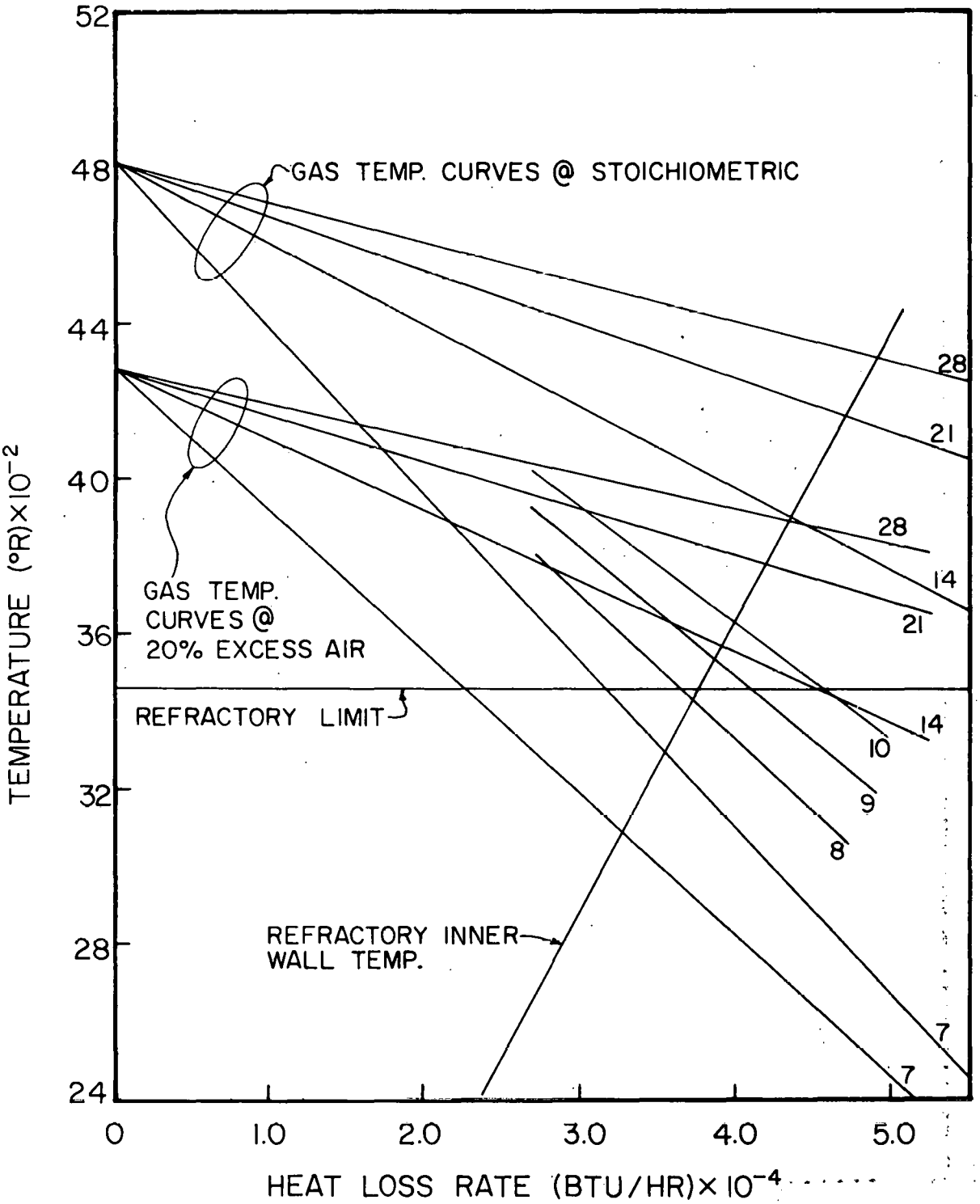

Figure 16. Reactor Heat Loss Rate vs. Temperature Curves

Figure 16 indicates that the upper limit to combustion placed by the refractory temperature may be as low as 9 lbm coal/hr for stoichiometric conditions and 14 lbm coal/hr for 20% excess air. This assumes that the refractory temperature equals the gas temperature. In fact refractory temperatures will be lower. Based on conservative assumptions (Heat transfer over-estimated) concerning the gas-wall energy exchange, Appendix C shows that the gas temperature will be 60°R higher than the wall temperature at stoichiometric and 9 lbm/hr, and 65°R higher at 20% excess air and 14 lbm/hr.

While these figures indicate some curtailment of combustion flow rates, they also show that heat losses for gasification will be minimized. Achieving stable combustion is virtually assured even at low flow rates; higher flow rates are available to compensate for errors due to the simplicity of the model.

4.4 Ignitor. A spark initiated methane/air ignitor is positioned to fire across the coal jet. The ignitor will be used to preheat the chamber and to stabilize the coal flame until the walls are hot enough to insure a self-sustaining coal flame. A similar ignitor has undergone testing in the cyclone chamber and was found to be stable and easy to light-off.

4.5 Cooling Coil and Exhaust Piping. As the hot gases leave the reaction chamber, they encounter the water-cooled coil shown in Fig. 11. This coil begins cooling the gases and protects the vessel from overheating at the exhaust opening. Exhaust piping downstream of the cooling coil will be water jacketed.

The cooling coil will be made of 3/8" stainless steel tubing coiled to fit inside a 4 inch pipe. Initially the cooling coil will be exposed directly to the hot gases leaving the chamber, providing the maximum cooling. If slag plugging occurs, or the coil suffers from excessive abrasion or overheats, a 3/4 inch layer of refractory will be applied to reduce cooling and protect the coil.

It is not clear how the coal ash will behave in this system. If the particles follow stream lines and avoid wall contact, they will be cooled by radiation in the exhaust section and collected as dust particles. The ash will certainly be liquid at the chamber temperatures we have predicted, so some wall slagging may occur. This can be controlled by appropriate exit modifications; for example, using the lower ash collection pipe as a water bath slag quench, and in extreme cases, providing radiant cooling surfaces inside the vessel. Other investigators using laboratory scale reactors (Pershing & Wendt, 1975; Smoot and Hanks, 1977) have not reported slag problems, so we are delaying any specific slag control measures until ash behavior is more clearly defined.

4.6 Pressure Vessel. The pressure vessel is a piece of 24" schedule 20 seamless pipe with standard pipe flanges and a welded end cap. All portions meet or exceed the requirements of the ASME Boiler and Pressure Vessel Code for a design of 650°F and 300 psig. The vessel will be constructed by the Purdue Machine Shop; material procurement has begun with a tenative completion date near the end of October.

The entire pressure vessel will be supported from trunions placed just below the upper flange (just above the center of gravity). By disconnecting the exhaust and inlet lines, the reactor can be tilted 30° in either direction. Additionally, the reactor can be lowered 24" from its normal operating position. The reactor must be vertical to operate, but inlet and exhaust lines will be designed to allow operation in either the up or a partially lowered position. Safety brackets will prevent the reactor from shifting in the event of an hydraulic cylinder failure. Trunion, safety bracket, hydraulic cylinder, and flange bolt inspections will be included in a periodic maintenance schedule.

4.7 Probing. A stationary probe will be inserted through the exhaust gas cleanout cap. This probe will be used to obtain initial reactor performance data; it will also serve as a safety check for ignition and confirm gross reactor behavior after internal probing is initiated.

A traversing offset probe will be inserted through the lower vessel head and used to map concentration and temperature profiles inside the chamber. Probe travel is restricted to 24 inches by the test cell

ceiling height, so a single probe will not cover the entire chamber. As noted in Table V, the wall contact point is less than 16 inches from the jet exit for swirl numbers greater than 0.6. A single probe will therefore allow probing of the most significant portion of the reactor. If necessary, a second probe can be constructed to traverse the lower half of the chamber.

The probe will be water-cooled with a 1" diameter at the base, reducing to a 3/8" diameter near the tip. The large base is required to aid in stabilizing the long unsupported probe; the small tip should minimize flow disturbances. A ceramic tip would be very desirable, but initial efforts to design an economical ceramic probe have not been successful.

A preliminary design of the probe traversing mechanism was considered during vessel design to insure that enough clearance would be available. A ball screw device will be used to position a translating platform which supports the probe. A second motor will rotate the probe through 180° to provide full radial profiles.

5. Summary

As designed, the reactor will provide an effective tool for investigating the combustion and gasification of pulverized coal or char in a swirling jet. Sufficient flexibility is available in the reactor to compensate for off-design firing conditions and to study the effects of varying reactor configuration. Optical access is provided for visual observation of the flame. Internal probing of the entire reactor chamber can be accomplished with two probes.

D. Sampling System

In our gasification program we will attempt to measure gas-phase composition and temperature, not only at the exhaust but also within each gasifier. The presence of water and particulates will present special problems; however, the measurements can be made by an appropriately designed mass spectrometer-probe system.

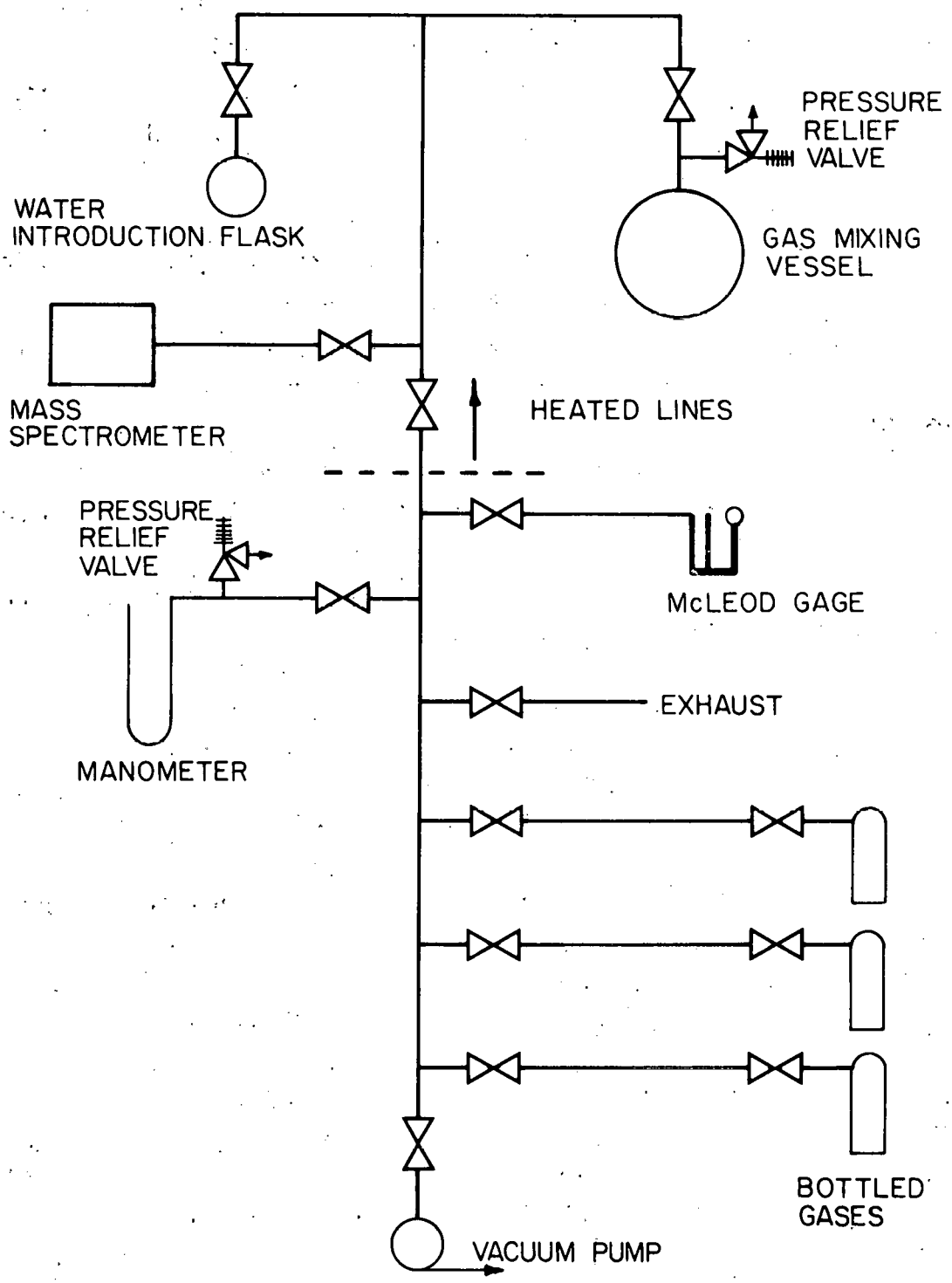

Figure 17. Mass Spectrometer Calibration System Schematic

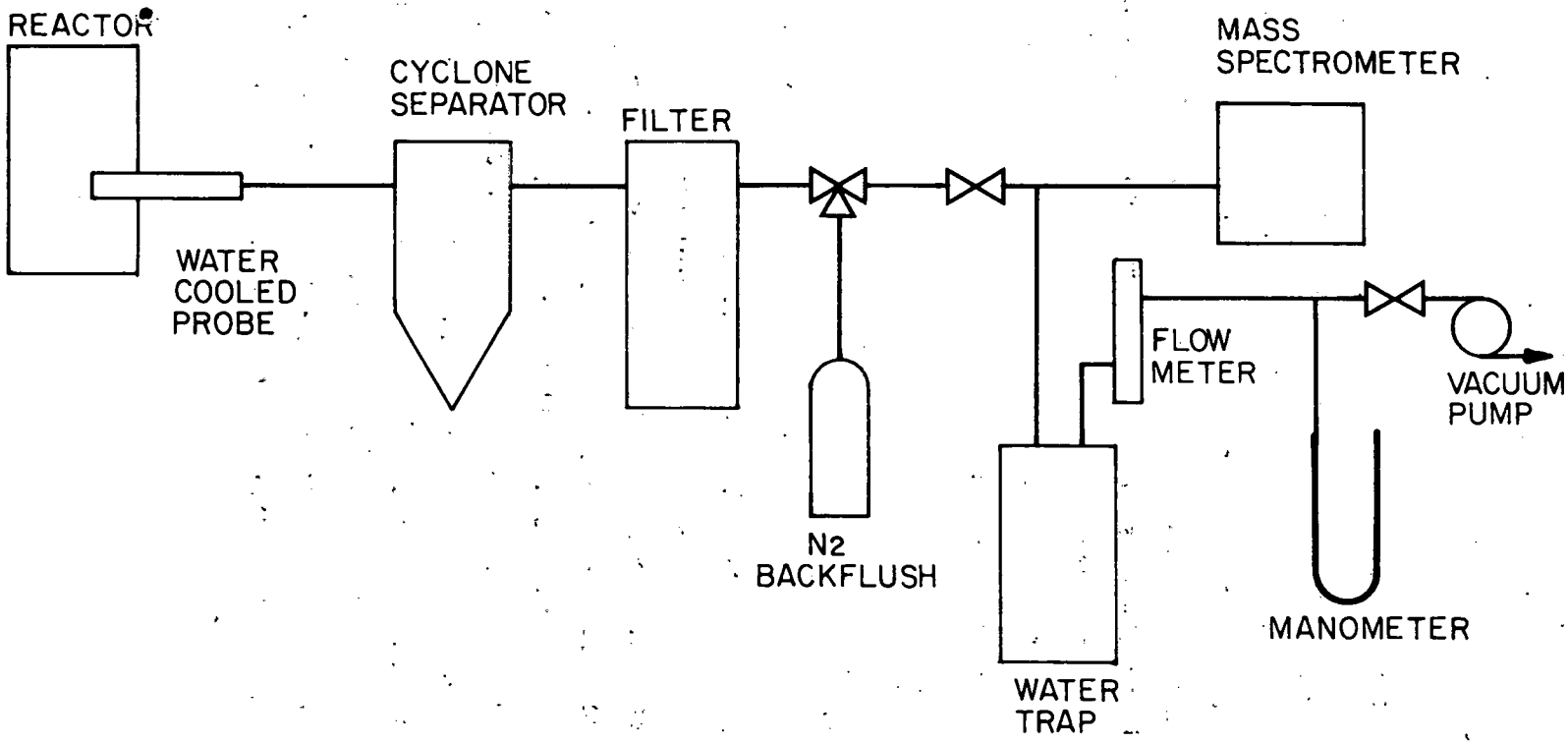

Figure 18. Sampling System Schematic

1. Mass Spectrometer

The UTI-30C quadrupole mass spectrometer system is in working order and has been successfully calibrated. Tests reveal that the Q-30C is suitable to resolve gas mixtures similar to those expected during coal gasification (see Appendix D).

2. Calibration System

A simple calibration system has been designed and built (Fig. 17). The system is capable of mixing calibration gases of known compostion from pure gases by carefully monitoring the partial pressures. Pure bottled gas is introduced into the manifold and then into the glass mixing vessel. A manometer monitors the pressure each time more gas is introduced into the mixing vessel. The heated portion of the system allows mixtures containing known amounts of water vapor to be made. System leaks can be detected by a McLeod or Pirani gage.

3. Sample Inlet System

A schematic diagram of the sampling system is shown.in Fig. 18. Sample gases enter the water-cooled stainless steel probe where the chemical reactions are quenched (Chedaille and Braud, 1972). Heated, teflon lined tubing (Technical Heaters Inc.) is used to minimize water adsorption and condensation, catalytic reactions and adherence of tars and solids between the probe and the mass spectrometer (Fuchs et al., 1974). A Universal Oil Products ½ inch cyclone and a Balston 95A filter are used to remove particulates from the sample gas, as particles may damage the mass spectrometer. Together they are capable of removing all particles greater than 0.6 microns in diameter and most of the smaller particles. The vacuum pump pulls the sample to the mass spectrometer and regulates the sample gas flow rate and pressure at the mass spectrometer inlet. The N_2 back flow system will allow high pressure flow through the probe to remove any blockages which may occur.

4. Probes

Presently, water cooled stainless steel probes are used to sample product gases from the exit stream. Consideration is being given to long water cooled or steam cooled probes for internal reactor sampling. The design may incorporate a thermocouple for temperature measurement and a screen to prevent entry of large particles. A mechanism allowing probe movement is being examined.

IV. PRELIMINARY EXPERIMENTAL RESULTS

A. Coal Feeder

During the Spring of 1977 the coal feeder was equipped with remote control devices and calibrated. The feeder is a Vibra Screw Live Bin Feeder, and it employs a rotating, vibrating auger fed from a vibrating bin. The bin capacity is three cubic feet, and the feed rate range is 4 to 40 lb/hr for a material of density 40 lb/ft^3, approximately that of loosely compacted pulverized coal.

A non-contact magnetic sensor (Electro Products Corporation model 3030AN) was installed to provide a signal proportional to the rotational speed of the auger. An iron gear with 120 teeth was attached to a shaft geared directly to the auger shaft; the magnetic sensor thus produces a voltage spike each time a gear tooth passes it. A Heathkit model SM4100 frequency counter counts the spikes and provides a display proportional to the auger rotational speed. The overall sensitivity of the system is two Hz per rpm auger speed.

In order to provide remote rotational speed control, a servo motor (Bodine Electric Company model 415) was installed to drive the feeder speed adjusting crank. The motor is a reversible induction motor with a rated torque of 32 in-lbs and a maximum speed of 14 rpm. Push buttons on a remote controller are used to position the adjusting crank, and limit switches shut the servo motor off when the adjusting crank reaches maximum and minimum settings. Figure 19 is a schematic of the feeder control/monitoring system.

The feeder was calibrated with Southern Indiana bituminous coal, which is to be used for the initial gasification experiments. After pulverizing, the coal was found to have a Rosin-Rammler particle size distribution as follows:

$$RR = 100 \exp[-(x_s/56)]^{1.23}$$

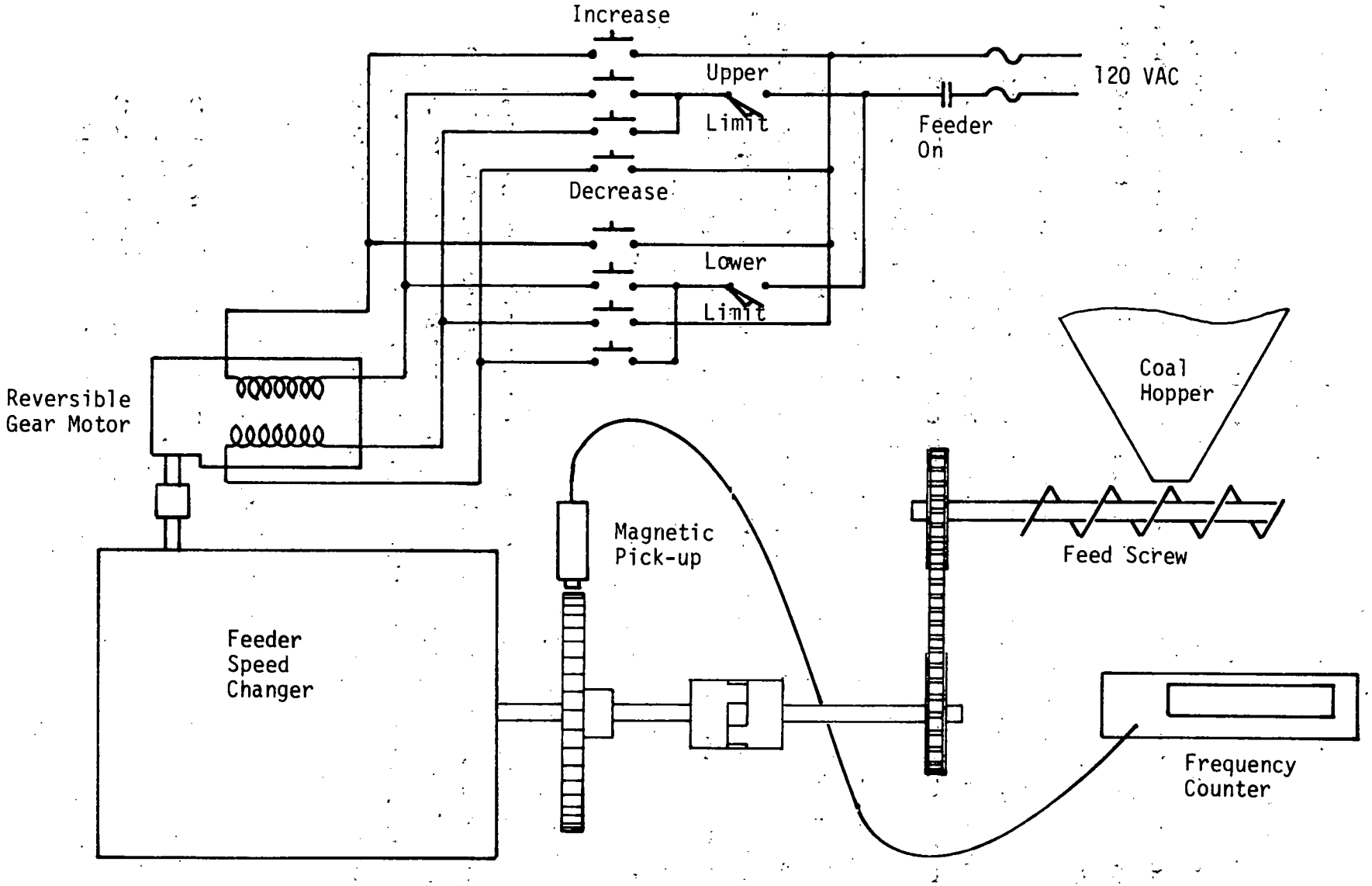

Figure 19. Feeder Contrcl/Monitoring Schematic

where: x_s = screen size (μm)

RR = weight percent of particles retained at a given screen size.

It was found that 75.2% of the coal passed through a 200 mesh screen.

Results of the feeder calibration are shown in Fig. 20. A least squares fit showed that the feeder calibration could be most conveniently represented by the piece-wise linear plot shown. Using sixty second samples, the maximum experimental error using this calibration was found to be less than one percent.

Tests were also run to determine the feeder percent error as a function of sampling time and mass flow rate. Figures 21 and 22 are plots of percent error versus sampling time and percent error versus flow rate, respectively. As one might expect, percent error decreases rapidly with increased sampling time. In order to help alleviate the minute variations in feed rate observed, a vibrating wooden cone has been installed between the feeder discharge and the coal entrainment vessel. The coal leaves the auger and falls onto the center of the cone and gradually slides off the smooth, sloping surface, falling into the entrainment vessel. Variations in feed rate due to the cyclic nature of the auger are thus reduced to an even lower level. This design is undergoing further testing and should become an integral part of the feeder mechanism.

B. Operational System Checkout

A series of informal hot and cold flow tests and the formal methane tests covered in section E have shown that the completed portions of the cell and the cyclone reactor can be expected to conform to design. The informal tests were conducted to show only the general behavior of various systems and to confirm the safety of the overall design prior to reactive tests.

1. Cold Testing and Dry Run Operation

Prior to any operation of the system, a detailed operating procedure was developed and approved by the Combustion Laboratory safety committee. The procedure includes item by item checklists for start-up, operation, shutdown and monitoring of the reactors, specific operator

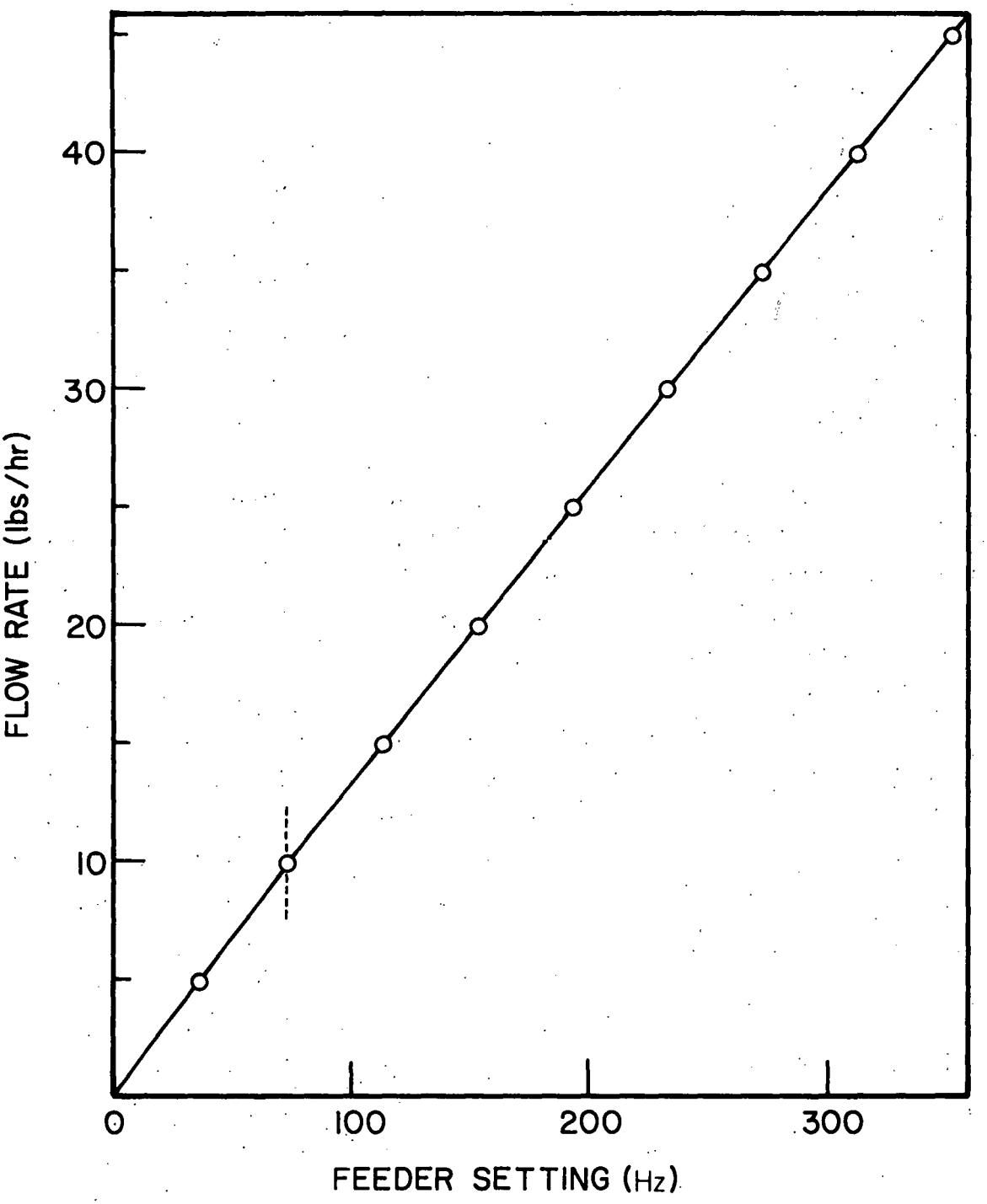

Figure 20. Coal Feeder Calibration

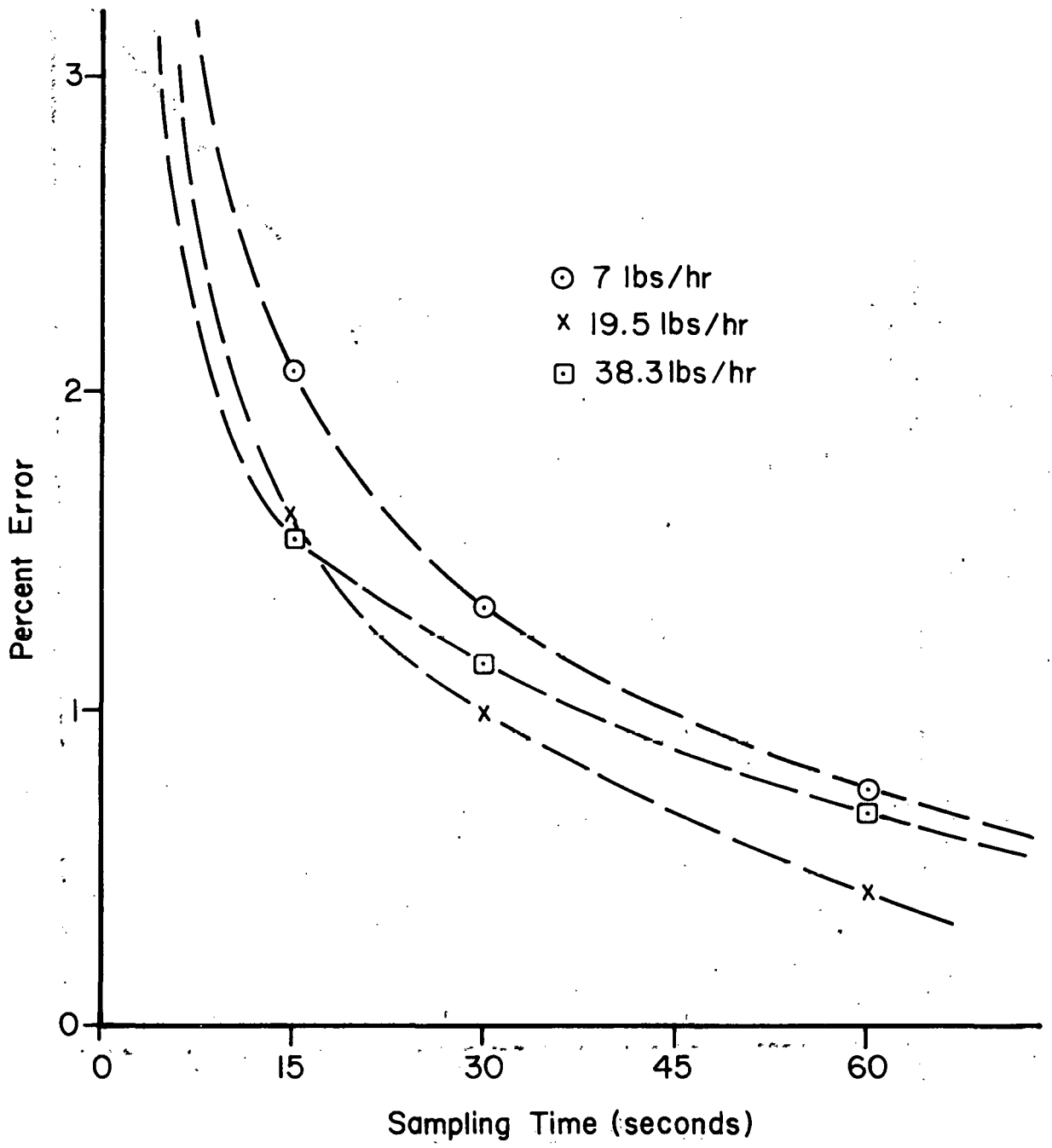

Figure 21. Feeder Percent Error vs. Sampling Time

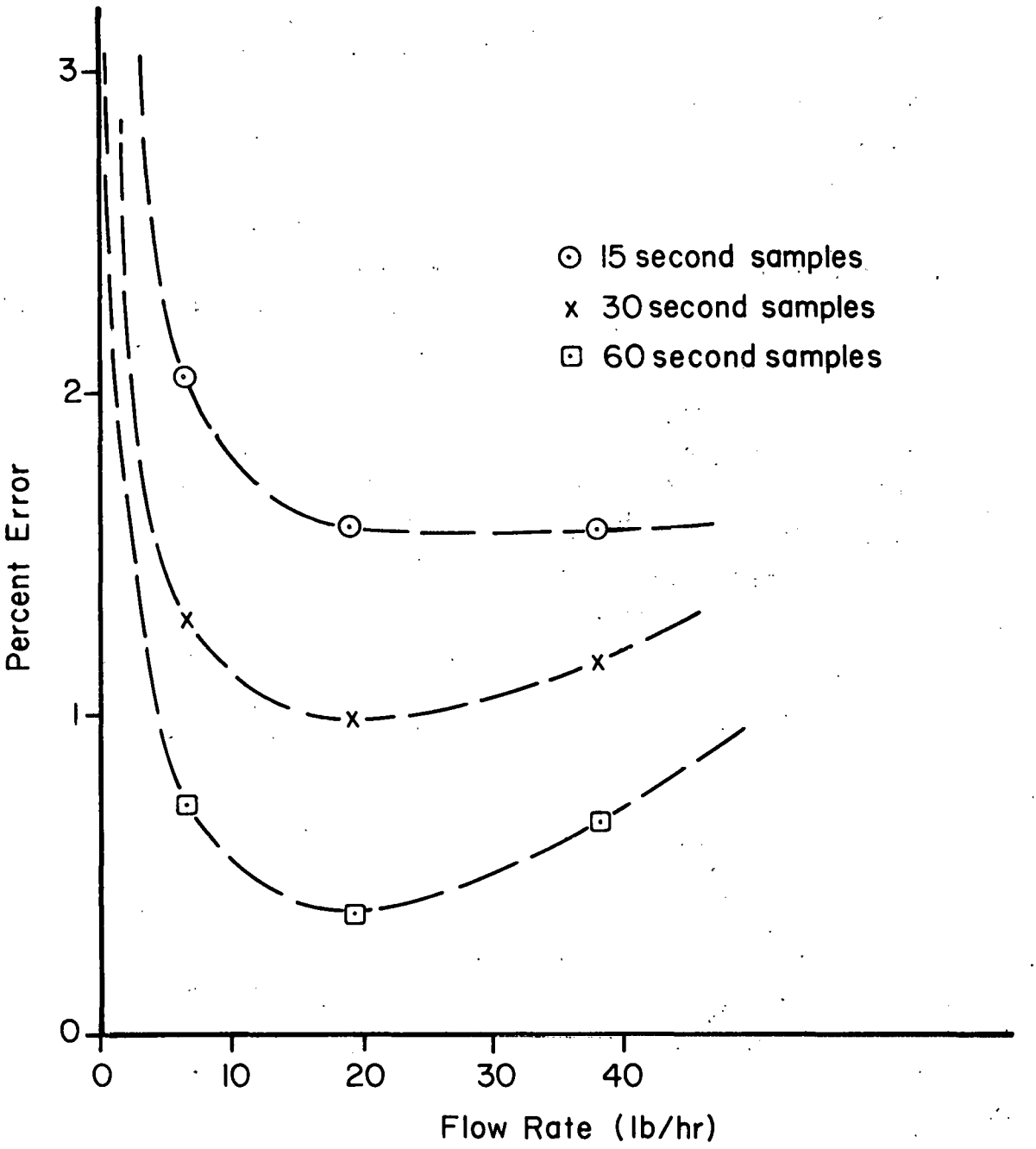

Figure 22. Feeder Percent Error vs. Flow Rate

responsibilities and an outline of emergency procedures. A dry run operation was done with all potential operators present to insure familiarity with the system and solve any remaining problems.

Each system was independently tested under flow conditions. Initially, pressure surges which blew the fluid out of the flow metering manometers were encountered upon opening a remotely operated valve. This problem was overcome by installing snubbers and a manometer bypass valve in the sensing lines. With the exception of the surges, the systems all performed as expected. Flows were stable and controllable. With proper settings on the selector valves downstream of the controller (insuring adequate back pressure at the regulator), very precise control is possible.

During the cold flow tests all systems required for initial operation were tested and found to be in good operating condition. Trips were simulated and we found that a 30 second purge effectively cleared the cyclone reactor.

2. Hot testing

The performance of the air heaters and reactor heater were checked during the hot unreacting tests. The reactor heater was used to heat the refractory for final curing and prior to methane firing. Set-point increases have not been automated, but otherwise, the heaters are completely automatic, reaching and holding temperature well.

The incoming air heater maintains temperature at the orifice meters at 45°C for all flow rates, simplifying the flow measurement process. It responds to changes of flow rapidly and with good stability. The secondary air heaters also worked well. Secondary air temperatures have been as high as 400°C. However, the fast response of these heaters to flow rate changes has created some stability problems. Since the flow is controlled on the basis of pressure, increasing system resistance as temperature increases reduces the flow rate. The reduced flow rate requires less heat, so the heaters turn down and the flow rate goes up again. Flow rate fluctuations on the order of 2% were observed. We believe that a thermocouple averaging technique will solve this problem.

During methane tests, we found that the heater shells overheated at very low flow rates (much less than for coal runs). When the air flow

interlocks are installed, they will prohibit operation of the heaters at dangerously low flow rates. All heaters are surrounded by explosion cases to prevent personal injury should a shell failure occur.

3. Methane Combustion Tests

The methane tests (see Section E) provided an opportunity to observe the system under combustion conditions. Although the flow rates were low, the system behaved well. Exhaust temperatures were as high as 1000°C at the reactor exit. The ceramic tube which formed the reactor exit throat broke during the tests, apparently due to thermal shock. This was the only adverse condition observed with the exhaust cooling system; other exhaust components performed well.

The ignitor was stable and easy to light off under the operating conditions of the tests. Some problems were noted with long term stability, apparently due to dielectric breakdown after operation for periods over 1 hour. Since the ignitor will only be used for short periods during start-up and shut-down, this will not be a limitation. The dielectric regained its initial strength after a 15 minute cooling time in all cases where problems were encountered.

During the methane tests, the thermocouple monitoring system provided rapid temperature indication of ignition and data acquisition was very easy for all forty thermocouples. Flow data were much more difficult to record due to the necessity of reading manometers and pressure gages. When the electronic flow system is complete, it will be similar to the thermocouple system and data acquisition will be much faster and more accurate since a signal proportional to flow will be read directly.

The methane flow tests were the first indication of how valuable the mass spectrometer is to the operation and testing of the coal gasifiers. It provided a rapid (<5 seconds) indication of ignition. Additionally, the operator can tell at a glance how the system is performing. The presence of primary gases such as oxygen or methane can indicate both the occurrence of ignition and the efficiency of combustion.

During the methane tests, the primary orifice meter was placed in the exhaust system to measure exit gas flow. The mass flow indications from this meter confirmed the input flows. This indicates that our system

is leak free, and that the flow meter calibrations are accurate. Figure 23 is a plot of the exhaust flow versus input flow for one set of cold flow conditions.

When the jet reactor, coal and steam systems are installed, they will receive a similar shakedown. Based on our experience so far, we expect the systems to perform reliably as designed so that a minimum of time is required for hardware maintenance. A maximum effort can be placed on obtaining effective experimental results to both demonstrate the feasibility of these systems and back up our modeling efforts.

C. Mass Spectrometer Calibration

Calibration and testing of the UTI Q-30C mass spectrometer system is complete. Calibration tests have been performed with gas mixtures containing H_2, CH_4, H_2O, N_2, CO, O_2 and CO_2. Gas mixtures similar to those expected in combustion and gasification experiments can be resolved to within five percent of the actual mole fraction for each species.

1. Mass Spectrometer

A UTI Q-30C quadrupole mass spectrometer system is used to analyze the cyclone and jet reactor product gases. The Q-30C system has several features essential for our program requirements. The inlet system is designed for continuous sampling, has rapid response, and can tolerate high pressures (50 psia). High concentrations of water vapor can be measured, as the inlet is heated. A Faraday cup is used rather than an electron multiplier to enhance response linearity. Hydrogen can be measured for concentrations under 15%. A completely automatic bakeout cycle provides for eliminating large background interference.

2. Calibration Methods

A simple calibration system was designed and built to make sub-atmospheric gas mixtures of known composition (Fig. 17). Pure gases purchased from Matheson Inc. were used to prepare gas mixtures. The concentration of each gas in a mixture is determined from its partial pressure, which is measured by a mercury manometer (with the exception

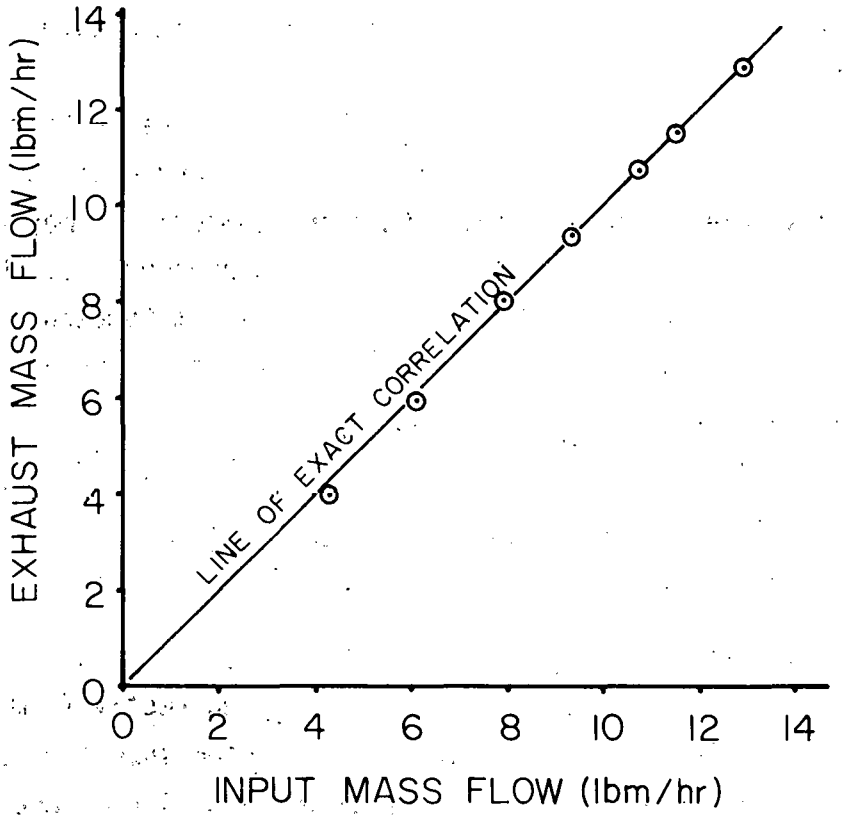

Figure 23. Exhaust Flow vs. Input Flow

of H_2O). Gas mixing was aided by a magnetic stirrer. The total pressure of each calibration mixture was approximately 500 torr.

Water was handled by heating the calibration system such that the lowest system temperature was at the liquid-vapor interface within the water reservoir (Fig. 17). The interface temperature determines the equilibrium water vapor pressure within the system. Water vapor can then be allowed to enter the evacuated mixing flask. After equilibrium is attained, subsequent gases can be introduced to form a water-containing mixture of known composition.

In all calibration tests, efforts were made to keep sampling conditions close to those expected in combustion and gasification experiments. The sample pressure, temperature and composition may all cause variations in the calibration data. The inlet pressures of the gas samples were always between 400 and 600 torr; inlet temperature was kept at 200°F. Calibration gas mixture compositions were confined to a range expected in actual experiments.

The gases considered in calibration were H_2, CH_4, H_2O, CO, N_2, O_2 and CO_2. Binary gas mixtures consisting of N_2 and a second gas were monitored to calculate the sensitivity of each gas relative to nitrogen (with the exception of CO). Each binary mixture contained 50 to 95 percent N_2, as experimental product gases will consist largely of N_2. The relative sensitivity of CO was determined indirectly from CO/Ar and Ar/N_2 mixtures. Fragmentation patterns were determined from both pure gases and binary mixtures. The fragmentation data for CO and the magnitude of the CH_4 14-peak were determined from the pure gases.

Test gas mixtures of progressively increasing complexity were prepared to check the relative sensitivity and fragmentation pattern data. Further adjustments in the calibration data were made from these tests. A final set of mixtures, similar to those expected in experimental sampling, were used to test the ability of the mass spectrometer system to determine the mole fraction of each gas. Results from these tests appear in Appendix D.

3. Data Reduction

The gases considered in calibration have interfering fragmentation patterns (more than one gas producing a signal at a given mass/charge ratio).

To resolve the complex gas mixtures, 10 separate peaks were monitored for the 7 gases considered. A system of 10 equations and 7 unknowns must therefore be solved. The computer program of McLean and Sawyer (1967), which utilizes a least squares technique to solve an overspecified system of equations, is used to resolve the gas mixture data. The program calculates the mole fraction of each gas, the standard error of calculation and the residuals left for each peak height.

The actual composition of each calibration mixture is known from pressure measurements when making the mixture. This known composition can then be compared to the computer program results, as calculated from the mass spectra. Appendix D contains the results of several calibration tests of complex gas mixtures and a discussion of errors. These calibration experiments clearly show that the mass spectrometer can be used to resolve mixtures expected in our coal gasification experiments.

D. Cyclone Reactor Tests

Two phases of cyclone reactor testing have been completed: a particulate residence time study of the cyclone using a Plexiglas model and initial methane combustion runs with the torch ignitor. The residence time study confirms that sufficient combustion time is available to nearly all coal particles. Methane combustion in the cyclone enables both qualitative assessment of various reactor design features and preliminary product gas analysis via the mass spectrometer under relatively clean operating conditions. The results of these tests provide the basis for several conclusions and recommendations for future cyclone operation.

1. Particulate Residence Time Study

A Plexiglas cyclone, fabricated to the design dimensions of the cyclone reactor, was used to observe coal particle behavior under cold flow conditions. Coal particles (100% through 400 mesh) were injected into the cyclone through one of four tangential nozzles; air was injected through all four nozzles. Due to limitations in the air system, volumetric flow rates were restricted to the lower half of the range anticipated under combustion conditions.

Injected particles either left the cyclone immediately or remained indefinitely in one of three regions: at the intersection of the wall and roof, at the intersection of the wall and floor, or at the center of the floor (in contrast to the sloped floor and slag tap in the reactor, the floor of the model is level and has no slag tap). It is assumed that particles leaving the cyclone are the smallest, those remaining at the center of the floor slightly larger, and those remaining at the wall larger still. If sufficient burning time is available to those particles leaving the cyclone, it follows that sufficient burning time is available to all particles.

Figure 24 illustrates the relationship between particulate residence time/burning time ratio (τ_r/τ_b) and critical particle radius for both "short circuit" and total cyclone flow volumes. Development of this relationship is presented in Appendix E. The critical particle radius is the radius of that particle whose radial position at equilibrium is the same as the radius of the cyclone throat. Note that both particulate residence time τ_r and critical particle radius are functions of the volumetric flow rate. It is assumed that no particles having radii greater than the critical particle radius exit the cyclone. Consequently, sufficient burning time is available to all particles when the value of τ_r/τ_b is greater than or equal to unity for a particular critical particle radius. From Fig. 24, it is apparent that for only very low values of critical particle radius will particles leave the cyclone incompletely combusted.

The discontinuity in each of the curves is due to a change in the rate controlling step for particle combustion. On the basis of Fig. 31 (Appendix E), it is assumed that the rate controlling step for combustion of particles having radii less than approximately 16 μ is chemical kinetics. Combustion of particles with radii greater than 16 μ is assumed to be controlled by diffusion.

2. Reactor System Assessment

Early combustion runs were hampered by failure to achieve agreement between input and output carbon/nitrogen ratios, ignitor instabilities and an inability to obtain reliable H_2O sampling data.

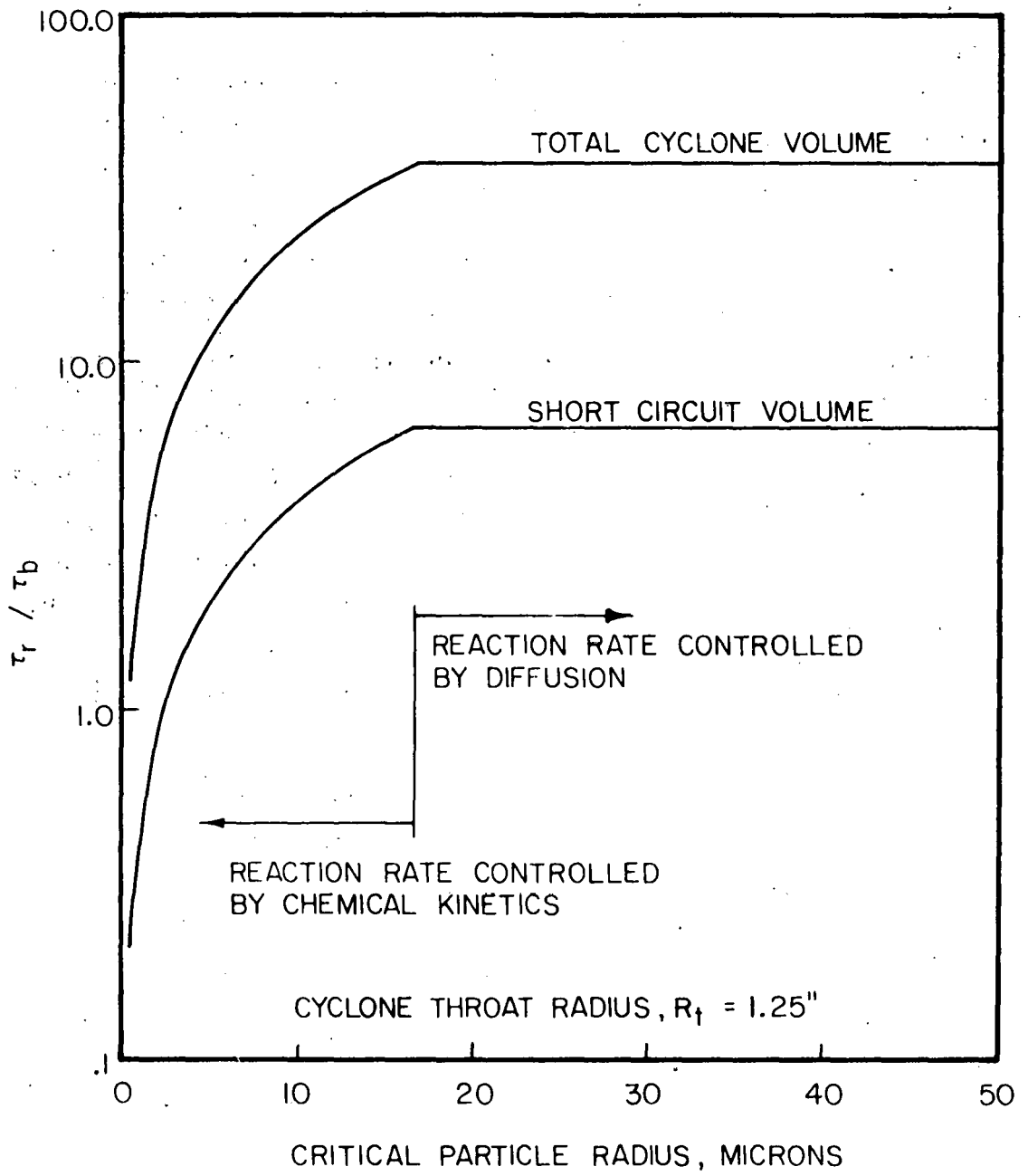

Figure 24. Residence Time/Buring Time Ratio as a Function of Critical Particle Radius

Lack of agreement in the carbon/nitrogen ratios was primarily attributed to an error in computing the calibration curves for the ignition air and gas rotameters. Agreement improved when these rotameters were recalibrated. Ignitor performance was enhanced as operating experience increased. The H_2O sampling problem has not been resolved.

Two difficulties characterized ignitor performance: (1) sudden sustained exit gas temperature drops after periods of stable combustion and (2) occasional relight failure after shutdown periods. The sustained temperature drops were apparently due to ignition spark degradation. The dielectric provided by the mullite insulator failed due to spark heating. Instead of being drawn from the end of the tungsten electrode, the spark crept up the mullite insulator to the ignition air tube (Fig.10), thus discharging in a poorly mixed zone. Inspection of the ignitor following relight failure generally indicated that either the tungsten electrode needed to be cleaned of soot or the spark gap needed readjustment.

To sustain satisfactory ignitor performance, the ignition air supply tube was slightly shortened, thus exposing a greater length of the mullite insulator. This apparently inhibited spark creep and promoted cooling. To prevent soot buildup and maladjustment of the spark gap, frequent maintenance is required; however, this procedure is quite simple.

The cause of unwarranted increases in the H_2O concentration of the sampled product gas during experimental runs has not been isolated. Possible sources of the H_2O are the water cooled sampling probe or condensation on the probe resulting from methane combustion. Investigation of these sources has been inconclusive; continued investigation is required.

Inspection of the cyclone following the combustion runs revealed that the 2.5 inch diameter mullite tube extending into the reactor from the chamber roof had shattered, probably due either to thermal shock or thermal cycling. Since it is likely that further ceramic replacements would also shatter, a steam cooled stainless steel tubing arrangement is being considered.

Performance of the internal reactor thermocouples was quite satisfactory. Refractory temperature profiles using the preheated walls were roughly parabolic in shape. Under combustion conditions, however, this profile was skewed due to the downward firing of the ignitor. Outer

wall temperatures of the three lower refractory cylinders all increased, while that of the uppermost cylinder decreased. Since the thermocouples providing feedback to the reactor heater temperature controllers are located outside the refractory wall opposite the reaction zone, the time-proportioning controller remained off during most of a combustion run. Consequently, directional firing of the ignitor resulted in an increase in lower refractory temperature and a decrease in upper refractory temperature.

Confirmation of ignition was obtained as planned via the product gas thermocouple, the mass spectrometer sampling system, and the observation window. Response times of both the thermocouple and the mass spectrometer were excellent. Visual observation of combustion activity was hampered by clouding of the window and non-luminous flames.

3. Product Gas Analysis

Reliable data were obtained using the ignitor for 16 methane combustion runs at the stoichiometries indicated in Fig. 25. At each run condition, two sets of flow and temperature data and a minimum of three mass spectra were recorded. The flows and compositions determined from these data were then averaged.

Combustion temperatures measured by the product gas thermocouple ranged from approximately 775°K under fuel rich conditions to 1175°K under slightly fuel lean conditions. In Fig. 26, product gas compositions of N_2, O_2, and CO_2 for the 16 combustion runs are compared on a dry basis to N_2, O_2, and CO_2 equilibrium compositions at 1000°K for a carbon-air-steam system. Comparison on a dry basis was done due to the unreliability of the H_2O data.

Concentrations of H_2, CH_4, and CO were detected only at stoichiometric and fuel rich conditions. Since these concentrations were relatively small, considerable uncertainty exists concerning their accuracy. In particular, dilute concentrations of CO were difficult to distinguish from N_2 since they have identical molecular weights (George et al., 1977). Under gasification conditions, however, concentrations of these species will increase. Consequently, detection will be more accurate.

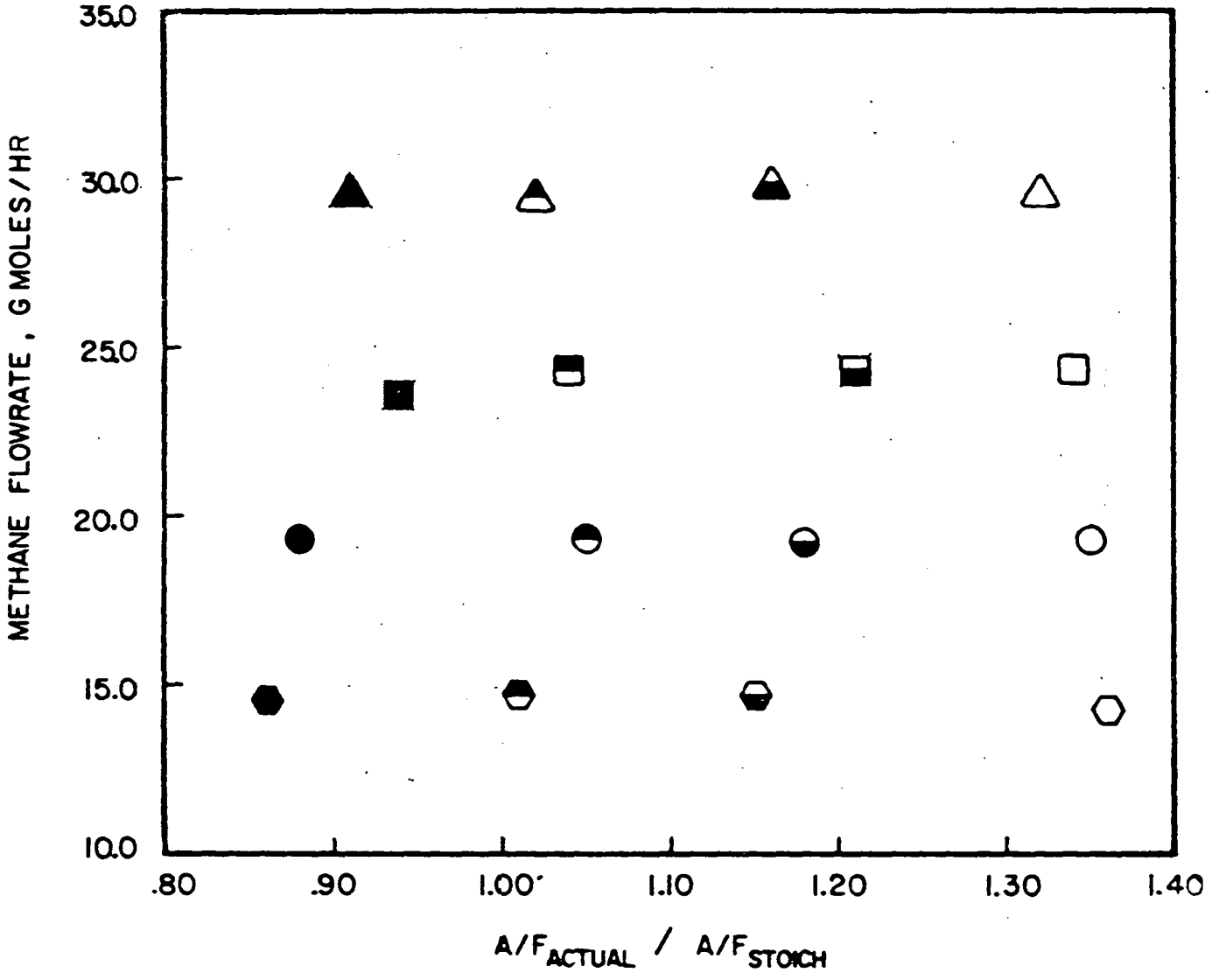

Figure 25. Stoichicmetries of Methane Combustion Runs

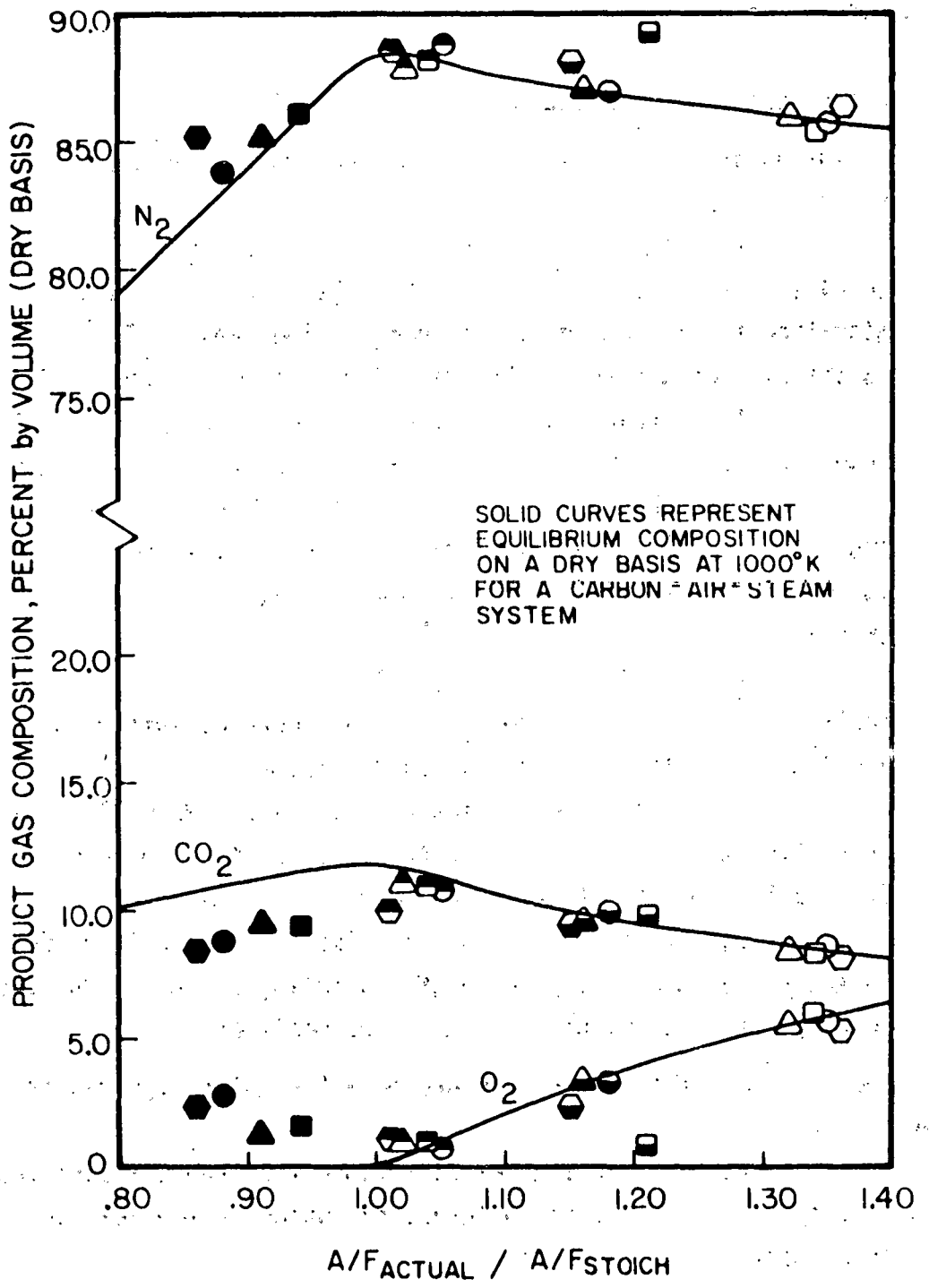

Figure 26. Dry Product Gas Composition of Methane Combustion Runs

From Fig. 26 it is apparent that reaction products approached thermodynamic equilibrium under stoichiometric and air rich conditions. Under fuel rich conditions, however, the presence of oxygen indicates that reactants were insufficiently mixed; the low CO_2 concentration is consistent with this behavior.

4. Conclusions and Recommendations

On the basis of the previous discussion, the following conclusions can be drawn:

(1) Adequate residence time is available for complete burning of nearly all particles. However, particles migrating to the center of the reactor floor may be lost to the slag quench bath, thus reducing percent carbon gasified.

(2) Ceramic tubes projecting into the reaction zone from the cyclone throat are unsuitable for use in the reactor.

(3) The mass spectrometer sampling system and the product gas thermocouple provide fast and reliable response to ignition. The observation window, although useful, is not as reliable.

(4) Satisfactory combustion can be achieved with the ignitor. Stable methane combustion runs were of sufficient duration to ignite incoming air/coal streams.

(5) At low CO concentrations, CO and N_2 will continue to be difficult to distinguish via the mass spectrometer. However, it is believed that the H_2O problem can be solved.

(6) Tests performed under fuel lean conditions demonstrate that the mass spectrometer sampling system can be used to accurately determine product gas compositions.

The following recommendations are made for future cyclone reactor operation:

(1) During initial coal combustion runs, assess the effect of operation with no throat extension in the reactor on percent carbon gasified.

(2) Incorporate a steam injection system in the development of a new throat extension.

(3) Avoid prolonged unnecessary operation of the ignitor. This will help reduce shutdown time for reactor maintenance.

(4) Determine extent of steam addition from the water-filled slag quench bath.

E. Data Analysis for Coal Runs

Data accumulated during gasification test runs will be analyzed in terms of common independent and dependent variables associated with gasification processes (Lenzer et al., 1976; George et al., 1977). Independent variables are defined as those that can be varied at will (but are generally held constant during a given run). Dependent variables are functions of the independent variables, and are divided for our purposes into two categories: those which can be measured directly, and those which must be calculated through knowledge of measured quantities. Table VII classifies the important variables for coal gasification as independent, dependent and measured, or dependent and calculated.

Many of the dependent variables can be calculated with relative ease once the independent and measured dependent quantities are known. The make gas yield is simply the ratio of the make gas flow rate to the coal feed rate. The combustible mass fraction can obviously be calculated through knowledge of the make gas composition. The combustible make gas yield is simply the product of the make gas yield and the combustible mass fraction. The H_2/CO ratio is also very easily found from the make gas composition.

Calculation of steam decomposition is complicated by the fact that some steam is produced from combustion of hydrogen released during devolatilization. If it is assumed that all coal hydrogen is converted to steam in the oxidation zone, the steam decomposition can be calculated as follows:

$$\text{steam decomposition} = \frac{H_2O_{in} - H_2O_{out} + H_2O_D}{H_2O_{in}}$$

where $H_2O_{in} \equiv$ steam feed rate, kg/hr

$H_2O_{out} \equiv$ steam discharge rate, kg/hr

$H_2O_D \equiv$ steam produced from coal hydrogen, kg/hr.

TABLE VII

Gasification Variable Classification

Variable Name and Units	Classification
coal throughput, kg/m^3hr	independent
coal feed rate ($\dot{m}_c$), kg/hr	independent
air/coal input ratio, kg air/kg coal	independent
steam/coal input ratio, kg steam/kg coal	independent
reactor pressure, atm	independent
reactant inlet temperatures, °C	independent
gas exit temperature, °C	dep.-measured
make gas composition, percent by volume	dep.-measured
make gas flow rate ($\dot{m}_g$), kg/hr	dep.-measured
make gas yield (Y), kg make gas/kg coal fed	dep.-calculated
combustible make gas yield (Y_p), kg comb. gas/kg coal fed	dep.-calculated
combustible mass fraction (ω_p)	dep.-calculated
chemical yield (ε_y), kg gas produced/kg coal reacted	dep.-calculated
make gas heating value (Q), kcal/kg gas produced	dep.-calculated
H_2/CO ratio	dep.-calculated
steam decomposition, percent	dep.-calculated
heat loss, percent	dep.-calculated
carbon efficiency (η_c), percent	dep.-calculated
cold gas efficiency (η_{cg}), percent	dep.-calculated
hot gas efficiency (η_{hg}), percent	dep.-calculated

Note that H_2O_{out} is determined from make gas composition and flow rate and includes unreacted steam plus any steam produced through hydrogen combustion in the oxidation zone. H_2O_D is found from the coal analysis and feed rate.

The reactor heat loss is the difference between the total heat input (chemical plus sensible enthalpy) and the total heat output. Percent heat loss is then calculated as follows:

$$\%H.L. = 100 \times \frac{H_{in} - H_{out}}{H_{in}}$$

where $H_{in} \equiv$ chemical plus sensible enthalpy in

$H_{out} \equiv$ chemical plus sensible enthalpy out.

The make gas heating value is defined to be the energy released by combustion of one kilogram of product gas, and is calculated as follows:

$$Q = \frac{1}{\bar{M}} \sum_{i=1}^{n} x_i H_{c,i}$$

where $Q \equiv$ make gas heating value, kcal/kg gas

$n \equiv$ number of product gas constituents

$x_i \equiv$ mole fraction of species i in product gas

$\bar{M} \equiv$ average molecular weight of make gas, kg/g mole

$H_{c,i} \equiv$ enthalpy of combustion of species i, kcal/g mole.

Carbon efficiency is typically calculated through knowledge of coal feed rate and carbon present in slag, ash and carryover of fines. However, separator inefficiency may make an accurate analysis of unburned carbon impossible. Fortunately, carbon efficiency can also be determined if the coal feed rate and composition plus make gas flow rate and composition are known by performing a mass balance on carbon:

$$\dot{m}_c \omega_C = \dot{m}_g \left(\omega_{CO} \frac{M_C}{M_{CO}} + \omega_{CO_2} \frac{M_C}{M_{CO_2}} + \omega_{CH_4} \frac{M_C}{M_{CH_4}} \right) + \dot{m}_{uc} \quad (1)$$

where $\dot{m}_c \equiv$ coal mass flow rate, kg coal/hr

$\dot{m}_g \equiv$ make gas flow rate, kg gas/hr

$\dot{m}_{uc} \equiv$ unburned carbon mass flow rate, kg carbon/hr

$\omega_C \equiv$ carbon mass fraction, g C/g coal

$\omega_{CO} \equiv$ CO mass fraction, g CO/g gas

$\omega_{CO_2} \equiv$ CO_2 mass fraction, g CO_2/g gas

$\omega_{CH_4} \equiv$ CH_4 mass fraction, g CH_4/g gas

$M_i \equiv$ molecular weight of species i, g/g mole

Carbon efficiency is then calculated as follows:

$$\eta_C = \frac{\dot{m}_c\omega - \dot{m}_{uc}}{\dot{m}_c\omega_C} = \frac{\dot{m}_g\left(\omega_{CO}\frac{M_C}{M_{CO}} + \omega_{CO_2}\frac{M_C}{M_{CO_2}} + \omega_{CH_4}\frac{M_C}{M_{CH_4}}\right)}{\dot{m}_c\omega_C} \qquad (2)$$

Note that the mass flow rate of unburned carbon is eliminated by using the second expression in eq. (2). Once the carbon efficiency is known, the chemical yield may be found as follows:

$$\varepsilon_y = \dot{m}_g/\eta_C\dot{m}_c = \frac{1}{\eta_C}\left(\frac{\dot{m}_g}{\dot{m}_f}\right) = Y/\eta_C$$

Cold gas efficiency is defined as follows:

$$\eta_{cg} = H_p/H_c$$

where $H_p \equiv$ product gas enthalpy of combustion, kcal/kg coal

Hc $\equiv$ input coal enthalpy of combustion, kcal/kg coal.

H_c is found during proximate analysis of the coal by burning a measured amount in a calorimeter. Since the product gas enthalpy of combustion can be expressed as

$$H_{pg} = QY = Q\varepsilon_y\eta_C \ ,$$

the cold gas efficiency becomes

$$\eta_{cg} = Q\varepsilon_y\eta_c/H_c \ .$$

The hot gas efficiency is a parameter of considerable interest in low BTU gasification (Laurendeau and Waite, 1977). It includes the difference in sensible enthalpy between reactants and products as well as the change in chemical enthalpy and is calculated as follows:

$$\eta_{hg} = (H_p + \Delta H_{pr})/H_c = \eta_{cg}' + (\Delta H_{pr}/H_c)$$

where $H_p \equiv$ product gas enthalpy of combustion, kcal/kg coal
$H_c \equiv$ input coal enthalpy of combustion, kcal/kg coal
$\Delta H_{pr} \equiv$ difference in sensible enthalpy between products and reactants, kcal/kg coal

ΔH_{pr} can be easily calculated from the make gas composition and yield, plus the air and steam to coal ratios, coal feed rate, and reactant and product temperatures.

V. FUTURE EFFORTS

During the next contract year, we expect to meet the following schedule:

(1) Construction and installation of the confined jet gasifier and associated equipment. Integration of the coal feeder and electronic flow measurement instrumentation into the test cell flow system. Refine the gas sampling system and begin initial cyclone reactor coal combustion tests. Begin development of combustion modeling techniques (3 months).

(2) Complete cyclone atmospheric coal combustion tests and confined jet methane combustion tests. Develop probe system for internal reactor sampling. Compare initial experimental and analytical model results (3 months).

(3) Complete atmospheric confined jet coal combustion experiments. Finalize construction of the steam system, and begin cyclone reactor atmospheric gasification tests. Interpret experimental results in light of our entrained flow combustion models (6 months).

In summary, the gasification facility provides two reactors representing a microcosm of most practical combustion and gasification devices using pulverized coal and char. Successful probing both externally and internally will allow assessment of the combustion and gasification characteristics of many solid fuels over a range of operating pressures. We are designing the facility with flexibility in mind; thus the reaction vessels can be used for future investigations concerned with related fuels or new reactor configurations can be easily developed.

VI. APPENDIX A: SWIRL NUMBER CORRELATION FOR THE SWIRL GENERATOR

The swirl number (S) is the most useful parameter for characterizing swirling jets. In order to determine the swirl number, it is generally desirable to perform a velocity and pressure traverse at the jet exit and use the relations

$$G_\phi = \int (w \cdot r)\, \rho u \, dA \tag{A.1}$$

$$G_x = \int u(\rho u)\, dA + \int p \, dA \tag{A.2}$$

$$S = \frac{G_\phi}{G_x R} \tag{A.3}$$

where A is the area of the jet cross-section being probed, ρ the jet density, u and w the axial and tangential velocity components, p the static pressure, r the radius and R the burner radius. A complete traverse is fortunately not necessary when the IJmuiden swirl generator is used. Beer and Chigier (1972) report data for this swirl generator which indicates good agreement between the measured and predicted swirl numbers. To the extent that the critical assumptions remain valid for our generator, we expect an equally good correlation.

If the flow is assumed incompressible and inviscid, the angular momentum flux (G_ϕ) at the nozzle exit must equal the angular momentum flux at the swirl block exit. If the pressure term in Eqn. A.2 is neglected, then the axial momentum (G_x) can be predicted on the basis of input parameters. Since recirculation zones develop primarily as the result of pressure gradients which cannot be overcome by fluid momentum, the pressure term is not necessarily negligible, but it is none the less a common assumption and will be retained.

As the flow is assumed both incompressible and inviscid, Bernoulli's equation,

$$\frac{P_2 - P_1}{\rho} + \frac{V_2^2 - V_1^2}{2} = 0$$

can be applied to the slots of the swirl generator (see Fig. 27). For equal pressure drop through the radial and tangential slots, it follows that

$$V_r = V_t = V$$

where subscripts r and t refer to the radial and tangential slots, respectively. The mass flow through each slot then becomes proportional to the area of the slot, and the ratio of tangential to radial mass flow is equal to the area ratio of the tangential and radial slots.

Since the flow is inviscid, the velocity is uniform at each slot exit. The streamlines through the tangential slot must each make an angle α with a radial line at the slot exit. Thus, as Fig. 27 shows, the streamlines are all tangent to a circle of radius r_1 so that $(w \cdot r)$ is simply $(V \cdot r_1)$ = constant.

The flux of angular momentum is constant and only the flow through the tangential slots contributes to the angular momentum. Eqn. A.1 thus becomes

$$G_\phi = \int (V \cdot r_1) \rho V \, dA = z V^2 r_1 \rho a_t \qquad (A.4)$$

where a_t is the area of one tangential opening and z the number of tangential slots.

The slot exit area is the area of a plane perpendicular to the bisector of the slot as shown in Fig. 27. Noting that the magnitude of line $\overline{ed}$ is

$$|\overline{ed}| = 2R_1 \sin\left(\frac{\xi}{2}\right),$$

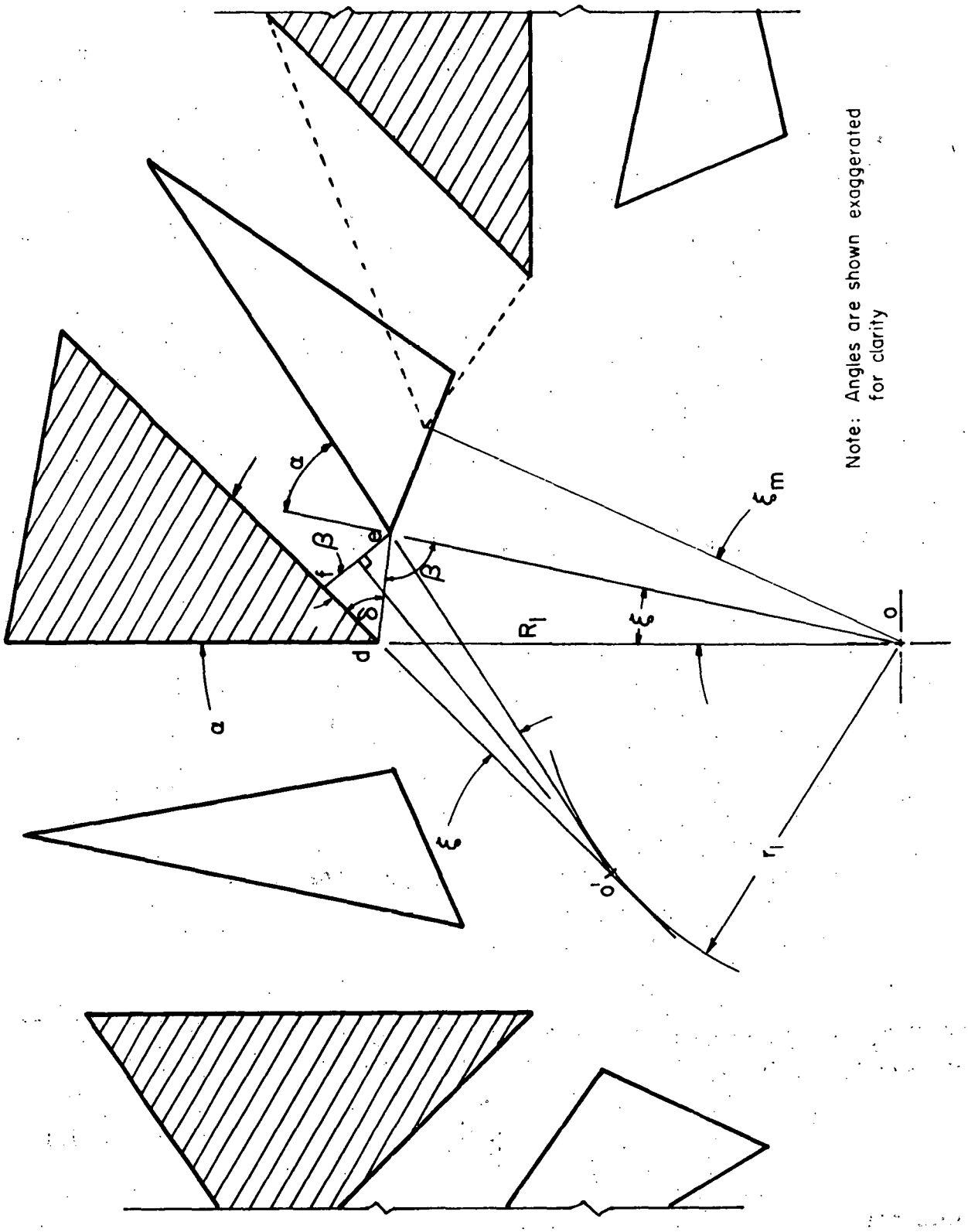

Figure 27. Swirl Generator Geometry

then by the law of sines,

$$|\overline{ef}| = 2R_1 \sin\left(\frac{\xi}{2}\right)\left[\frac{\sin\delta}{\sin\beta}\right] . \qquad (A.5)$$

However,

$$\delta = 90 - \alpha + \frac{\xi}{2}$$

and

$$\beta = 90 - \frac{\xi}{2}$$

so that

$$\sin\delta = \cos\left(\alpha - \frac{\xi}{2}\right) \qquad (A.6)$$

and

$$\sin\beta = \cos\left(\frac{\xi}{2}\right) . \qquad (A.7)$$

Now,

$$a_t = B\,|\overline{ef}| \qquad (A.8)$$

where B is the thickness of the blocks. Substituting Eqns. A.5, A.6 and A.7 into Eqn. A.8, we obtain

$$a_t = 2BR_1 \tan\left(\frac{\xi}{2}\right)\cos\left(\alpha - \frac{\xi}{2}\right) ; \qquad (A.9)$$

similarly, the area of one radial opening is given by

$$a_r = 2BR_1 \sin\left(\frac{\xi_m - \xi}{2}\right) . \qquad (A.10)$$

The velocity through the slots can be expressed as:

$$V = \frac{\dot{m}_s}{\rho_s A_s}$$

where $\dot{m}_s$ is the secondary air mass flow rate, ρ_s the density of the secondary air and A_s the total free area of the swirl block. Eqn. A.4 then becomes

$$G_\phi = zr_1\left(\frac{1}{\rho_s}\right) a_t \left[\frac{\dot{m}_s}{A_s}\right]^2 . \qquad (A.11)$$

Note that

$$A_s = z(a_t + a_r) \qquad (A.12)$$

and

$$r_1 = R_1 \sin \alpha \quad . \tag{A.13}$$

Beer and Chigier (1972) define a swirl parameter (σ) such that

$$G_\phi = \sigma \frac{\dot{m}_s^2}{\rho_s 2\pi B} \quad . \tag{A.14}$$

For an unswirled primary jet, we thus have from Eqn. A.11,

$$\sigma = 2\pi B \left(z r_1 \frac{a_t}{A_s^2}\right) \quad ;$$

hence, applying Eqns. A.9, A.10, A.12, and A.13, we have

$$\sigma = \frac{\pi}{z} \left(\frac{\tan(\frac{\xi}{2}) \cos(\alpha - \frac{\xi}{2}) \sin \alpha}{\left[\tan \frac{\xi}{2} \cos(\alpha - \frac{\xi}{2}) + \sin\left(\frac{\xi_m - \xi}{2}\right)\right]^2} \right) \quad . \tag{A.15}$$

When only the secondary swirl number is required, the axial momentum of the jet is expressed as

$$G_x = \frac{\dot{m}_s^2}{\rho_s A_e} \tag{A.16}$$

where A_e is the secondary throat area. From Eqns. A.3, A.14, and A.16 we have

$$S_s = \frac{\sigma A_e}{2\pi B R} \quad . \tag{A.17}$$

The secondary swirl number is therefore independent of flow rate.

To determine the total swirl number, G_x must be redefined to include both the primary and secondary axial momenta:

$$G_x = \int u(\rho u)\, dA_e + \int U(\rho_p U)\, dA_p \tag{A.18}$$

where the subscripts e and p refer to the secondary and primary streams respectively; U is the axial velocity of the primary stream and the

pressure terms have been neglected.

We now define

$$f = \dot{m}_c/\dot{m}_p$$

where $\dot{m}_c$ is the mass flow rate of coal and $\dot{m}_p$ is the mass flow rate of primary air or steam alone. If we assume that the coal occupies no space in the flow then the primary stream density is given by

$$\rho_p = \rho_a\ (1 + f)$$

where ρ_a is the density of the primary air alone. Expressing the primary velocity as

$$U = \frac{\dot{m}_p}{\rho_a A_p} \tag{A.19}$$

and substituting Eqns. A.16 and A.19 into Eqn. A.18, we obtain

$$G_x = \frac{\dot{m}_s^2}{\rho_s A_e} + \frac{\dot{m}_p^2\ (1 + f)}{\rho_a A_p} \tag{A.20}$$

Letting

$$\psi = \dot{m}_p/\dot{m}_s$$

we have

$$G_x = \frac{\dot{m}_s^2\ [\rho_a A_p + \rho_s A_e\ (1 + f)\ \psi^2]}{\rho_s A_e \rho_a A_p}\ ; \tag{A.21}$$

by substituting Eqns. A.14 and A.21 into Eqn. A.3,

$$S_t = \frac{\sigma A_e A_p \rho_a}{2\pi B R\ [\rho_a A_p + \rho_s A_e\ (1 + f)\ \psi^2]} \tag{A.22}$$

The total swirl number is not a function of flow rate, but includes the non-dimensional flow ratios f and ψ to account for changes in stoichiometry and the portion of the air used for coal transport.

VII. APPENDIX B: PREDICTED SWIRLING JET DEVELOPMENT

In order to develop approximations for the behavior of a swirling jet confined by a cylindrical chamber, the Thring-Newby analysis presented by Field et al. (1967) was extended to swirling jets by extrapolating the spread and entrainment data presented by Kerr and Fraser (1965). The density was assumed constant since the usual density correction factor $[(\rho_a/\rho_o)^{\frac{1}{2}}$ where ρ_a is the ambient density and ρ_o the jet density] cannot account for a jet initially at a higher density than ambient which becomes, due to combustion, a jet with lower than ambient density.

Figure 28 shows the general development of a confined jet. The jet spreads due to entrainment until it contacts the wall at a point P. Because no fluid is supplied externally, fluid is stripped from the jet prior to point P to satisfy the initial entrainment requirements. This creates the recirculation zones shown. Assuming that the jet initially develops as a free jet, that the jet boundary is given by 2ϕ where ϕ is the half-velocity half-angle, and that disentrainment follows the same relation as entrainment, we can analyze the system as follows.

Kerr and Fraser (1965) reported swirled jet development for swirl numbers $S \leq 1.4$ according to

$$\tan \phi = (1 + C_1 S) \tan \phi_o \qquad (B.1)$$

$$\frac{\dot{m}}{\dot{m}_o} = \frac{x}{d} (C_2 + C_3 S) \qquad (B.2)$$

where C_1, C_2, and C_3 are empirical constants, ϕ_o is the unswirled jet half-velocity half-angle, x the distance from the jet exit, d the jet exit diameter, and $\dot{m}/\dot{m}_o$ the ratio of total to initial mass flow rate. Field et al. (1967) suggest that the values for the constants be taken as: $C_1 = 2.85$, $C_2 = 0.35$, $C_3 = 0.7$ and $\phi_o = 4.85°$.

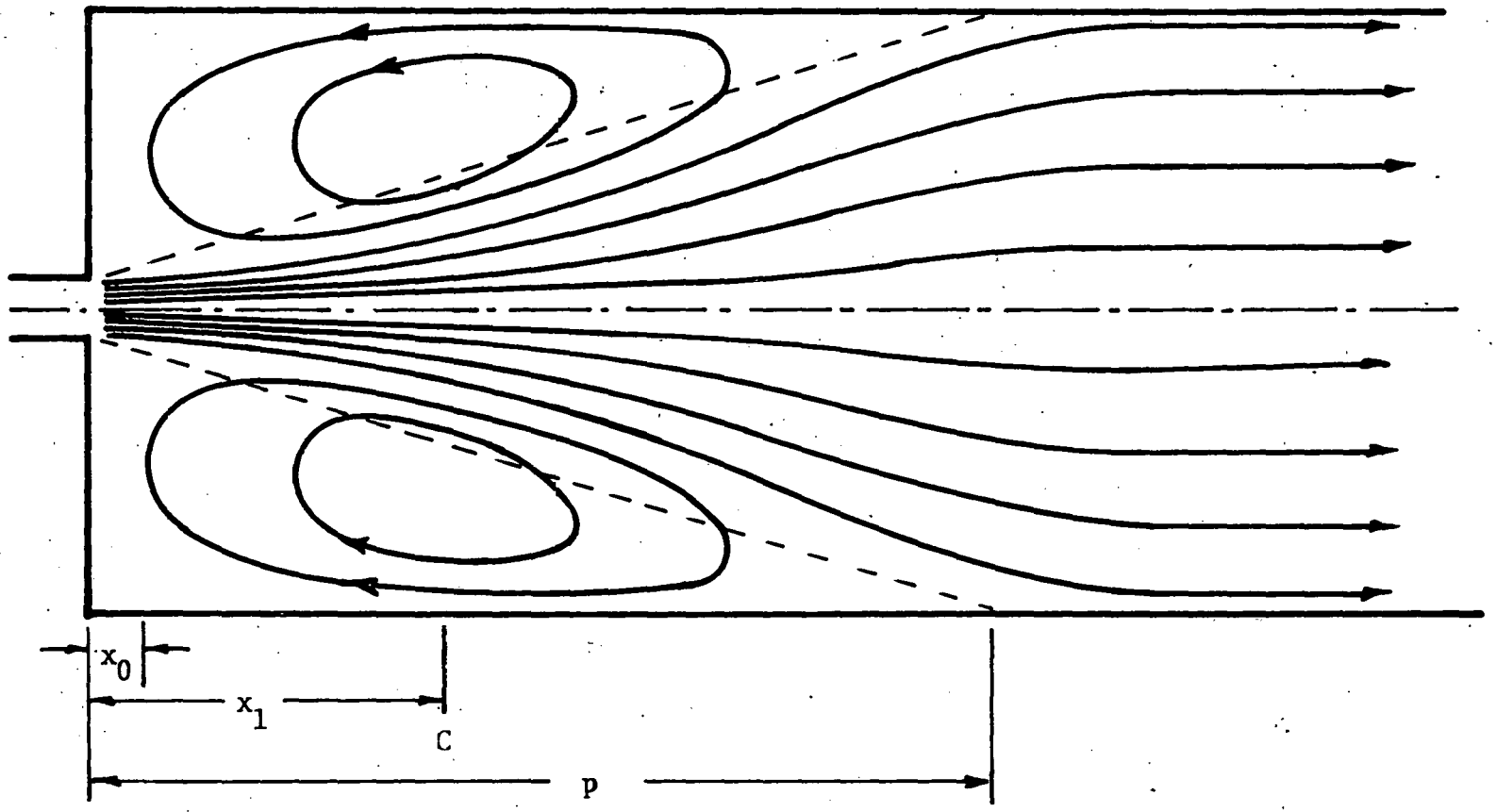

Figure 28. General Impression of Flowlines in a Confined Jet

The point P where the jet strikes the wall is given by

$$P = \frac{D}{2 \tan 2\phi} \tag{B.3}$$

where D is the chamber diameter. From Eqn. B.2, note that theoretical entrainment begins at $\dot{m}/\dot{m}_o = 1$, which yields

$$x_0 = \frac{d}{(C_2 + C_3 S)} \tag{B.4}$$

By conservation of mass, the amount of fluid entrained prior to x_1 equals the amount disentrained between x_1 and P; therefore

$$\int_{x_0}^{x_1} \frac{d\dot{m}}{dx}\, dx = \int_{x_1}^{P} \frac{d\dot{m}}{dx}\, dx \tag{B.5}$$

From Eqn. B.2 and the third assumption, we have $\frac{dm}{dx}$ = constant so that Eqn. B.5 becomes

$$(x_1 - x_0) = (P - x_1)$$

and thus

$$x_1 = \frac{p + x_0}{2} \tag{B.6}$$

Eqn. B.2 may be rewritten to consider the recirculated mass flow ($\dot{m}_r$):

$$\frac{\dot{m}_r}{\dot{m}_o} = \frac{x_1}{d} (C_2 + C_3 S) - 1 \quad ;$$

then from Eqns. B.4 and B.6,

$$\frac{\dot{m}_r}{\dot{m}_o} = \frac{P}{2d} (C_2 + C_3 S) - 0.5 \tag{B.7}$$

From Eqns. B.1 and B.3, we also have

$$P = \frac{D}{2} \left(\frac{1}{\tan \left[2 \tan^{-1} (0.0849 + 0.242\, S) \right]} \right) \tag{B.8}$$

so that Eqn. B.7 becomes

$$\frac{\dot{m}_r}{\dot{m}_o} = \frac{0.5}{\Gamma} - 0.5 \qquad (B.9)$$

where

$$\Gamma = \frac{d}{P(C_1 + C_2 S)} = 2\left(\frac{\tan\left[2 \tan^{-1}(0.0849 + 0.242\ S)\right]}{0.35 + 0.70\ S}\right)\frac{d}{D} \qquad (B.10)$$

Note that for zero swirl, Γ reduces to

$$\Gamma = 0.98\ \frac{d}{D} = 0.98\ \theta$$

where θ is the constant density Thring-Newby parameter (Beer and Chigier, 1972). Eqn. B.9 then becomes

$$\frac{\dot{m}_r}{\dot{m}_o} = \frac{0.51}{\theta} - 0.5$$

which compares favorably with the equation for an unswirled jet given by Field et al. (1967):

$$\frac{\dot{m}_r}{\dot{m}_o} = \frac{0.47}{\theta} - 0.5 \quad .$$

Eqns. B.8 - B.10 are used to develop the wall contact and mass recirculation ratio values presented in Table V.

VIII. APPENDIX C: THERMAL ANALYSIS OF THE JET REACTION CHAMBER

To determine the suitability of the reactor refractory and insulation design and to give an indication of exhaust gas temperatures a simple PSR equilibrium model was employed. The assumptions governing the model are as follows:

(1) The coal burns to completion inside the reactor.
(2) Reactor composition is uniform throughout and coal particles are uniformly distributed.
(3) Radiation transfer is the result of coal particles alone; effects of CO_2 and H_2O are neglected. No radiation reduction due to particle burnout is included.
(4) Convective transfer in the chamber is approximated by pipe flow.
(5) Coal particles are assumed to be black body spheres of 60μm diameter.
(6) The exit gas composition is assumed to be as follows for all cases regardless of input stoichiometry: $X(N_2) = 76\%$, $X(CO_2) = 16\%$, $X(H_2O) = 6\%$, $X(O_2) = 2\%$. Ash is less than 2% of the products by weight and is neglected.
(7) Heat transfer is approximated as one-dimensional through the cylindrical reactor wall. End losses are included by multiplying the wall heat transfer by 1.18 to reflect the increased area.
(8) Heat is lost from the vessel by convection and radiation into a 100°F environment.

Heat balances and mass flow rates are based on combustion. Initial flow rates and temperatures are listed in Table VIII. Based on the assumed exit gas composition, the enthalpy of the products (BTU/lbm of product gas) can be calculated from

$$H_p = 0.0253\, H_{N_2} + 0.0020\, H_{H_2O} + 0.0053\, H_{CO_2} + 0.00067\, H_{O_2} \qquad (C.1)$$

TABLE VIII

Initial Conditions for Reactor Thermal Analysis

	Temperature (°R)	Stoichiometric	20% Excess Air
Coal* Flow Rate	660	7 - 28 lbm/hr.	7 - 28 lbm/hr.
Primary Air Flow Rate	660	1.5 lbm air/lbm coal	1.5 lbm air/lbm coal
Secondary Air Flow Rate	1210	7.66 lbm air/lbm coal	9.57 lbm air/lbm coal
Total Enthalpy Input (H_o) Per lbm Product Gas		1.30×10^3 BTU/lbm	1.12×10^3 BTU/lbm

* HHV(Dry Basis) = 11904 BTU/lbm

where H_i is the sensible enthalpy per pound of the i^{th} gas (reference to 537°R). Fig. 16 (Heat Loss Rate vs. Gas Temperature) was generated by calculating the exit enthalpy for a series of gas temperatures. Heat loss rate (Q_L) was determined by

$$(H_o - H_p)\,\dot{m}_t = Q_L \qquad (C.2)$$

where $\dot{m}_t$ is the total mass flow rate of dry coal and air.

Heat is lost through the wall by conduction and from the surface of the vessel by natural convection and radiation. Conduction losses (BTU/hr) were calculated by:

$$Q = \frac{(T_w - T_v)\,2\pi L}{\frac{\ln(r_2/r_w)}{k_r} + \frac{\ln(r_3/r_2)}{k_K} + \frac{\ln(r_v/r_w)}{K_s}} \qquad (C.3)$$

where: T_w = refractory inner wall temperature
T_v = vessel outer wall temperature
L = chamber length = 50"
r_w = inner wall radius = 7.625"
r_2 = refractory/Kaowool interface radius = 9.625"
r_3 = vessel inside radius = 11.625"
r_v = vessel outside radius = 12.00"
k_r = refractory conductivity = 0.58 BTU/(hr•ft•°R) @ 3060°R
k_K = Kaowool conductivity = 0.11 BTU/(hr•ft•°R) @ 2060°R
K_s = steel conductivity = 21 BTU/(hr•ft•°R) .

Substituting the above values into Eqn. C.3 gives

$$Q_1 = 12.35\,(T_w - T_v) \quad .$$

Natural convection from the vessel wall was calculated by applying the heat transfer coefficient (Holman, 1968)

$$h = 0.29\left(\frac{T_v - 560}{L_w}\right)^{\frac{1}{4}}$$

to the general convective heat transfer equation to give

$$Q_2 = 6.09\ (T_v - 560)^{1.25} \qquad (C.4)$$

where the heat transfer area was based on a cylinder 60" long and 24" in diameter. In effect, the extra length assumes that the high conductivity of the shell and the two-dimensional effects at the end of the cylinder can be compensated for by using a larger convective area.

Radiation from the vessel wall (Q_3) was modeled via

$$Q_3 = A_v \varepsilon \sigma_B (T_v^4 - 560^4) = 4.09 \times 10^{-8} (T_v^4 - 560^4) \qquad (C.5)$$

where A is the area and σ_B the Stefan-Boltzmann constant. The emissivity ε was taken as 0.76, the value for high temperature black paint (Chapman, 1974). Eqns. C.3, C.4 and C.5 were solved graphically ($Q_1 = Q_2 + Q_3$) to determine the heat loss rate and vessel wall temperature as functions of inner wall temperature (T_w). In order to partially compensate for the heat loss through the ends, the heat loss calculated was multiplied by 1.18 to include the top and bottom chamber areas. Heat loss rate vs. T_w is shown in Fig. 16, along with the heat loss rate vs. gas temperature curves. Figure 15 shows the vessel wall temperature as a function of T_w.

If the gas temperature (T_g) is assumed to be equal to the wall temperature, then the intersection of a gas temperature line with the wall temperature line represents a stable operating point. The line of constant temperature at 3460°R shown on the graph represents the upper recommended use temperature of the refractory.

For an estimate of the gas to wall heat transfer, convection heat transfer was assumed to follow the relation for pipe flow presented by Holman (1968),

$$Nu = 0.023\ (Re)^{0.8}\ (Pr)^{0.3} \qquad (C.6)$$

where Nu(hD/k) is the Nusselt number, Re the Reynolds number and Pr the Prandlt number. The Prandlt number is assumed equal to 0.7 and the Reynolds number is given by

$$Re = 15.28\ (\dot{m}_t/D\mu)$$

where m_t is the air mass flow rate (lbm/hr), D the chamber diameter and μ the viscosity. Using appropriate air values for thermal conductivity (k) and viscosity (Bird, Stewart and Lightfoot, 1960), the heat transfer coefficient (h) is obtained:

$$h = 41 \left(\frac{\dot{m}_t}{\sqrt{T_g}}\right)^{0.8} \frac{BTU}{hr \cdot ft^2 \cdot {}^\circ R} \quad . \tag{C.7}$$

The total heat transfer by convection (BTU/hr) from the gas to the wall is then

$$Q_{cv} = hA\ (\Delta T) = 680 \left(\frac{\dot{m}_t}{\sqrt{T_g}}\right)^{0.8} (T_g - T_w)\ \frac{BTU}{hr} \quad . \tag{C.8}$$

For gas to wall radiation transfer, the emissivity of the gas is calculated as follows. The particle mass (M_p) is given by

$$M_p = 3.53 \times 10^{-17}\ \rho_c \left(\frac{\pi (D_p)^3}{6}\right) = 3.19 \times 10^{-10}\ \frac{lbm}{particle} \tag{C.9}$$

where ρ_c is the density of coal (assumed to be 80 lbm/ft^3) and D_p the diameter of the particle (60μm). The cross-sectional surface area (a_p) per particle is given by

$$a_p = \pi (D_p)^2 = 3.04 \times 10^{-8}\ \frac{ft^2}{particle} \tag{C.10}$$

and the particle concentration (C) by

$$C = \chi \left(\frac{1}{M_p}\right) \rho_g\ \frac{particles}{ft^3} \tag{C.11}$$

where χ is the coal/air ratio and ρ_g is the density of the gas at the temperature of interest. The adsorption coefficient K can be determined from (Field et al., 1967)

$$K = C a_p\ ft^{-1} \tag{C.12}$$

and the emissivity of the gas (ε_g) is then given by

$$\varepsilon_g = 1 - \exp(-\ 8.33 \times 10^{-2}\ f_r K\ D) \qquad (C.13)$$

where f_r is a shape factor and D the chamber diameter in inches.

Letting the shape factor equal 0.75 (Field et al., 1967), expressing the density of the gas as

$$\rho = 39.8 \left(\frac{1}{T_g}\right) \text{ lbm/ft}^3$$

and substituting Eqns. C.9 through C.12 into C.13, the gas emissivity becomes

$$\varepsilon_g = 1 - \exp(-\ 3.59 \times 10^3\ \frac{\chi}{T_g}) \quad . \qquad (C.14)$$

If the emissivity of the walls is assumed to be 0.5, the net radiant energy exchange can then be expressed as (Field et al., 1967)

$$Q_r = \left(\frac{1}{\frac{1}{\varepsilon_g} + \frac{1}{\varepsilon_w} - 1}\right) A\sigma_B\ (T_g^4 - T_w^4)$$

or

$$Q_r = \left(\frac{1}{\frac{1}{\varepsilon_g} + 1}\right) (2.845 \times 10^{-8})\ (T_g^4 - T_w^4)\ \frac{\text{BTU}}{\text{hr}} \quad . \qquad (C.15)$$

The total net energy exchange between the gas and the wall (Q_t) is

$$Q_t = Q_r + Q_{cv} \qquad (C.16)$$

Thus, Eqns. C.8, C.14, C.15 and C.16 can be used to determine the heat flux for any set of conditions specified. By applying these equations iteratively to Fig. 16, ($Q_L = Q_1 = Q_t$) it is possible to determine the gas and wall temperatures for a given flow rate and stoichiometry. For example, at 9 lbm/hr and stoichiometric feed rates, the predicted gas temperature is 3555°R and the wall temperature 3495°R; at 14 lbm/hr coal flow and 20% excess air, the gas temperature is 3585°R and the wall temperature 3520°R.

IX. APPENDIX D: MASS SPECTROMETER CALIBRATION DATA

The following data (Tables IX and X) are the result of the Q-30C mass spectrometer analysis for several complex gas mixtures. Gas mixture compositions are known from partial pressure measurements and are compared with the mole fractions calculated from the mass spectrometer data by the computer program of McLean and Sawyer (1967).

Calibration errors come from several sources. Readability errors are encountered when measuring partial pressures and mass spectrometer peak heights. These errors are generally less than one percent and are reduced further by repeated measurements. Error is caused by time dependent changes in the mass spectrometer system, but frequent calibration checks minimize this type of error. Adsorption and desorption phenomena, backgrounds, and inherent system nonlinearities appear to be the major sources of calibration errors.

Examination of the data reveals that measurement errors of less than three percent can be expected with a high degree of confidence for CH_4, N_2, O_2, and CO_2 concentrations. Similarly, H_2 measurements can be made to within five percent accuracy. The CO concentration is the most difficult to measure; errors averaging five percent are expected when CO concentrations are larger than four percent of the sampled gas. CO measurability increases as the CO/N_2 and CO/CO_2 ratios increase.

TABLE IX

Comparison of Measured and Calculated Mole Fraction Data†

Trial		H_2	CH_4	H_2O	CO	N_2	O_2	CO_2
	M	.0666			.0588	.756	.0309	.0878
1	C	.0644			.0581	.761	.0300	.0869
	E	-3.3			-1.2	+0.7	+2.9	+1.0
	M	.0555			.0597	.790	.0320	.0626
2	C	.0527			.0585	.792	.0324	.0645
	E	-5.0			-2.0	+0.3	+1.3	+3.0
	M	.0478			.0525	.785	.0422	.0728
3	C	.0490			.0450	.792	.0425	.0717
	E	+2.5			-14.3	+0.9	+0.9	-1.5
	M	.0576	.0259		.0708	.769	.0303	.0365
4	C	.0703	.0260		.0677	.770	.0292	.0365
	E	+4.0	+0.4		-4.4	+0.1	-3.6	--
	M	.0335	.0268		.0339	.780	.0570	.0689
5	C	.0333	.0263		.0395	.773	.0580	.0693
	E	-0.6	-1.9		+16.5	-0.9	+1.8	+0.6

TABLE IX (cont.)

Trial		H_2	CH_4	H_2O	CO	N_2	O_2	CO_2
	M	.0620	.0253		.0582	.751	.0438	.0601
6	C	.0604	.0250		.0611	.750	.0438	.0601
	E	-2.6	-1.2		+5.0	-0.1	--	--
	M	.0660	.0355		.0627	.734	.0334	.0682
7	C	.0687	.0360		.0626	.732	.0338	.0670
	E	+4.1	+1.4		-0.2	-0.3	+1.2	-1.8
	M	.0550	.0257	.0703	.0611	.716	.0291	.0429
8	C	.0583	.0236	.0706	.0642	.710	.0294	.0440
	E	+6.0	-8.2	+0.4	+5.1	-0.8	+1.0	+2.6
	M	.0415		.0907	.0509	.708	.0445	.0645
9	C	.0425		.0911	.0490	.708	.0449	.0647
	E	+2.4		+0.4	-3.7	--	+0.9	+0.3

†M -- measured mole fraction
C -- calculated mole fraction
E -- % error

TABLE X

Example Sensitivity and Fragmentation Data

Species	Relative Sensitivity	Mass/Charge 2	12	14	15	16	17	18	28	32	44
H_2	0.633	100									
CH_4	0.941		1.89	13.7	84.4	100	1.33				
H_2O	0.875	2.32				2.46	25.06	100			
CO	1.034		3.07	0.33		0.84			100		
N_2	1.00	0.37		5.67					100		
O_2	0.625					8.66				100	
CO_2	1.095		4.00			8.25			8.90		100

X. APPENDIX E: DEVELOPMENT OF THE RELATIONSHIP BETWEEN τ_r/τ_b AND CRITICAL PARTICLE RADIUS

Assume the following (Perry et al, 1950):

(1) Flow in the cyclone can be modeled as an ideal free vortex.

(2) Flow at the cyclone wall has an inward radial velocity U_1 defined as

$$U_1 \equiv Q'/(2\pi R_1 L) \qquad (E.1)$$

where $Q' \equiv$ volumetric flow rate, ft^3/sec
$R_1 \equiv$ cyclone radius, ft
$L \equiv$ cyclone length, ft.

(3) The entire flow Q' passes through the area A shown in Fig. 29 at uniform tangential velocity V_1. Thus

$$V_1 = Q'/A = Q'/[(L - \ell)\cdot(R_1 - R_t)] \; . \qquad (E.2)$$

(4) Constant gas density.

(5) Conservation of mass in the radial direction. Thus,

$$U_1 R_1 = U_2 R_2 \qquad (E.3)$$

where $R_2 \equiv$ arbitrary radius within cyclone, ft
$U_2 \equiv$ radial velocity at R_2, ft/sec.

The following are also given (Perry et al., 1950):

(1) Centrifugal force on a particle $\equiv (4/3)\,\pi a^3 \rho v^2/r$.

(2) Viscous drag force on a particle $\equiv 6\pi a \mu u$.

(3) From conservation of angular momentum for a free vortex,

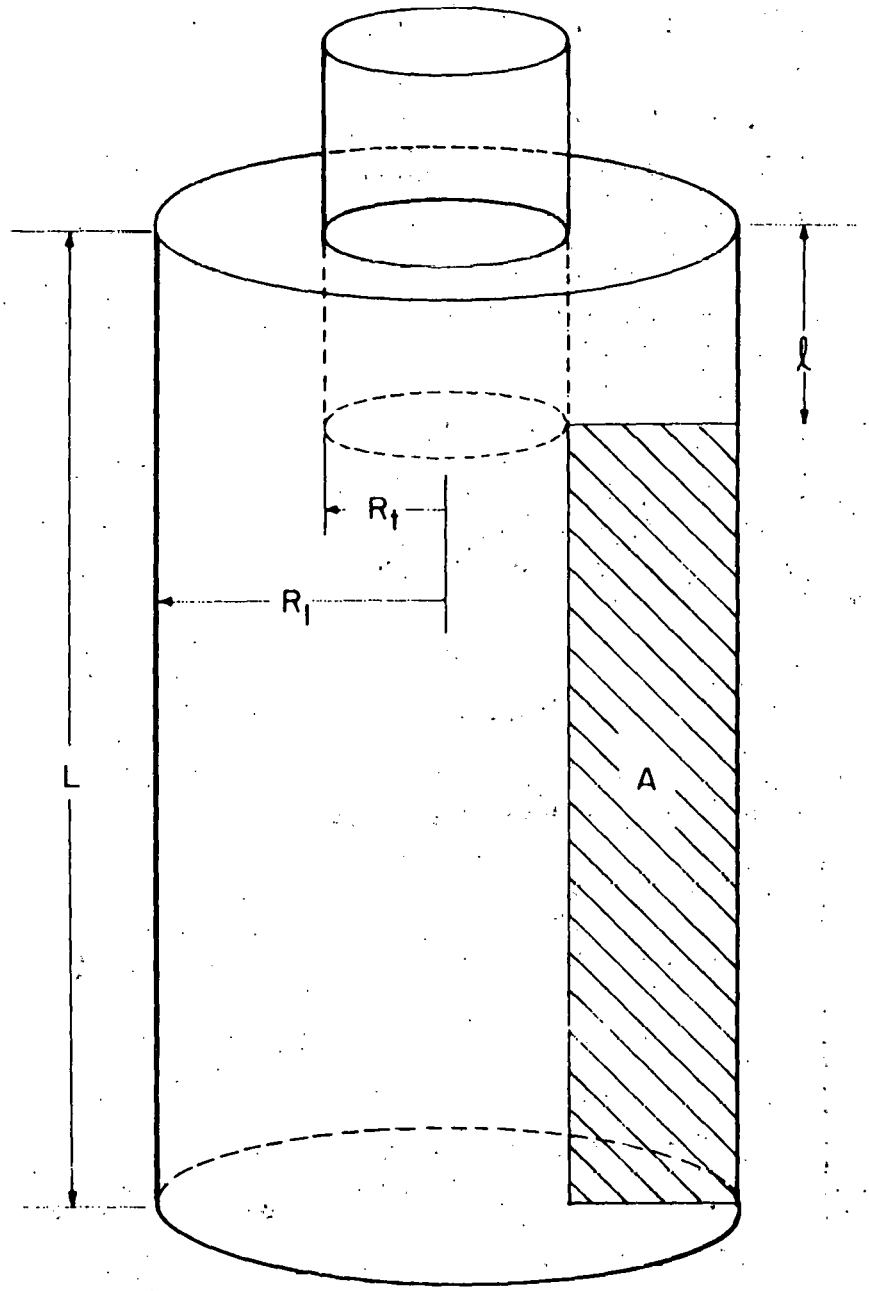

Figure 29. Cyclone Model Schematic

$$M_1 V_1 R_1 = M_2 V_2 R_2 \qquad \text{(E.4)}$$

where $a \equiv$ particle radius, ft

$\rho \equiv$ particle density, lbm/ft^3

$r \equiv$ radius at any point in cyclone, ft

$v \equiv$ tangential velocity of gas, ft/sec

$u \equiv$ radial velocity of gas, ft/sec

$\mu \equiv$ viscosity of gas, lbm/ft sec

$m_1 \equiv$ mass flow rate at cyclone wall, lbm/sec

$m_2 \equiv$ mass flow rate at radius R_2, lbm/sec

$V_2 \equiv$ tangential velocity at R_2, ft/sec .

For a particle at equilibrium, opposed radial forces are equal:

$$(4/3)\,\pi a^3 \rho v^2/r = 6\pi a \mu u \quad .$$

Therefore,

$$v^2 = (9\mu u r)/(2a^2\rho) \quad .$$

Now, let

$$u = U_2,\ v = V_2,\ r = R_2;$$

then

$$V_2^2 = (9\mu U_2 R_2)/(2a^2\rho) \quad .$$

Substituting for V_2^2 from Eqn. 4:

$$V_1^2 = \left(\frac{M_2}{M_1}\right)^2 \left(\frac{R_2}{R_1}\right)^2 (9\mu U_2 R_2)/(2a^2\rho) \quad . \qquad \text{(E.5)}$$

Combining Eqns. E.1 and E.3 yields

$$U_2 = Q'/(2\pi R_2 L) \quad . \qquad \text{(E.6)}$$

Substituting Eqn E.6 into E.5 and solving for a gives

$$a = \frac{3}{2}\left(\frac{1}{V_1}\right)\left(\frac{M_2R_2}{M_1R_1}\right)\sqrt{\frac{\mu Q'}{\pi L\rho}} \quad . \tag{E.7}$$

Substituting Eqn. E.2 into E.7 yields the final result

$$a = \frac{3}{2}(L - L_t)(R_1 - R_t)\left(\frac{M_2R_2}{M_1R_1}\right)\sqrt{\frac{\mu}{Q'\pi L\rho}} \quad . \tag{E.8}$$

Equation E.8 relates the radius a of a particle to its equilibrium radius R_2 as a function of the volumetric flow rate Q'. The critical particle radius for a given volumetric flow rate is determined by setting R_2 equal to the throat radius R_t. Figure 30 presents this relationship graphically for the following conditions:

$L = .833$ ft
$L_t = .167$ ft
$R_1 = .250$ ft
$R_t = .104$ ft
$M_1 = M_2$
$R_2 = R_t$
$\mu = 4 \times 10^{-7}$ (lbf·sec/ft^2)
$\rho = 85$ lbm/ft^3
$g_c = 32.2$ (lbm·ft/lbf·sec^2) .

To verify this relationship and to check the validity of the assumptions made, coal particles having a known Rosin-Rammler size distribution were injected to the cyclone model at measured gas flow rates. The mass of particles remaining in the cyclone was then measured to determine (via the Rosin-Rammler Distribution) the radius of the largest particle exiting the cyclone at that flow rate. These data are also presented in Fig. 30. If it is assumed that all particles migrating to the throat radius exit the cyclone, then the critical particle radius should equal the radius of the largest particle to leave the cyclone.

All experimental points indicate particle radii greater than predicted. This may be an indication that there are defects in the initial assumptions, particularly assumption 3. Furthermore, measurement errors may be introduced by the slight mass differences between injected and

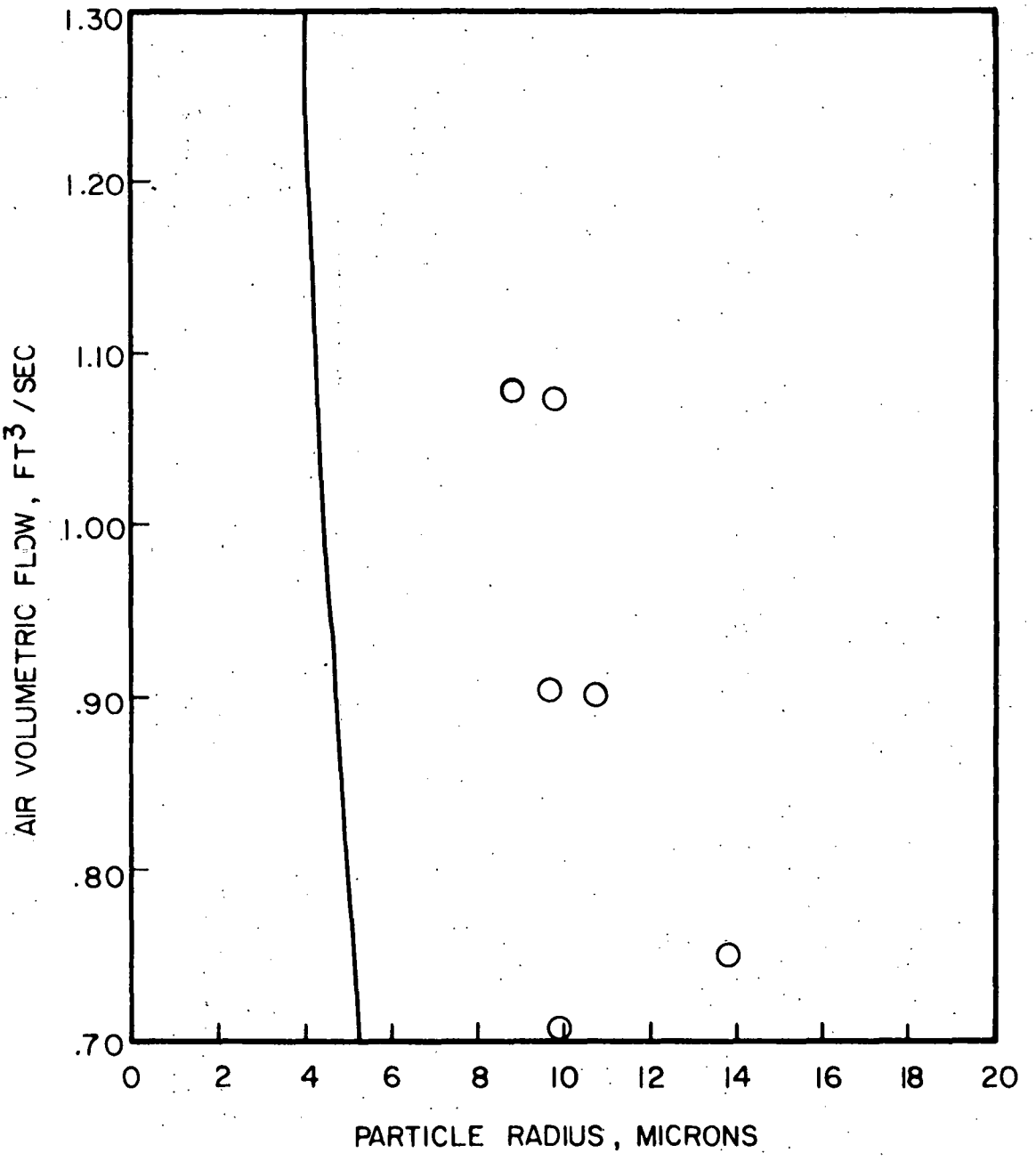

Figure 30. Radius of Largest Escaping Particle vs. Air Volumetric Flow Rate

recovered particles. Considering these errors, a factor of two difference between theory and experiment should not be surprising. In any event, the data indicate that only a small mass fraction of the particles escape, even for incoming particles smaller than 400 mesh.

To determine if sufficient burning time is available to particles leaving the cyclone, particulate residence time τ_r and particulate burning time τ_b were both obtained as functions of the critical particle radius. Particulate residence time was obtained by dividing the flow volume by the volumetric flow rate, which can be expressed as a function of critical particle radius by rearrangement of Eqn. E.8. Two flow volumes were used (Fig. 29): a "short circuit" flow volume given by

$$V_f = \pi(R_1^2 - R_t^2) \cdot L_t$$

and the entire flow volume given by

$$V_f = \pi R_1^2 L - \pi R_t^2 L_t \quad .$$

Particulate burning times are available in the literature (Thring and Essenhigh, 1963) and are illustrated in Fig. 31. In calculations, the longer burning time was used at each particle radius. The relationship between the τ_r/τ_b ratio and critical particle radius is presented in Fig. 24 of Section IV.D.

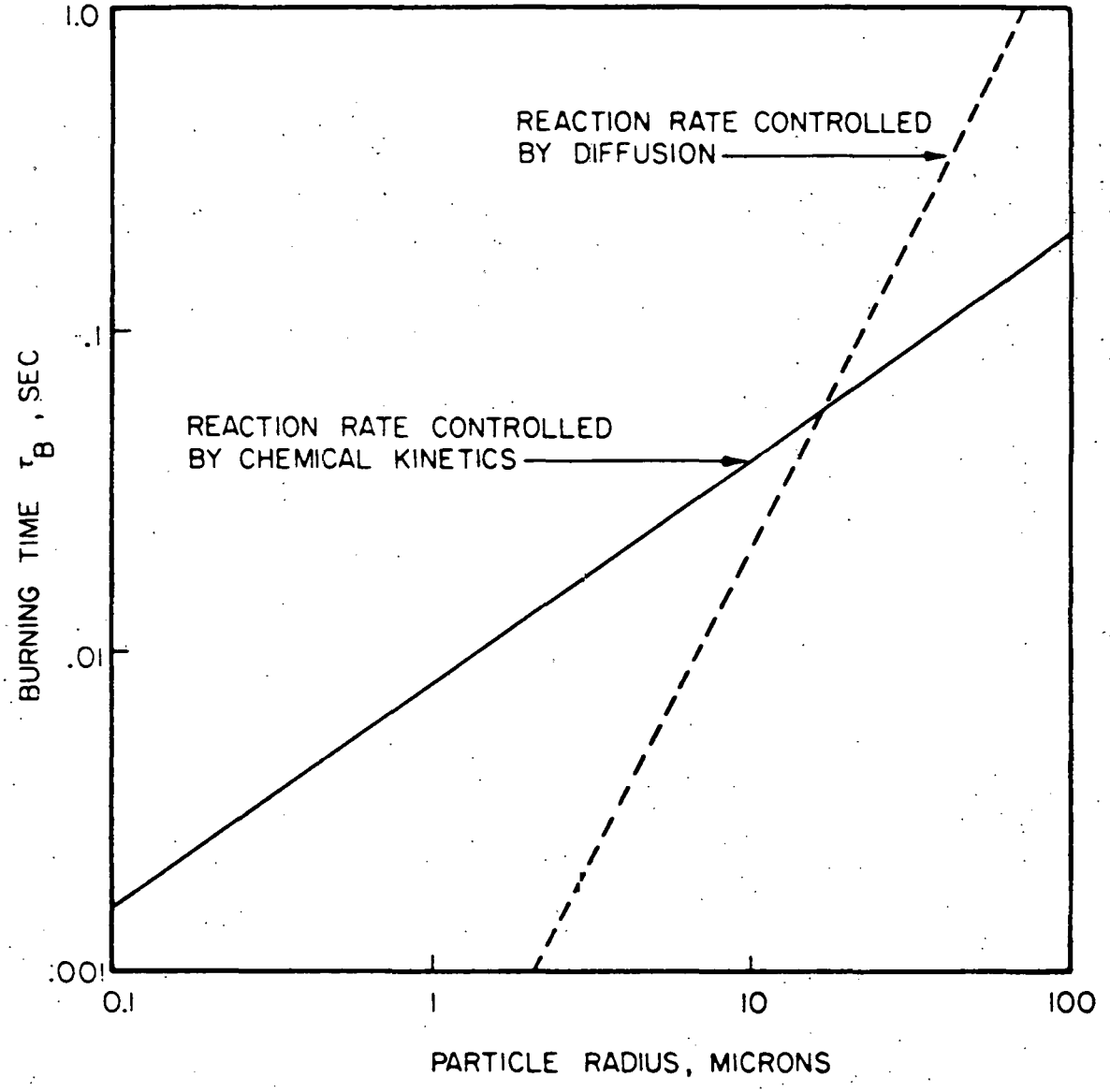

Figure 31. Calculated Burning Times for Pulverized Coal with 10% Excess Air vs. Critical Particle Radius

LIST OF REFERENCES

Agrest, J. (1965), "The combustion of vegetable materials: A cotton husk combustion problem," J. Inst. Fuel 38, 344.

Anthony, D. B. and Howard, J. B. (1976), AIChE J. 22, 625.

Babcock and Wilcox (1963), Steam: Its Generation and Use, Chapter 17.

Baluev, E. D. and Troyankin, Yu. V. (1967), "Study of the aerodynamic structure of gas flow in a cyclone chamber," Thermal Eng. 14 (1), 84.

Batchelder, H. R., Busche, R. M. and Armstrong, W. P. (1953), "Kinetics of coal gasification," Industrial and Engineering Chemistry 45, 1856.

Beer, J. M. and Lee, K. B. (1965), "The effect of residence time distribution on the performance and efficiency of combustion," Tenth Symposium (International) on Combustion, The Combustion Institute, 1187-1202.

Beer, J. M. and Chigier, N. A. (1969), "Stability and combustion intensity of pulverized coal flames - effect of swirl and impingement," J. Inst. Fuel 42, 443.

Beer, J. M. and Chigier, N. A. (1972), Combustion Aerodynamics, Wiley, New New York.

Beer, J. M. (1976), Massachussets Institute of Technology, Cambridge, Mass., Personal Communication.

Bird, R. B., Stewart, N. E. and Lightfoot, E. N. (1960), Transport Phenomena, Wiley, New York.

Blake, T. R. (1977), "Computer modeling of coal gasification reactors," Qarterly Technical Progress Report, ERDA Fossil Energy Program Contract No. EX-76-C-01-1770, Systems, Science, and Software, La Jolla, California.

Chapman, A. J. (1974), Heat Transfer, 3rd Edition, Macmillian Publishing Co., Inc., New York.

Chedaille, J. and Braud, Y. (1972), Measurements in Flames, International Flame Research Foundation -- Crone Russak, New York, 95-98.

Colket, M. B., Stefucza, J. M., Peters, J. E. and Mellor, A. M. (1977), "Radiation and smoke from gas turbine flames, Part 2: Fuel effects on performance," Final Technical Report, Contract No. DAAE07-76-C-0063, Purdue University, West Lafayette, Indiana.

Field, M. A., Gill, D. W., Morgan, B. B. and Hawksley, P. G. W. (1967), Combustion of Pulverized Coal, BCURA, Leatherhead, U. K.

Fuchs, W., Berman, M., Stradey, J. P., Jr., Ergun, S. (1974), "An automated monitoring system for an experimental coal gasifier," Chem. Inst. 5 (3), 155.

George, P. E., Lenzer, R. C., Thomas, J. F. and Laurendeau, N. M. (1977), ERDA Report FE-2029-5, Purdue Univ., W. Lafayette, Indiana.

Godsave, G. A. E. (1953), "Studies on the combustion of drops in a fuel spray--the burning of single drops of fuel," Fourth Symposium (International) on Combustion, The Williams and Wilkins Company, Baltimore, 818.

Grant, J. R., Rice, J. G. and Thomas, W. C. (1977), "An experimental study of the combustion of a low heating value gas in a swirl burner," Spring Meeting, Central States Section/The Combustion Institute, Cleveland, Ohio.

Heap, M. P., Lowes, T. M., Walmsley, R. and Bartelds, H. (1973), "Burner design principles for minimum NO_x emissions," EPA Coal Combustion Seminar, Research Triangle Park, North Carolina.

Holman, J. P. (1968), Heat Transfer, 2nd Edition, McGraw-Hill, New York.

Hottel, H. C. and Howard, J. B. (1971), New Energy Technology: Some Facts and Assessments, MIT Press, Cambridge, Massachusetts.

How, M. E., Kear, R. W. and Whittingham, G. (1954), "The design and development of a laboratory-scale pulverized-coal-fired furnace," J. Inst. Fuel 27, 598.

Kerr, N. M. and Fraser, D. (1965), "Swirl. Part I: Effect on axi-symmetrical turbulent jets," J. Inst. Fuel 38, 519.

Kurtzrock, R. C., Bienstock, D. and Field, J. H. (1963), "Process development in removing sulfer dioxide from hot flue gas; Part 2: laboratory-scale pulverized-coal-fired furnace," Bur. Mines R16307.

Laurendeau, N. M. (1975), "Theoretical and practical concepts governing production of power gas from coal," Spring Meeting, Central-Western States Section/The Combustion Institute, San Antonio, Texas.

Laurendeau, N. M. (1977), "Heterogeneous kinetics of coal char gasification and combustion," Prog. in Energy and Combustion Sci., (in press).

Laurendeau, N. M., and Waite, D. M. (1977), "Performance parameter for coal gasification to power gas," Fuel 56, 108.

Lenzer, R. C., George, P. E., Thomas, J. F. and Laurendeau, N. M. (1976), ERDA Report FE-2029-4, Purdue Univ., W. Lafayette, Indiana.

Lenzer, R. C. and Laurendeau, N. M. (1976), "Gasification of pulverized coal within swirling flows: An interpretive review," Spring Meeting, Western States Section/The Combustion Institute, Salt Lake City, Utah.

Lenzer, R. C. (1977), "Design and development of a pulverized coal cyclone gasifier," M. S. Thesis, School of Mechanical Engineering, Purdue University, West Lafayette, Indiana.

Levenspiel, O. (1972), Chemical Reaction Engineering, Wiley, New York.

Lewellen, W. S., Segur, H. and Varma, A. K. (1977), "Modeling two phase flow in a swirl combustor," Final Report, ERDA Contract No. EY-76-C-02-4062, Aeronautical Research Associates of Princeton, Inc., Princeton, New Jersey.

McLean, W. J. and Sawyer, R. F. (1967), "Mass spectrometer data reduction and error analysis," Report No. TS-67-4, College of Engineering, University of California, Berkeley.

Mehta, A. K. (1976), "Mathematical modeling of chemical processes for low BTU/gasification of coal for electric power generation," Final Report, ERDA Contract No. E(49-18)-1545, Combustion Engineering, Inc., Windsor, Connecticut.

Osborn, E. F. (1974), "Coal and the present energy situation," Science, 183, 477.

Perry, H., Corey, R. C. and Elliott, M. A. (1950), "Continuous gasification of pulverized coal with oxygen and steam by the vortex principle," ASME 72, 599.

Pershing, D. W. and Wendt, J. O. L. (1975) "Pollutant control through staged combustion of pulverized coal," ERDA Report No. FE-1817-1, University of Arizona, Tucson, Arizona.

Schmidt, K. R. (1970), "The rotary flow furnace of Siemens-Agrest," V. D. I. Berichte 146, 90.

Semenov, V. S. and Semenenko, N. A. (1969), "Pattern of combustion and gasification of coal in a cyclone chamber," Thermal Eng. 16 (12), 108.

Smith, J. M. (1970), Chemical Engineering Kinetics, McGraw-Hill, Inc.

Smoot, L. D. and Hanks, R. W. (1976), "The mixing and gasification of coal in entrained flow systems," Quarterly Technical Progress Report, ERDA Report FE-1767-4, Brigham Young University, Provo, Utah.

Squires, A. M. (1974), "Clean fuels from coal gasification," Science 184, 340.

Strickland, L. D. (1973), "A cold flow mixing study of a vortex coal gasifier," Ph.D. Thesis, West Virginia University, Morgantown, W. Va.

Syred, N. and Beer, J. M. (1974), "Combustion in swirling flows: A review," Comb. and Flame 23, 143.

Thring, M. W. and Essenhigh, R. H. (1963), "Thermodynamics and kinetics of solid combustion," in Chemistry of Coal Utilization, Supplementary Volume, H. H. Lowry, Ed., Wiley, New York, 754-772.

Tuttle, J. H., Colket, M. B. and Mellor, A. M. (1976), "Characteristic time correlation of emissions from conventional aircraft type flames," Final Report, EPA Grant No. R-802650-02, Purdue University, West Lafayette, Indiana.

Ustimenko, B. P. and Bukhman, M. A. (1968), "Turbulent Flow structure in a cyclone chamber," Thermal Eng. 15 (2), 90.

von Fredersdorff, C. G. and Elliott, M. A. (1963), "Coal gasification," in Chemistry of Coal Utilization, H. H. Lowry, Ed., Wiley, New York, 892-1022.

Yagi, S. and Kunii, D. (1957), "Studies on combustion and gasification of pulverized coal in a model cyclone generator," Sixth Symposium (International) on Combustion, Reinhold Publ. Corp., New York, 584-590.

BIBLIOGRAPHIC DATA SHEET	1. Report No. ERDA-FE-2029/6	2.	3. Recipient's Accession No.

4. Title and Subtitle
GASIFICATION IN PULVERIZED COAL FLAMES
Second Annual Progress Report

5. Report Date
August 1977 (I)

6.

7. Author(s) P. E. George, R. C. Lenzer, J. F. Thomas, J. S. Barnhart, N. M. Laurendeau

8. Performing Organization Rept. No. PURDU-CL-77-04

9. Performing Organization Name and Address
The Combustion Laboratory
School of Mechanical Engineering
Purdue University
W. Lafayette, Indiana 47907

10. Project/Task/Work Unit No.

11. Contract/Grant No.
E(49-18)-2029

12. Sponsoring Organization Name and Address
Energy Research and Development Administration
Fossil Energy Division
20 Massachusetts Ave., N.W.
Washington, D. C. 20545

13. Type of Report & Period Covered
(July 1976-July 1977)

14.

15. Supplementary Notes

16. Abstracts

The objective of this program is to investigate the feasibility of using currently available pulverized coal burners to produce power or synthesis gas from coal. Two configurations will be considered: (1) the annular confined jet with secondary swirl, and (2) the vortex tube with tangential entry. The first burner is characterized by a single axial injector of high primary velocity; secondary swirl is used to control mixing and residence times. The second burner is modeled after the cyclone combustor; large residence times and slagging operation should lead to high carbon efficiencies.

Species concentrations and temperature are measured both within and downstream of the gasifier chambers. These profiles are used to assess the influence of process variables such as pressure, solid/gas feed rates, swirl intensity, inlet temperature and geometrical injection pattern on both the rate and extent of coal conversion. Simple models governing entrained flow systems will be developed to further interpret the experimental data.

17. Key Words and Document Analysis. 17a. Descriptors

Pulverized Coal Gasification
Coal Gasification
Pulverized Coal Combustion
Pulverized Coal Burners
Cyclone Burners

17b. Identifiers/Open-Ended Terms

17c. COSATI Field/Group

18. Availability Statement	19. Security Class (This Report)	21. No. of Pages
Release Unlimited	UNCLASSIFIED	132
	20. Security Class (This Page) UNCLASSIFIED	22. Price

☆U.S. GOVERNMENT PRINTING OFFICE: 1978-740-306/300 REGION NO. 4